TÉCNICO LISBOA

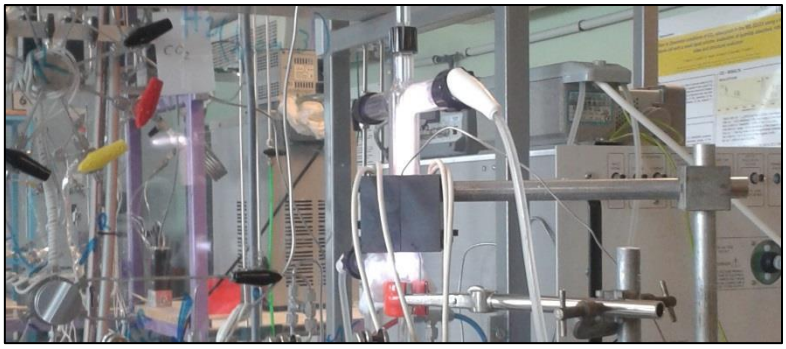

Plasma-assisted Catalytic CO_2 Hydrogenation

Diogo Miguel Cardona de Sousa Bento

Thesis to obtain the Master of Science degree in

Chemical Engineering

Supervisors: Prof. Carlos Manuel Faria de Barros Henriques

Dr. Federico Azzolina-Jury

Examination Committee

Chairperson: Prof. Sebastião da Silva Alves

Supervisor: Prof. Carlos Manuel Faria de Barros Henriques

Members of the Committee: Prof. José Manuel Madeira Lopes

November 2015

This page was intentionally left blank

Acknowledgements

In the first place, I would like to express my gratitude towards the LCS laboratory, to ENSICAEN and IST for the opportunity to carry out this internship in the LCS lab and learn so much about catalysis, especially on the topic of CO_2 hydrogenation. To the LCS personnel for kindly receiving me and for all the technical support and scientific advises that were so useful throughout this work.

I would also like to thank in particular to Dr. Federico Azzolina-Jury and Dr. Frédéric Thibault-Starzyk from LCS as well as to Dr. Carlos Henriques from IST for the supervision and knowledge they were willing to share with me that allowed the completion of this thesis.

To my family, who gave me all the necessary support not only during this work, but during this whole journey to complete the Master's Degree in Chemical Engineering.

At last I would like to thank to my good friends. The ones I was fortunate enough to meet during my personal and academic life in IST as well as the ones that I met during the internship in Caen. Thank you for all the advises, support and motivation that pushed me towards the finish line. In particular to Ameessa, who has been such a big support and role model in terms of compromise and dedication towards one's goals.

This page was intentionally left blank.

Abstract

Ni-based USY and ZSM-11 catalysts were prepared with different amounts of metal and by different impregnation methods for application on the CO_2 hydrogenation reaction. Their characterization was performed by determining their external and internal surface areas, micro- and mesopores volume, crystallinity, Ni reduction level on the catalysts surface and by analysing SEM images of each sample. All the analyzed catalysts revealed crystallinity above 99%. Crystal sizes of 250 and 500 nm were exhibited by the ZSM-11 and USY catalysts, respectively. The H_2TPR-MS method was used to determine the fraction of reduced Ni of each sample *in-situ*. The hydrogenation reaction was performed in a packed-bed reactor under vacuum under conventional heating and plasma-assisted conditions. The activity of each sample was found to be influenced by the amount of reduced nickel on the catalyst. The reaction was also performed under two different plasma-catalytic configurations at different volumetric flows: In-plasma catalysis (IPC) and Post-plasma catalysis (PPC), with IPC presenting the highest activity. The results were found to be influenced by the residence time of the gas in plasma. An unreported phenomenon was verified while performing the IPC reaction. The plasma induced enhancement of the catalyst adsorption capacity, resulting on methane storage during plasma activity and its release upon plasma's extinction. This occurrence was evidenced by IR measurements that were performed on Ni-based USY, ZSM-11, SiO_2 and Al_2O_3 catalysts.

Key words: CO_2 Methanation, Hydrogenation, Glow-Discharge Plasma, Zeolite Catalysts

This page was intentionally left blank.

Resumo

Catalisadores de níquel em zeólitos USY e ZSM-11 foram preparados com diferentes teores de metal e através de diferentes métodos de impregnação para aplicação na reacção de hidrogenação de CO_2. A sua caracterização foi feita através da determinação da área superficial externa e interna, volume de micro- e mesoporos, cristalinidade, fracção de Ni reduzido no catalisador e analisando as imagens SEM de cada amostra. Todos os catalisadores analisados apresentaram uma cristalinidade superior a 99%. Cristais de 250 e 500 nm foram observados para os zeólitos ZSM-11 e USY, respectivamente. Foi usado o método H_2TPR-MS para determinação *in-situ* do teor de Niº à superfície de catalisador. A reacção de hidrogenação foi conduzida num reactor de leito fixo sob vácuo em condições de aquecimento tradicional e assistido por plasma. A actividade de cada amostra demonstrou ser influenciada pela quantidade de Ni reduzido no catalisador. A reacção foi também realizada sob duas diferentes configurações plasma-catalíticas: catálise em plasma (IPC) e catálise pós-plasma (PPC), com IPC apresentando mais actividade. Estes resultados demonstraram estar relacionados com o tempo de residência da mistura reaccional no plasma. Um fenómeno não reportado foi verificado durante as experiências com a configuração IPC: a melhoria da capacidade de adsorção do zeólito por acção do plasma que resultou em acumulação de metano no catalisador e na sua consequente libertação após extinção do plasma. Este fenómeno foi posteriormente estudado em ensaios de IV realizados utilizando catalisadores de Ni em USY, ZSM-11, SiO_2 e Al_2O_3.

Palavras-chave: Metanação de CO_2, Hidrogenação, Plasma Glow-Discharge, Catalisadores de Zeólitos

This page was intentionally left blank.

Table of Contents

List of Figures

List of Tables

This page was intentionally left blank.

Acronyms

AC	Alternating Current
BBU	Basic building unit
BET	Brunauer-Emmet-Teller
BJH	Barrett-Joyner-Halenda
CBU	Composite building unit
CCP	Capacity coupled plasma
CO_x	Carbon oxide
Co-Imp	Co-Impregnation
DBD	Dielectric barrier discharge
DME	Dimethyl-Ether
ECR	Electron cyclotron resonation
FAU	Faujasite
FTIR	Fourier-Transform Infrared
GHG	Greenhouse gas
H_2TPR-MS	Hydrogen Temperature-Programmed Reduction – Mass Spectroscopy
ICP	Inductively coupled plasma
IE	Ion Exchange
Imp	Impregnation
IPC	In-plasma catalysys
IR	Infrared
IWI	Incipient wetness impregnation
MEL	Mobil Eleven
MS	Mass spectroscopy
NTP	Non-thermal plasma
PPC	Post-plasma catalysis
PtF	Power-to-Fuels
PtG	Power-to-Gas
PtL	Power-to-Liquids
RF	Radio frequency
rME	Reverse microemulsion
RWGS	Reverse water-gas shift
SEM	Scanning electron microscope
SNG	Synthetic natural gas
TPR-MS	Temperature-programmed reduction – Mass spectroscopy
USY	Ultrastable zeolite Y
XRD	X-Ray diffraction
ZSM-11	Zeolite Socony Mobil #11

This page was intentionally left blank.

List of Symbols

$\%Ni$	Nickel load (%)
A	Area (A.s)
a	Experimental parameter
A_s	Section area (m^2)
b	Experimental parameter related to the adsorption of an adsorbate in a material
C	Adimensional constant
$C_{balance}$	Carbon balance (%)
$C_{baseline}$	Concentration obtained with the baseline intensity (ppm)
C_{CH4}	CH_4 concentration (ppm)
C'_{CH4}	Corrected CH_4 concentration (ppm)
CH_x*	Methyl radicals
$CO*$	CO radical
CO_2Conv	CO_2 conversion (%)
$CO2_{in}$	Amount of CO_2 at the inlet (mL/min)
CO_{2out}	Amount of CO_2 at the outlet (mL/min)
d	Spacing between diffraction plans
E_a	Activation energy (kJ/mol)
$F_{initial}$	Initial flow (mL/min)
H	Height of the catalyst bed (m)
H_2/Air	Hydrogen to air molar ratio
I	Ion current intensity (A)
i	Product I
I'	Corrected ion current intensity (A)
$I_{baseline}$	Baseline ion current intensity (A)
$I_{initial}$	Initial ion current intensity (A)
$I'i_{initial}$	Corrected initial ion current intensity (A)
$i_{produced}$	Produced amount of a product i (mL/min)
m	Sample mass (g)
m_{Ni}	Nickel mass (g)
M_{Ni}	Molecular weight of Ni (g/mol)
$m_{Ni(NO3)2.6H2O}$	$Ni(NO_3)_2.6H_2O$ mass (g/mol)
$M_{Ni(NO3)2.6H2O}$	Molecular weight $Ni(NO_3)_2.6H_2O$ (g/mol)
$mol\%$	Molar percentage
m_{USY}	USY mass (g)
m/z	Mass to charge ratio
n	Gas quantity (mol)
N_a	Avogadro's number
n_{Air}	Quantity of air (mol)

n_C	Quantity of C (mol)
n_{Cin}	Quantity of C at the inlet (mol)
n_{CO}	Quantity of CO (mol)
$n_{CO2consumed}$	Quantity of CO_2 consumed (mol)
n_{Cout}	Quantity of C at the outlet (mol)
n_{H2}	Quantity of H_2 (mol)
$n_{H2consumed}$	Quantity of H_2 consumed (mol)
Ni^*	Total unreduced Ni amount (mol)
$Ni^{2+}{}_{max}$	Maximum limit of Ni^{2+} (mol)
Ni^o	Metallic nickel (mol)
$Ni^o{}_{frac}$	Fraction of reduced Ni (%)
$Ni_{reduced}$	Reduced nickel amount (mol)
Ni_{total}	Total amount of nickel (mol)
n_{Ni^o}	Quantity of Ni^o (mol)
O^*	Oxygen radical
p	Pressure (atm or Torr)
$p.d$	Pressure multplied by distance between electrodes
P	Parcial pressure of the adsorbate vapor at the working temperature (Pa)
P_0	Standard pressure (Torr)
P^*	Saturation pressure of the adsorbate. (Pa)
P_r	Pressure of the reactor (Torr)
Q_0	Volumetric flow at standard conditions (mL/min)
Q_r	Volumetric flow at the reactor conditions (mL/min)
R	Gas constant ($L.atm.K^{-1}.mol^{-1}$)
S	Specific surface area (m^2/g)
S_i	Selectivity towards the product *i*
T	Temperature (ºC or K); Si or Al atom in a BBU
T_0	Standard temperature (K)
T_r	Temperature of the reactor (K)
$t_{res\ plasma}$	Residence time in plasma (ms)
u	Spatial velocity (m.s)
V_a	Adsorbed gas volume at STP conditions. (mL)
V_B	Breakdown voltage (V)
V_{cat}	Catalyst volume (cm^3)
V_m	Adsorbed gas volume necessary to the monolayer formation at STP conditions. (mL)
vol.%	Volumetric percentage
V_{plasma}	Plasma volume (cm^3)
$V_{reactor}$	Reactor volume (cm^3)
$V_{unit\ cell}$	Unit cell volume ($Å^3$)
wt.%	Weight percentage

Y_i	Yield towards a product *i*
ΔH	Variation of enthalpy (kJ/mol)
ΔG_f^o	Standard Gibbs free energy (kJ/mol)
ΔP	Pressure drop (Torr)
ε	Packed-bed porosity
λ	Wavelenght (cm^{-1})
θ	X-Ray diffraction angle (º)
μ	Viscosity (Pa.s)
ρf	Specific mas of the fluid (kg/m^3)

This page was intentionally left blank.

1. Introduction

1.1. Contextualization of the CO_2 hydrogenation subject

Since the end of the industrial revolution, after the XIX century, the energetic needs across the world have been increasing [1]. Due to this augmentation, and the consequent growth of the fuel prices, the interest about renewable energy sources has been rising, in particular since the end of 2004 [2]. Nevertheless, these kinds of energy sources are still not as reliable as resources like fossil fuels such as petroleum or coal [3] due to disadvantages such as: high development costs, unavailability in certain areas, inability of large quantity production or difficulty in energy storage.

Consequences of the use of fossil fuels to this extent include the release of abnormal quantities of carbon dioxide as well as of other pollutants such as sulfur, carbon and nitrogen oxides, contributing to air, land and water pollution. A very well-known consequence of these emissions is the greenhouse effect which contributes to the global warming phenomenon [4]. Water and methane also contribute to the greenhouse effect. However, the water in the atmosphere does not accumulate as other gases. Whenever its concentration reaches certain levels it causes rain and its consequent atmosphere concentration decrease. Methane is a dangerous gas which is also considered as heat-trapping, however its concentration in atmosphere is far from the one of CO_2, thus justifying more attention being paid to the latter.

Attending to this information, it is important to research and develop technologies that allow us to efficiently produce energy from clean and preferably renewable sources.

Discovered in the 1910s, the Sabatier reaction allows the conversion of carbon dioxide to methane [5], thus consuming an unwanted product of a great variety of processes in order to produce a valuable fuel. This reaction also requires Hydrogen, which can be produced by the electrolysis of water through environmental clean processes.

Several kinds of catalysts have been developed and tested for this reaction, most of them containing Nickel as it has a fairly low cost [6, 7]. The possibility of combining the application of a catalyst with non-thermal plasma (NTP) technology seems to be very interesting from the industrial point of view. Through this method, higher yields of methane production can be achieved at the expense of less heating power, rendering it a good alternative as a clean fuel source.

1.2. Main Goals

The purpose of this work is to study the influence of nickel-supported catalysts over MEL and FAU zeolites as well as over silica and alumina on the CO_2 hydrogenation reaction. The reaction was performed under partial-vacuum (≈3 mbar) in a specific temperature range within a packed-bed reactor, under conventional heating, plasma and both simultaneously.

Different configurations of plasma catalysis, in-plasma and post-plasma, were tested using the packed-bed reaction in order to increase the knowledge about the plasma-catalyst interaction and its influence on the reaction product selectivity under different reaction conditions.

In addition, an infrared study of the carbon dioxide hydrogenation reaction assisted by plasma was performed in order to obtain more information about the adsorbed species on the catalyst.

1.3. Thesis Outline

This thesis is written according with the following outline: Chapter 2 presents some general information about the major motivation of this study, some introductory basis about the subjects that were approached during this work as well as some information about the industrial applications that were or may be performed based on the CO_2 hydrogenation process. In Chapter 3 the experimental methods used throughout the reactions performance and catalyst preparations are explained. Chapter 4 is dedicated to the presentation of the results obtained and its interpretation. At last, in Chapter 5 the main conclusions that emerged from this work are presented as well as some suggestions for future work.

2. Bibliographic revision

As a consequence of the worldwide energy consumption increase, as well as the depletion of fossil fuels, much interest has been shown on the research and development of sustainable energy resources and in ways of decreasing pollutant gases emissions to the atmosphere.

The emission of carbon dioxide is one of the main contributors for greenhouse effect, hereby contributing for the aggravation of global warming.

Anthropogenic CO_2 emissions, mostly due to the electricity production, transportation and industry activity, have been increasing with the world's economy growth, Figure 1. This is especially noticeable in strongly industrialized developing countries such as China or India.

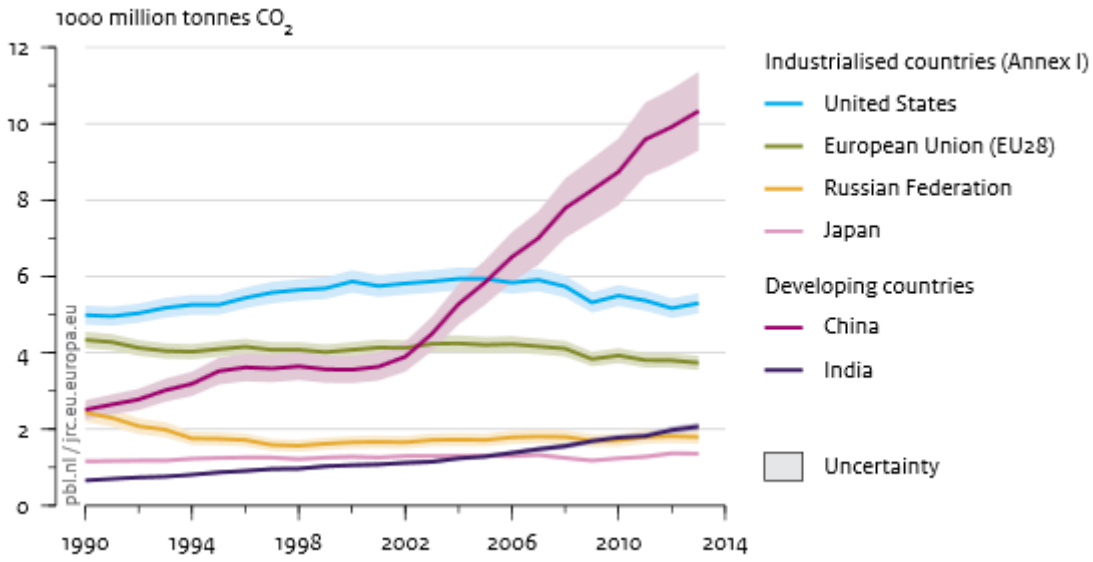

Figure 1 - CO_2 emission evolution on the most relevant industrialized and developing countries [8].

Due to human activity, especially since the beginning of the industrial revolution around 1750 the CO_2 equilibrium that would normally occur between its emission and natural conversion into other compounds has been unbalanced. This led to an uncommonly high concentration of carbon dioxide in the atmosphere which, together with the emission of other heat-trapping gases such as halocarbons, hydrocarbons and carbon sulfur and nitrogen oxides, causes noticeable climate changes. The sudden emission increase after 1750 is shown in Figure 2.

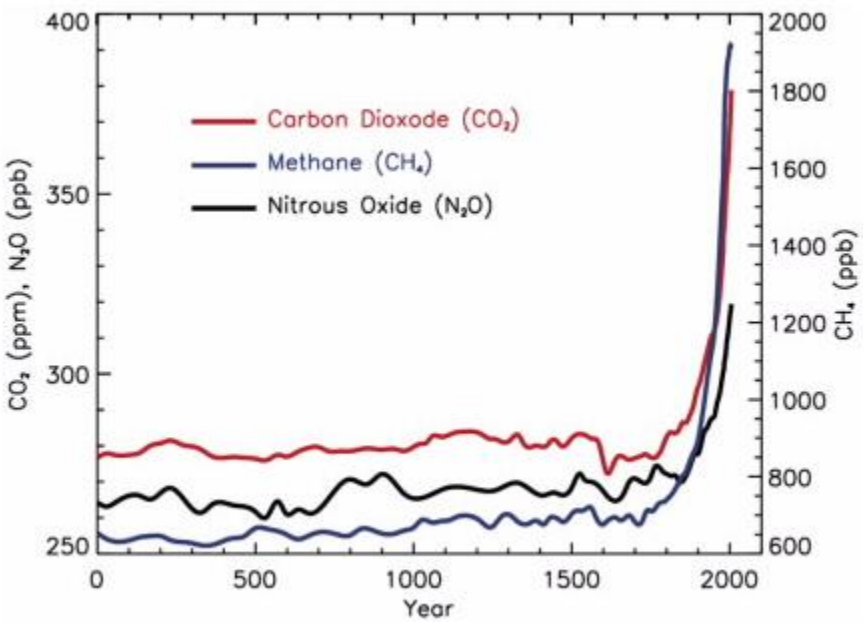

Figure 2 - GHG emission evolution since year 0 to 2000 [9].

As CO_2 is the one of the more abundant greenhouse gases in the atmosphere, and due to the awareness of its impact on the environment, in the past few decades an attempt at output reduction has been made. Methods such as the reduction of CO_2 production in industrial processes, its storage or its conversion into more valuable species, have been investigated in the past few years [10].

The conversion of CO_2 into CH_4 is possible through the Sabatier reaction [5]. This reaction has been attracting interest of the scientific community due to its possible application as a fuel.

Methane is the main component of natural gas. It is a relatively abundant gas on Earth, usually found below the ground, being easier to extract than other fuels such as petroleum. The combustion of CH_4 is described in equation 2.1. It is considered as a clean fuel since the products of its complete combustion are CO_2 and water. As a consequence of having only one atom of carbon per molecule, it is the hydrocarbon that releases less carbon upon its burning. This makes it less harmful than any other hydrocarbon combustion. Methane also has the advantage of, unlike Hydrogen, having relatively simple manipulation and storage, being easily used as a fuel in any plant with lower risks.

$$CH_4 + 2O_2 \rightarrow CO_2 + 2H_2O \quad (2.1)$$

The utilization of methane as a fuel has advantages such as reduced carbon emissions (compared with coal or oil), easy storage, transport and usage, abundance, versatility and safety (i.e. compared with H_2). These advantages may overpass disadvantages such as its toxicity, flammability, or possible difficult and expensive infrastructure development if it is necessary.

2.1. CO_2 hydrogenation reaction

According to the Sabatier reaction, it is possible to perform hydrogenation of CO_2 into methane (CO_2 methanation), hereby generating water as a by-product, in the presence of Nickel catalysts (equation 2.2).

$$CO_2 + 4\,H_2 \rightarrow CH_4 + 2H_2O \quad (2.2)$$

This is an exothermic reaction that takes place at high temperatures, optimally between 200 and 500ºC, and preferentially at atmospheric pressure or higher [7,11]. In this interval of temperatures the reaction enthalpy varies between -172.7 kJ/mol and -179.9 kJ/mol, respectively.

Simultaneously with this reaction, secondary products may be formed. Table 1 shows a list of possible reactions than can occur in the presence of CO_2 and H_2.

Table 1 - List of reactions that can take place in the presence of carbon oxides and hydrogen (adapted from [12]).

	Reaction	ΔH_{298K} (kJ/mol)	Reactions name
R1	$CO_2 + 4H_2 \rightleftarrows CH_4 + 2H_2O$	-165.0	CO_2 methanation
R2	$CO_2 + H_2 \rightleftarrows CO + H_2O$	+37.7	Reverse water-gas shift
R3	$CO + 3H_2 \rightleftarrows CH_4 + H_2O$	-206.1	CO methanation
R4	$2CO + 2H_2 \rightleftarrows CH_4 + CO_2$	+247.3	Inversed methane CO_2 reforming
R5	$2CO \rightleftarrows C + CO_2$	+172.4	Boudouard reaction
R6	$CH_4 \rightleftarrows 2H_2 + C$	+74.8	Methane cracking
R7	$CO + H_2 \rightleftarrows C + H_2O$	-131.3	CO reduction
R8	$CO_2 + 2H_2 \rightleftarrows C + 2H_2O$	-90.1	CO_2 reduction

Figure 3 shows the effect of temperature and pressure in the equilibrium conversion of CO_2. These values were obtained based on the Gibbs free energy minimization considering the compounds CO_2, CO, CH_4, H_2 and H_2O, involved in studied reactions using Aspen Plus V8.4. A flow of 20 mL/min with a molar composition of H_2/CO_2/Ar=4/1/5, like the one used throughout this study, was used in the inlet stream to the Gibbs reactor.

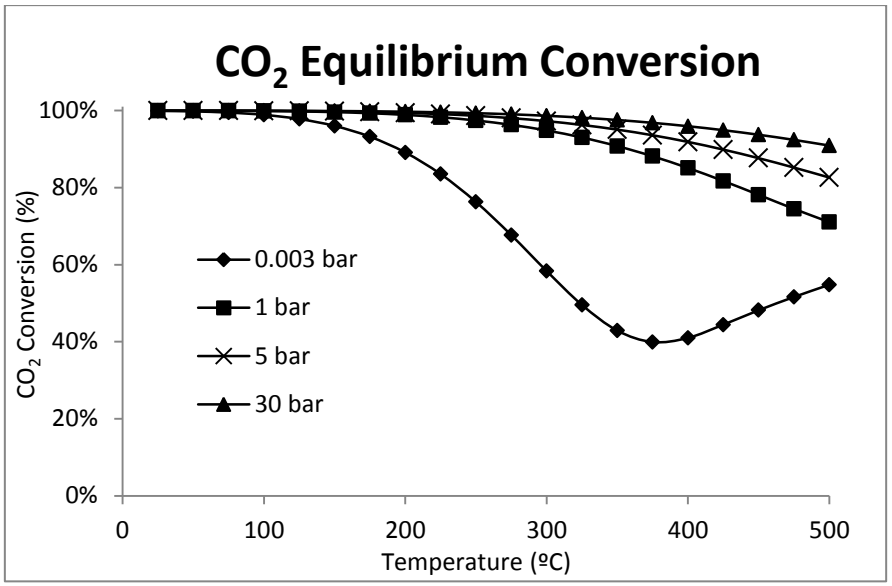

Figure 3 – Equilibrium conversion of CO_2 at different temperatures and pressure.

The thermodynamic analysis gives important information such as: type of thermodynamically stable products that may be expected, if the reaction is endo- or exothermical, or the effect parameters such as temperature, pressure and inlet ratio of the reactants. This information is useful to understand the thermodynamic limits/allowances of each reaction and, hereby, provide guidance in the catalyst development or enhancement.

Figure 3 reveals that, the conversion of carbon dioxide is thermodynamically favored at low temperatures, due to its exothermicity, and by high pressures as the hydrogenation of CO_2 is a volume reducing reaction. The H_2/CO_2 ratio used in the reaction also has an important role in these results. Gao *et Al.* reports that the hydrogenation, as well as the selectivity towards CH_4 is improved by the increase of hydrogen in the mixture. However, above a H_2/CO_2 = 6 molar ratio this increase loses significance. As CO_2 is a very stable molecule due to its double C=O bonds ($\Delta G_f^o{}_{CO2(g)}$ = -394.4 kJ/mol), by adding a higher Gibbs free energy reactant such as H_2 ($\Delta G_f^o{}_{H2(g)}$ = 0 kJ/mol), the equilibrium conversion becomes easier [13].

Despite of being thermodynamically favorable and having considerably high equilibrium conversions in this temperature range, this reaction requires a catalyst and some heating (≈200ºC) in order to take place. Due to the great stability of the CO_2 molecule high activation energy is necessary to start the reaction. Catalysts have been developed in order to overcome this barrier. In Appendix A1 are presented the basics of catalysis.

Some of the most used catalysts in the formation of methane according with Reaction R1 from Table 1 include Nickel and Ruthenium [14] based catalysts, since these metals have high selectivity towards methane. They activate the H_2 by its dissociative adsorption on the reduced metal particles surface. In general, metals of the group VIII, IX, X and XI transition metals can be used in the hydrogenation of CO_2. The incompletely filled *d*-orbitals of transition metals provide an easy electron exchange between the metal particles and the molecules. It has been reported [15] that the more active metals in CO_x methanation catalysis in decreasing activity order are Ru, Rh, Ir, Ni and Co.

Nickel is the preferred metal due to the relatively low cost comparing with ruthenium, rhodium or iridium.

Concerning the catalyst support, silica (SiO_2) [16], alumina (Al_2O_3) [6] and zeolites [11] are typically used. Recently, the application of zeolite based catalyst has been studied because of their good thermal stability [11], especially ultrastable zeolites such as USY. The CO_2 is adsorbed in these zeolites which, by bonding with it lower the activation energy to convert the CO_2 causing its activation.

The possibility of taking advantage of the CO_2 generated through the most varied processes to produce a valuable energy carrier as methane, which is environmental cleaner than most of the actually used fuels looks very attractive from the industrial and environmental point of view. The methanation of CO_2 can also be implemented together with CO_2 capture and storage processes in order to achieve even better results.

In Table 2 a list of some of the catalysts studied in the literature and the main results that were achieved are summarized.

The hydrogenation of CO_2 can also be carried according with the RWGS reaction (R2). This reaction is also of some interest since it allows the conversion of carbon dioxide to CO and water and can be applied to the synthesis of hydrocarbons such as methane or methanol. It can also be applied to the manufacture of higher hydrocarbons like ethylene and propylene by the Fischer-Tropsch reaction. High temperatures are necessary for carrying out this reaction since it is an endothermic (see Table 1) [77-79]. Catalysts for this reaction often include the use of noble metals as Pt or Cu in transition oxides [80]. However, like in the CO_2 methanation Ni can also be used [61].

As it is carried out with the same reactants as the R1 reaction, R1 and R2 are considered concurrent reactions.

Table 2 - Catalysts studied in the CO_2 methanation reaction and their results for the optimal conditions.

Catalyst	Preparation	Optimal conditions	H_2:CO_2 Ratio	Space velocity (h^{-1})	CO_{2Conv} (%)	CH_4 Selectivity (%)	CH_4 Yield (%)	Ref.
5%NiUSY	Imp	400 (ºC); Atm. pressure	4:1	43000	24.7	61.4	15.2	[17]
4%Ni3%CeUSY	Imp			43000	37.7	72.1	27.2	
4%Ni7%CeUSY	Imp			43000	44.3	75.5	33.4	
5%Ni15%CeUSY	Imp			43000	55	86.2	47.4	
10%NiUSY	Imp			43000	47.9	78.8	37.7	
8%Ni7%CeUSY	Imp			43000	51.7	85.6	44.3	
14%NiUSY	Imp			43000	65.5	94.2	61.7	
14%Ni7%CeUSY	Imp			43000	68.3	95.1	65.0	
CZ	Imp	400 (ºC); Atm. pressure	4:1	43000	0	-	-	[18]
5%Ni/CZ	Imp			43000	75	97	72.8	
10%Ni/CZ	Imp			43000	85	99	84.2	
15%Ni/CZ	Imp			43000	85	99	84.2	
Ru/CE	Imp	400 (ºC); Atm. pressure	4:1	10000	90	100	90	[19]
Ru/60CEAL	Imp			10000	90	100	90	
Ru/30CEAL	Imp			10000	90	100	90	
Ru/AL	Imp			10000	80	100	80	
10%Ni/Al_2O_3	Imp	350 (ºC); Atm. pressure	3:1	6000	70	95	66.5	[7]
15%Ni/Al_2O_3	Imp			6000	70	100	70	
20%Ni/Al_2O_3	Imp			6000	75	100	75	
25%Ni/Al_2O_3	Imp			6000	77	100	77	
1%Ni/MSN	Imp	400 (ºC); Atm. pressure	4:1	69105	11	100	11	[10]
3%Ni/MSN	Imp			69105	29	100	29	
5%Ni/MSN	Imp			69105	82	99.9	82	
10%Ni/MSN	Imp			69105	85	100	85	
Ni/Si	Co-Imp	400 (ºC); Atm. pressure	4:1	15000	73.2	98.7	72.2	[20]
Ni/Mg	Co-Imp			15000	38.9	9	3.5	
Ni/Si + Ni/Mg	Co-Imp			15000	66.5	96.8	64.4	
5%NiUSY	IWI	450 (ºC); -	4:1	43000	50	60	30.0	[21]
14%NiUSY	IWI			43000	70	95	66.5	
15%Ni/Al_2O_3	Imp	300 (ºC); Atm. pressure	4:1	15000	45	99	44.55	[22]
15%Ni-2%CeO_3/Al_2O_3	Imp			15000	71	99	70.29	

Pd/SiO_2	rME	450 (ºC); Atm. pressure	4:1	6000	40.8	10.4	4.3	[16]
Pd/SiO_2	Imp			6000	40.6	6.5	2.6	
Mg/SiO_2	rME			6000	0.8	10.3	0.1	
$Pd\text{-}Mg/SiO_2$	rME			6000	59.2	95.3	56.4	
$Mg/Pd/SiO_2$	Imp			6000	40	76.2	30.4	
$Pd\text{-}Fe/SiO_2$	rME			6000	44.7	2.8	1.3	
$Pd\text{-}Ni/SiO_2$	rME			6000	50.5	89	44.9	
Ni/SiO_2	rME			6000	36.8	81.8	30.1	
$Pd\text{-}Li/SiO_2$	rME			6000	42.6	88.5	37.7	
$4.29\%Ni/RHA\text{-}Al_2O_3$	IE	500 (ºC); Atm. pressure	4:1	48000	34	56	19.0	[23]
$4.09\%Ni/SiO_2$-gel	IE			48000	25	45	11.3	
$10\%Ni/A_{l2}O_3$	Imp	500 (ºC); 0.1 MPa	4:1	10000	20	25	<5	[24]
10%Ni/CTO	Imp	400 (ºC); 0.1 MPa	4:1	10000	75	100	75	

Note: Imp – Impregnation; IWI – Incipient wetness impregnation; Co-Imp – Co-Impregnation; rME – Reverse microemulsion; IE – Ion Exchange.

2.2. Catalytic processes industrial significance

Catalysts play a very important role in the modernization of the worldwide chemical industry. They allow a more efficient use of resources and can be used to treat effluents, contributing to the prevention of pollution and to turn the industry safer.

In the past century, catalysis turned out to be one of the most important fields in large-scale processes such as petrochemistry or bulk chemicals production. The recent evolution of the chemical industry demands has launched catalytic technology into new grounds. Lately, catalysis has been applied in the most varied fields, including smaller systems as batteries or fuel cells.

Nowadays, catalysts have high influence the chemical and energy industry, as well as environmental protection and sustainability. It is estimated that around 90% of the worldwide chemical processes involve catalysis at some point of their production process [25].

In the future it is highly expected that catalysis will play a key role, not only in the industrial development, but in the whole society. A good part of the catalytic processes are marked by its complexity and difficult of behavior prediction. One of the future challenges of catalysis will be the unravelling of their underlying complexity in order to improve their design. In the next decades more attention is going to be paid to the catalytic enhancement of efficiency in industrial processes. Due to the fossil fuel, as well as other natural resources, depletion it is important to find alternative ways of energy production keeping in mind the limits of environmental stamina.

Some of the areas that are predicted to play major roles in a near future are:

- Nanostructured heterogeneous catalysis. Including topics such as precise catalyst synthesis, further understanding of structure and environment impact on catalytic behavior and the development of catalytic devices.
- Molecular catalytic systems. By integrating multiple processes and development of complex and responsive adaptive catalysts.
- New catalytic conversions with atom efficiency such as CO_2 capture and conversion or electrochemistry for energy supply. This area may also be applied to liquid fuels and bulk chemical production.

2.3. Zeolites in catalysis

Zeolites are microporous aluminosilicate materials which result from the tridimensional union of tetrahedral TO_4, being T an atom of Si or Al and O an oxygen atom.

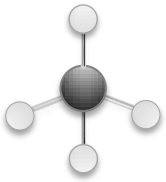

Figure 4 - Tetrahedral molecule (TO_4). Basic building unit (BBU) of a zeolite.

Due to their properties, zeolites have a very large application in the industry, being specially known for their utilization as adsorbents or as catalyst supports. Other known applications are such as ion exchange, as molecular sieves and wastewater treatments.

The general formula of zeolites can be expressed by the empirical formula:

$$M_{x/n}.(AlO_2)_x.(SiO_2)_y.mH_2O$$

being *n* the valence of the cation *M* and *m* the amount of water present in the voids of the zeolite.

The framework structure (Figure 6) of a zeolite consists in the infinite repetition the composite building units (CBUs) (Figure 5), which are structures obtained by the tridimensional connected arrangement of SiO_4 and AlO_4^- tetrahedrons, called basic building units (BBUs) (**Erro! Auto-referência de marcador inválida.**).

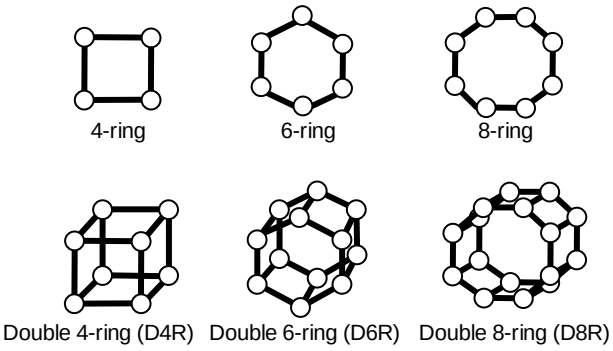

Figure 5 – Examples of composite building units (CBUs).

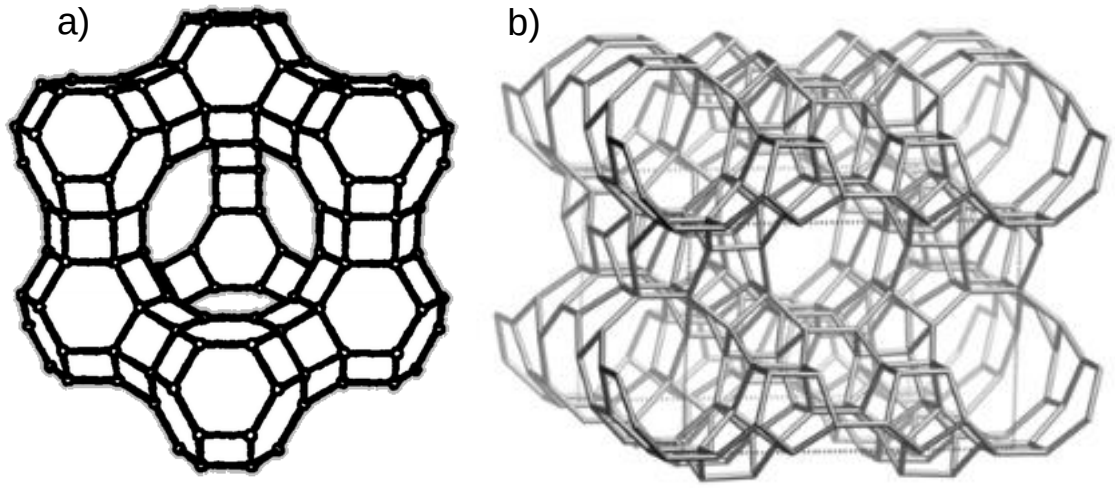

Figure 6 - Examples of zeolites frameworks: a)FAU b)MEL[26].

Each AlO_4 tetrahedron in the zeolite framework introduces a negative charge to it, which is neutralized by the presence of extra-framework cations such as Na^+, Ca^{2+} or Mg^{2+}. The presence of these cations does not affect the framework of the zeolite and they are mobile inside the structure, usually suffering ion exchange.

By looking into the tridimensional arrangement of the CBUs of the zeolite, based on their framework, we can identify different kinds of pores, cavities, channels, cages and supercages. Figure 7 shows examples of supercages (α-cages), sodalite cages (β-cages) and pores of FAU zeolite. Pores are the *n*-sized rings, with *n* equal to the number of T atoms in the ring that define the face of the polyhedral CBUs. If these polyhedral are smaller than six-rings they are called cages. They are small enough to block the passage of any molecule larger than H_2O. If the polyhedral have at least one face with a ring larger than a six-ring they are called cavities. Pores that are large enough to allow the passage of guest species (larger than six-rings) and extend infinitely in one dimension are called cannels. A framework can contain channels in one, two or three dimensions.

By knowing the framework of the zeolite it is possible to estimate which molecules can be adsorbed in it based on their sizes.

The zeolite structure includes the framework Si and Al atoms and the extra-framework cations.

So far, 229 zeolite frameworks have been identified [27], being it natural or synthetized. Each framework results from a different arrangement of the BBUs of the zeolite and has an impact on its properties, such as cation concentration, thermal stability and ion exchange selectivity.

In this work two kinds of zeolite were used:

- Faujasite (FAU) zeolites with a general formula of $M_{x/m}^{m+}Al_xSi_{192-x}O_{384}yH_2O$ [82]. These zeolites present a tridimensional pore structure made of 4,6 and 6-6 composite building units [81]. Two kinds of cavities are found within this structure. The supercages which have a diameter of 1.3 nm and are connected to sodalite cages with 0.65 nm of diameter by 4 dodecagonal windows (0.75 nm) in a tetrahedral arrangement.
- Mobil Eleven (MEL) zeolites with a general formula of $M_{x/m}^{m+}Al_xSi_{96-x}O_{192}$. This structure reveals straight channels which are intercepted by perpendicular channels (which are also straight). These channels are approximately circular with a diameter of 0.53 nm [82].

Recently it has been reported [28] that zeolite based catalysts may be used in plasma-catalytic systems in order to enhance CO and CO_2 methanation reaction. Plasma influences both catalyst and reactants and greatly improves the conversion of carbon oxides.

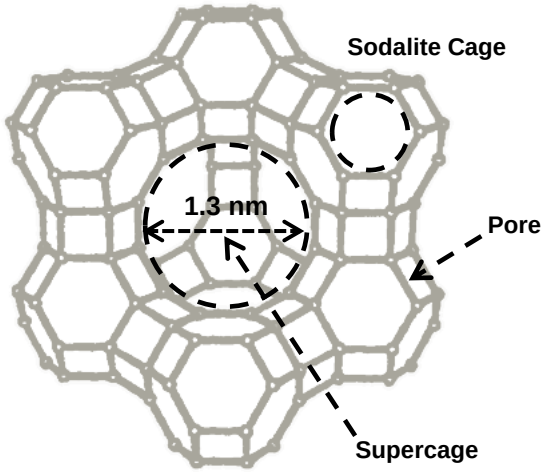

Figure 7 - Examples of cages, supercages and pores in FAU zeolite.

2.4. Plasma

Plasma is one of the four fundamental states of matter, along with gas, liquid and solid. Like gas, plasma does not have a fixed shape or volume. It consists in an electrically neutral medium of unbound charged particles. Overall, the number of positive charged particles should be paired with the negative charged. As these particles move they generate electric current with magnetic fields, thus affecting all the nearby particles, creating a very complex collective behavior. Unlike gas, in which there is only one independent-acting kind of specie, in plasma there is more than one kind of particles

interacting with each other. Based on the particle charge and its value different behaviors are obtained.

Ionization of particles is necessary to create plasma. Practically, this can be done by heating a gas or applying a strong electromagnetic field on it. This will ionize the gas particles and break existing molecular bonds.


<

Figure 8 - Plasma generation across a packed-bed reactor.

Plasma can be classified in different types depending on the way it is generated and on its properties. Some of the more known examples of industrial or commercial plasma are summed in Table 3 along with their main characteristics and applications.

Non-thermal plasma (NTP) is any kind of plasma that is not in thermal equilibrium. This term is applied whenever the temperature of the heavy particles in the plasma is not as high as the one from the electrons. In the NTP case, also called cold-plasma, it is estimated that the neutral particles have temperatures near ambient while the electrons that result from the partial ionization of the gas can reach temperatures of thousands of Celsius degrees. Usually in this type of plasma only a small fraction of the particles are ionized.

The application of this kind of plasma in chemical processes such as chemical synthesis, material fabrication, food processing and treatment of pollutants has been recently focus of study [29], [30]. It has additionally been reported by E. Jwa *et Al* [28] that non-thermal plasma-assisted catalytic hydrogenation of carbon oxides improves from CO_x conversion values lower than 15% at 180-260ºC to values near 90% in the same temperature range.

Table 3 - Types of plasma and its applications.

	Plasma type	Description	Applications
Low pressure	Glow-discharge plasma	Non-thermal plasma (NTP) generated by the application of direct current or low frequency electric field between two electrodes.	Fluorescent light tubes.
	Capacity coupled plasma (CCP)	Similar to glow-discharge, but generated with high frequency RF electric fields (≈13.56 MHz).	Microfabrication and integrated circuit manufacturing industry; plasma enhanced chemical vapor decomposition.
	Cascade arc plasma	High density NTP produced by a wall-stabilized thermal electric arc discharge.	Wastewater treatment.
	Inductively coupled plasma (ICP)	Similar to CCP with the electrode consisting in a coil wrapped around the chamber where plasma is created.	Metal content analysis in alimentary industry.
	Wave heated plasma	Microwave generated low-pressure discharge such as helicon discharge or electron cyclotron resonance (ECR).	Fusion research purposes.
Atmospheric pressure	Arc discharge	High power thermal discharge (≈10000K) that can be generated with different kinds of power supply.	Metallurgical processes.
	Corona discharge	NTP discharge generated by applying high voltage to sharp electrode tips.	Ozone generators; Particle precipitators.
	Dielectric barrier discharge (DBD)	NTP discharge generated by applying high voltages across small gaps coated with non-conducted material.	Web treatment of fabrics.
	Capacitive discharge	NTP generated by application of RF power (≈13.56 MHz) to one powered electrode with a grounded electrode held at a distance of approximately 1 cm.	Electronic technology industry.
	Piezoelectric direct discharge plasma	NTP generated on the high-side of a piezoelectric transformer.	Ozone generators; Medical technology.

2.5. Plasma-assisted catalysis

Since the last two decades of the 20th century, plasma-chemical and plasma-catalytic processes using low temperature plasma have been of interest of the scientific community [29].

Non-thermal plasma offers a unique way of initiating and enhancing the performance of chemical reactions. However, due to the non-selective nature of plasma processes, the addition of a catalyst may be implemented in order to increase conversion of reactants, selectivity towards desired products and, therefore, the process yield.

The types of plasma which are used in plasma-catalytic systems are glow-discharges, when the reactions are carried out under partial-vacuum and dielectric barrier discharges for atmospheric or higher pressures.

In plasma-catalytic processes, just like in the regular catalytic cases, the catalyst can be used in different forms such as pellets, foam, layers or coating.

In general, plasma catalysis can be divided into two distinct groups based on the configuration of the system:

- In-plasma catalysis (IPC): The plasma contacts with the catalyst, partially or totally, in one single step;
- Post-Plasma Catalysis (PPC): The plasma and catalysis steps can happen under independent conditions and the plasma step is usually done upstream the catalytic reactor.

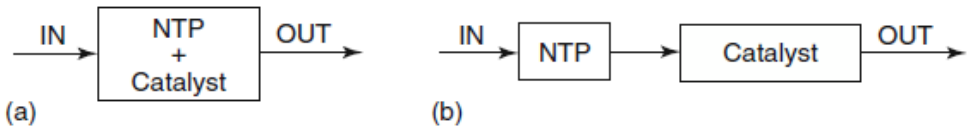

Figure 9 - Different kinds of plasma-catalysis configurations [29].

In the IPC configuration, Figure 9(a), plasma is generated across the catalytic bed, being in contact with reactants and catalyst as well as products of the reaction. This creates a great variety of active species that interact with each other and with the catalyst. The electric current that is applied to create the plasma also interacts with the catalyst.

On the other hand, in the PPC configuration, Figure 9(b), plasma can be created before the catalytic step, as the plasma is used for the purpose of creating chemically active species that can be sent to the catalyst afterwards in order to improve the catalytic activity. With this configuration the contact between the catalyst and short-living active species is avoided as well as the contact with plasma itself, which can affect the surface of the zeolite [29] and therefore change properties such as: adsorption capacity [31, 32], active sites [33], stability or activity [34]. Another characteristic of this configuration is that plasma processes are by nature non-selective, therefore, by having a catalytic step downstream the plasma step can combine both reactant conversion provided by plasma and high selectivity inherent to catalyst utilization. Its purpose is solely to modify the composition of the inlet stream to the catalyst bed, making can be more reactive.

The interaction of the plasma discharge with the catalytic bed results in many phenomena. It is known that, due to the high electric field within the packed-bed, microdischarges tend to happen between the voids of the catalyst particles. These microdischarges are favored by the existence of sharp-edged pellets and are more frequent in small are particles [36].

It has been reported that plasma treated catalysts may have their properties enhanced. Meng Guo *et Al.* verified that plasma treatment of the catalyst results in the enhancement of the dispersion of active components [34, 36]. It has been reported in [34] that improvements are also verified in the catalytic stability and activity as plasma activity prevents the catalyst from poisoning due to

enhancement of specific species' desorption [37-39] and sintering by decreasing the reaction temperature when plasma is used . Besides, the specific surface area of the sample can be increased after prolonged plasma activity, as it causes changes in the structure of the zeolite [34]. Overall, all these effects of plasma-catalyst interaction tend to increase its performance.

Due to the elastic and inelastic collisions between electrons and molecules, as well as vibrational-translational energy relaxation processes that occur during NTP activity the temperature of the gas increases which results in a heating of the catalyst surface. This temperature increase which was found in [40] to be dependent on the energy density of the medium, usually is not high enough to the thermal activation. However, the localized heating that may occur inside the catalytic packed-bed due to electric microdischarges (hot-spots) [29] is very likely to provide temperatures high enough to stimulate catalytic activity. This factor should not be neglected in plasma-catalytic studies. The energy density is given by the ratio between the input power and the flow rate.

Plasma-catalyst contact, due to a combination of factors already referred such as: enhancement of the electric field of the material [40], temperature increase, structure modification of the zeolite and dissociation and ionization of molecules, also influences the adsorption-desorption equilibrium of the existing species in the zeolites. This effect has particular significance whenever the IPC configuration is used once that the more adsorption occurs, more time inside the reactor is spent by the reactants, which means more conversion. Then, depending on the plasma-catalyst interaction outcome on the equilibrium, different results may be obtained. On the other hand NTP utilization can also promote desorption of reaction products, preventing the poisoning of the catalyst, maintaining catalytic activity.

The activation of the catalyst obtained by influence of NTP is different to the one obtained by classical heating. NTP creates a great variety of active species such as electrons, ions and radicals which interact between each other through mechanisms that are still not fully understood [29]. In order to comprehend it better detailed study in the plasma-catalysis topic is necessary.

But the influence of the NTP in plasma-catalysis does not rely merely in plasma-catalyst interaction. The interaction between plasma and the species in the gas phase also play a very important role in the reaction. As in PPC the plasma affected zone does not extend until the catalytic bed, this kind of interaction assumes a greater importance in the IPC reactions. Plasma contact with the gaseous stream forms a variety of short-living active species which are more reactive than the original ones. While the conventional non-plasma assisted catalytic reactions tend to happen according with the Langmuir-Hinshelwood model, Figure 10a), that is, the reaction happens between two species that are adsorbed in the catalyst, when these reactive species successfully reach the catalytic bed there is a chance that the mechanism changes. There in the possibility that these species may react with adsorbed reactants while being in the gas phase, following an Eley-Rideal mechanism path, Figure 10b). This possibility is even higher in IPC systems. Not only the gas-phase molecules can be excited at nearest distances to the catalyst surface but also the adsorbed species can become more active due to plasma excitation.

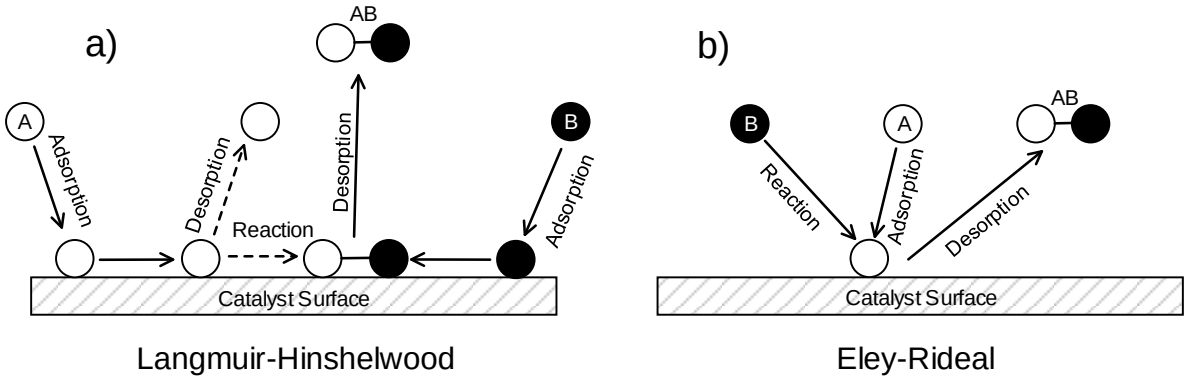

Figure 10 - Schematizations of: a) Langmuir-Hinshelwood and b) Eley-Rideal mechanisms.

In [28] it is reported that plasma-assisted CO_x conversion into methane reveals great improvements in comparison to the conventional heating reaction. A CO_2 conversion of ≈100% at 260ºC was accomplished under plasma while under conventional heating its value was under 15%.

2.6. Industrial application of the CO_2 hydrogenation reaction

The industrial hydrogenation of CO_2 can be performed aiming the creation of diverse products. A great majority of these applications is in the production of fuels. CO_2 can be reduced into CO by the reverse water-gas shift (RWGS) reaction for synthesis gas (syngas) chemistry purposes, competing with fossil fuels (coal and natural gas) based processes. The hydrogenation reaction can also be applied in order to obtain methane (synthetic natural gas or SNG) through the Sabatier reaction, formic acid, which can be used in fuel cells or in methanol synthesis which can be used in DME or biodiesel production.

Large scale conversion of CO_2 into valuable fuels can be, nowadays, achieved through the Power-to-Fuel (PtF) technology. This latter aims the production of synthetic fuels at the expense of CO_2, water and electric energy achieved by renewable sources. The usage of wind or solar power allows overcoming big disadvantages associated with this kind of sources by storing the energy produced outside the power grids, being possible to take advantage of the peak production hours of these kind of energy which, usually, are periods of the day where the energy consumption drops significantly. Besides that, there is still the advantage of producing clean energy [41].

The PtF concept can be divided in two kinds of processes: Power-to-Gas (PtG) and Power-to-Liquids (PtL) according with the kind of product that is desired.

At the moment PtF only pilot-scale plants have been implemented in Germany [42] and Iceland [43].

2.6.1. Power-to-Gas

The PtG technological concept aims the conversion of CO_2 and electric power into a valuable gaseous energy carrier such as H_2 or CH_4. Its first step is the high temperature electrolysis of water, which is preferentially performed using renewable energy sources for a more environmental friendly fuel production. The second step, that despite being optional is highly advised, is the conversion of CO_2 to CH_4 using the H_2 that was produced in the previous step [44] and the separation of the wanted product CH_4 from the water. The main advantage on the application of the methanation step is the reduction of costs and risks of Hydrogen manipulation, storage and usage. Figure 11 shows a simplified diagram of a PtG methane production unit.

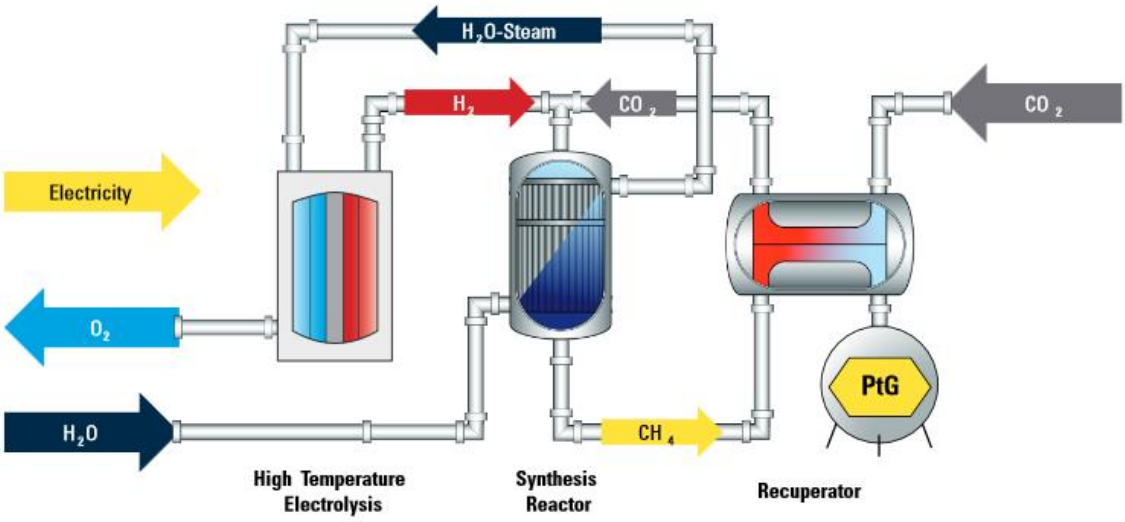

Figure 11 – Sunfire's PtG simplified process diagram for CH_4 production [44].

The produced fuel, H_2 or CH_4, can be stored and then injected in existing natural gas grids or used in transport or industry.

An efficiency of 51-65% was obtained for the electricity into methane production chain at atmospheric pressure. This value can be increased to values above 70% by the integration of the heat released during the process [45]. Efficiency values for the electricity to Hydrogen production chains are reported to be slightly better, as expected for a shorter process [46]. It was also reported a carbon rate of utilization higher than 98% and a minimum GHG mitigation potential of 85% [44].

In 2013 [42] Audi inaugurated the first industrial scale plant of production of methane based on electric energy and CO_2. This plant implemented the sunfire's Power-to-gas (PtG) technology, in which Hydrogen produced by the electrolysis of water is combined with CO_2 from a carbon source such as outlets of a woodgas generator or biogas plant in order to produce methane by the application of the Sabatier reaction or any other means. Figure 11, represents an example of a possible P2G process scheme.

2.6.2. Power-to-Liquids

In the PtL concept CO_2 and H_2 produces by H_2O electrolysis are used to produce $–CH_2–$ liquid hydrocarbons by the application of the reverse water-gas shift reaction to produce syngas which is then used to synthetize fuels with the Fischer-Tropsch [44,47]. The product stream of this process can

be then submitted to treatments such as refining and be treated as a conventional crude oil [48]. The synthetized fuels can be used in their pure form or mixed with the conventional correspondent fuels. In Figure 12 a simplified scheme of sunfire's PtL process is shown.

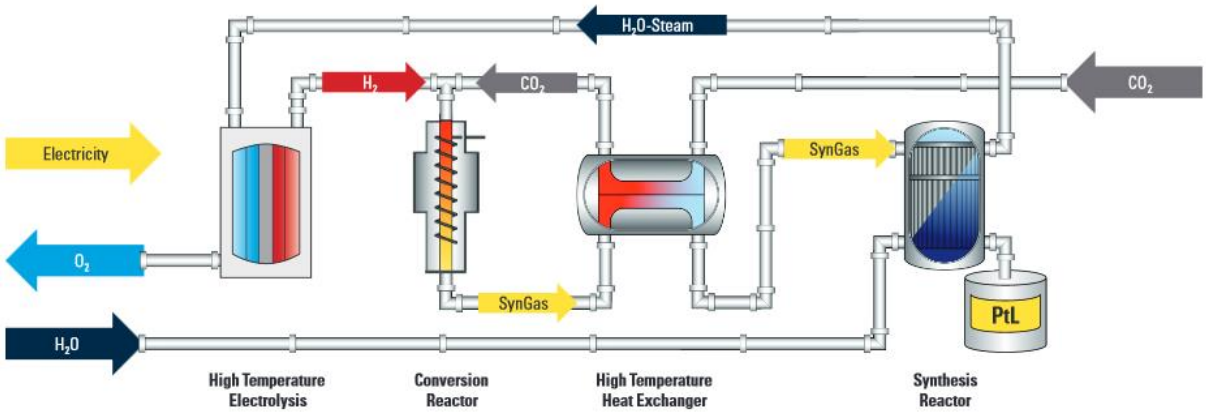

Figure 12 – Sunfire's PtL simplified process diagram[44]**.**

In November of 2014 a PtL demonstration plant, first of its kind, opened in Dresden, Germany [49]. An efficiency of ≈ 70% is achieved with a rate of carbon utilization higher than 95% and a GHG minimum mitigation potential of 85% [50].

3. Experimental

3.1. Preparation of the catalyst samples

3.1.1. Nickel impregnation

During this work the impregnation of the catalyst was performed on two Ni/USY (40) samples (each one with a different method) as well as for a sample of Ni/SiO_2. Every other catalyst sample used in this work was already previously synthetized and impregnated with the corresponding metal. The preparation of these samples consisted in the addiction of the metal, 14 wt. % of Nickel, to the chosen support, the USY(40) zeolite provided by Grace Davison (Ultrastable Zeolite Y), silica gel (ACROS Organics™, ultra-pure, 40-60μm, 40Å). The impregnation of the supports with Nickel was performed by two distinct methods, one for each sample:

- Wet impregnation method (Imp) [51];
- Incipient wetness impregnation method (IWI) [51].

The alumina and silica supported catalysts mentioned above were both prepared by the incipient wetness impregnation method.

In the first method, a solution of Nickel(II) nitrate hexahydrate is prepared and then added to the support in order to deposit the metal species on the supports surface. Then, by evaporation at 80ºC and under partial vacuum, the water present in the suspension was removed.

In this case, a solution of approximately 30 mL of $Ni(NO_3)_2.6H_2O$ (ACROS Organics™, 99%) was prepared with the necessary amount of salt in order to prepare a 14 wt.%Ni/USY(40) catalyst and added to around 4 g of zeolite. The quantities used on this method are displayed in Table 4.

Table 4 - Values used in the wet impregnation of the USY(40) sample.

	Value	Units
$M_{Ni(NO3)2.6H2O}$	290.81	g/mol
M_{Ni}	58.69	g/mol
m_{USY}	4.338	g
Target %Ni	14.0	wt.%
m_{Ni}	0.706	g
$m_{Ni(NO3)2.6H2O}$	3.498	g

After mixing it until obtaining homogeneity, the suspension was submitted to evaporation under vacuum at 80ºC in a *Buchi Rotavapor R* rotator-evaporator for approximately 3 hours, until complete water evaporation and the powder was recovered out of the walls of the rotator-evaporator recipient in order to collect the catalyst.

In the second method the impregnation the active metal (Nickel) was dissolved in an aqueous solution, under the form of $Ni(NO_3)_2.6H_2O$ with the volume corresponding to the total pore volume of the support (which was measured by BJH analysis). The solution was added to the zeolite drop by drop under agitation until it appears to be homogeneous. The quantities used in the impregnation by this method are shown in Table 5.

Table 5 - Values used in the incipient wetness impregnation of the USY(40) and SiO_2 supported samples.

	Units	USY(40)(IWI)	SiO_2
m_{USY}	g	4.344	3.001
Pore volume	cm^3/g	0.457	0.680
Total pore volume	cm^3	1.985	2.041
Solution volume	cm^3	2.0	2.0
Target %Ni	wt.%	14.0	14.0
m_{Ni}	g	0.707	0.489
$m_{Ni(NO3)2.6H2O}$	g	3.502	2.423

After the impregnation, the catalysts are calcined in order to remove volatile compounds and to make the nickel deposit in the catalyst surface.

The impregnation methods adopted for catalysts preparation are listed in Table 6.

Table 6 - Catalyst samples used and correspondent impregnation methods.

Catalyst	Impregnation method
14%Ni/USY(30)	Wet Impregnation
14%Ni/USY(40)	Wet Impregnation
14%Ni/USY(40)	Incipient Wetness Impregnation (IWI)
2.5%Ni/ZSM-11	Wet Impregnation
5%Ni/ZSM-11	Wet Impregnation
14%Ni/AL_2O_3	Incipient Wetness Impregnation (IWI)
14%Ni/SiO_2	Incipient Wetness Impregnation (IWI)

3.1.2. Catalysts Calcination

As the metal species in the catalyst, after impregnation, are present in the form of salt, it is necessary to perform calcination of each catalyst in order to remove all the volatile species in the catalyst and activate it. During this step the catalyst is submitted to a temperature of 500ºC under the flow of air or oxygen, in order to oxidize the impurities and the nickel towards NiO.

The calcination was usually performed in an oven under air. The samples were heated from room temperature until 500ºC at a heating rate of 10ºC/min. The set temperature was then held for 3 hours before cooling the oven down to room temperature.

Whenever it was necessary to calcine the catalyst under the shape of a wafer (for infrared spectroscopy measurements) the calcination was performed *in-situ* under a flow of 30mL of 79 vol.% N_2 and 21 vol.% O_2 and the outlet of the gas analyzed with the mass spectrometer.

Throughout the work all catalysts were submitted to a calcination step before each experiment.

3.1.3. Pellets and wafers preparation (Catalyst shaping)

Depending on the reactor that is used, the catalyst needs to be used in different forms. Throughout this work the catalyst samples were used under the shape of pellets of around 1 mm thickness and 3 mm of diameter in the packed-bed reactor, Figure 13 c), and circular wafers of around 18 mg of catalyst and 2 cm^2 of area, Figure 13b), for Infrared spectroscopy measurements.

The shape treatment of each catalyst (into pellets or wafers) was done in a *Specac* hydraulic press, Figure 13 a), using up to 1000 kgf of pressure per cm^2 of sample. Pressures above this value should not be used in order to avoid zeolite structural damages such as porosity and surface area diminution.

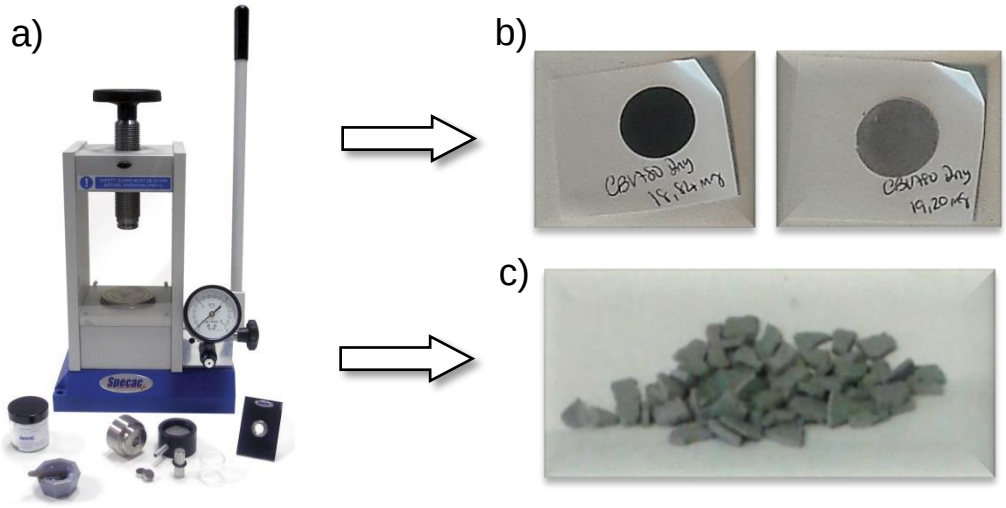

Figure 13 - a) Hydraulic press used in the preparation of: b) wafers; c) pellets.

3.1.4. Catalysts drying

Before the start of the experiments it may be necessary to dry the catalyst because of the atmospheric water that can be adsorbed over time by the contact of the catalyst with air. The water can block the active sites and/or induce deactivation – metal sintering – and as a consequence lower the catalysts activity. In order to remove this water, the drying step was performed *in-situ* (in the same system used to perform the catalytic activity tests), by heating the catalyst under inert flow (Nitrogen tends to be the most commonly used due to its low cost), at a temperature of 500ºC and pressure of approximately 1.9 Torr, during nearly 2 hours until the mass spectrometer signals are stable. The reactor is then cooled down under nitrogen flow.

3.2. Characterization of the catalysts

The basic principles of X-Ray diffraction, BET surface area and BJH pore volume and Scanning electron microscopy (SEM) analysis methods are summed in Appendix 2.

3.2.1. Verification of crystalline structure of the zeolites

The verification of the crystalline structure of the catalyst zeolite was done by X-ray diffraction in a PANalytical X'Pert PRO diffractometer with CuKα radiation (λ=0.15418 nm, 40 mA, 45 kV). The diffraction analysis of USY and ZSM-11 zeolites was performed between angles of 2θ = 5-60º and 2θ = 5-50º respectively with an increment of 0.1º and speed of 2º per min [52].

3.2.2. Determination of catalysts surface area, micro- and mesopores volume

The specific surface areas and micro and mesopores volumes of the FAU and MEL catalysts were determined by N_2 adsorption-desorption measurements at 77K using the Brunauer-Emmet-Teller (BET) method in a Micrometrics sorptometer Tri Star 3000. This analysis was performed after outgassing the samples at 200ºC overnight in order to remove the moisture adsorbed on the surface and inside the zeolites pores [52].

3.2.3. Scanning electron microscopy (SEM) of the catalysts

In order to evaluate the morphology and size of the zeolite crystals a Philips XL-30 scanning electron microscope with acceleration voltage of 30 kV was used [52].

3.2.4. Temperature-programmed reduction (H_2TPR-MS)

After calcination, the Nickel in the catalyst is present under the form of an oxide (NiO) or ion (Ni^{2+}).

In order to reduce the Nickel at the surface of the catalyst into Niº (equation 3.1) an *in-situ* reduction step is performed inside the reactor with the catalyst either in the shape of pellets or wafer. The reduction of the catalyst was performed by H_2TPR-MS (Hydrogen Temperature Programed Reduction – Mass Spectrometry), in which the gas outlet of the reactor is analyzed with a Pfeiffer Vacuum GSD 301 mass spectrometer. This procedure allows following the evolution of the hydrogen consumption during the experiment using the qualitative method of the *Quadstar* software and, thereafter, assuming the stoichiometry of equation 3.1, determines the fraction of reduced Ni on the catalyst. The reactor is heated from room temperature up to 500ºC at a rate of 10ºC/min under a 30

mL/min flow of 5% H_2, as shown in [7, 53, 54], and an inert such as Nitrogen or Argon and at a pressure of approximately 2.44 Torr.

$$NiO + H_2 \rightarrow Ni + H_2O \quad (3.1)$$

As the perfect isolation of the reactor was not possible to obtain, and being aware of the dangers of the manipulation of Hydrogen in the presence of Oxygen, some precautions were taken into account for security purposes. Some research was made in order to verify the flammability properties of the H_2/O_2 mixture and to see if the working conditions would lead to any danger. No evidence of risk was found. All the safety measures and calculations are displayed in Appendix A3.

3.3. Catalytic tests

3.3.1. Packed-bed system: Conventional heating *vs* plasma-assisted CO_2 hydrogenation

Prior to this work, the methanation reaction was studied using a wafer of about 20 mg of catalyst but CO_2 conversion was barely observed and very low amounts of CH_4 formed was observed, possibly due to the very low contact time between reactant mixture and catalyst. Working with 20 mL/min of flow at 2 Torr and 470ºC the contact time was estimated to be of a magnitude order of 10^{-5} seconds. Then, it was decided that the catalyst mass should be increased and used in the form of packed-bed in order to improve the contact time.

In order to study the influence of each catalyst in a packed-bed, the CO_2 methanation reaction was performed in a Pyrex® tube reactor with a height of around 12 cm height and 2 cm of inner diameter. This reactor was partially filled with ≈1,2 g of catalyst supported on a quartz frit, equipped with two tungsten electrodes. These electrodes were placed one above and one below the catalytic bed, and were connected to an AC power supply of 2 kV and 50 Hz, allowing the formation of non-thermal plasma all across the catalyst-bed. The reactor is also equipped with a cartridge heater connected to an EROElectronic (CORAME technology) temperature controller in order to control the temperature of the reactional system as schematized in Figure 14. The outlet of the reactor is connected to a vacuum pump and to a mass spectrometer in order to analyze its composition.

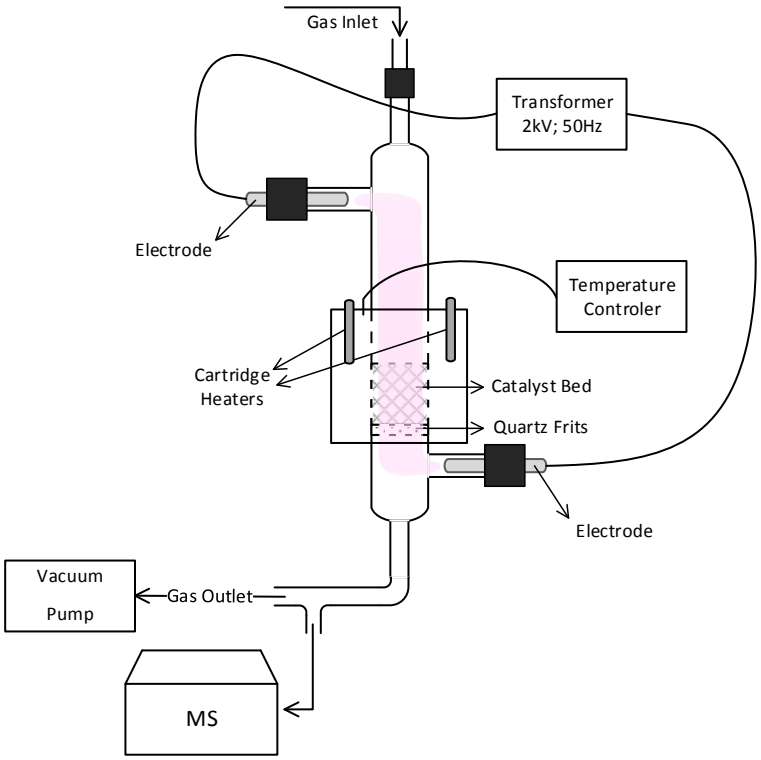

Figure 14 – Packed-bed reactor scheme.

The CO_2 methanation reaction was performed with a total volumetric flow of 20 mL/min. This flow was set in order to fulfill the requirements to the application of the calibration of CH_4, which below 10 mL/min did not seem to linearly match the concentration of methane with the intensity of the signal. It was also desired that the relative pressure drop of the gas across the catalyst bed and its support was not higher than 5% of the initial pressure (Appendix A4). A gas composition with the stoichiometric ratio of H_2/CO_2 = 4/1 in 50 molar % of Argon was applied in order to keep the hydrogen concentration low, as a security measure. The pressure inside of the reactor, after sending the reactional gas, was approximately 2.040 Torr, varying slightly with the change of temperature in the reactor as well as due to flow oscillations caused by the flow controller. The reaction is performed under vacuum since low pressures (P < 5 mbar) are needed to sustain the plasma due to the breakdown voltage of the gaseous mixture (Appendix A5).

The choice of Argon instead of Nitrogen as an inert was based on the comparison between the methanation reaction results under plasma of this two species. In a short test performed with the packed-bed reactor, a higher CH_4 production under plasma was obtained in an atmosphere of Ar instead of N_2 (Figure 15).

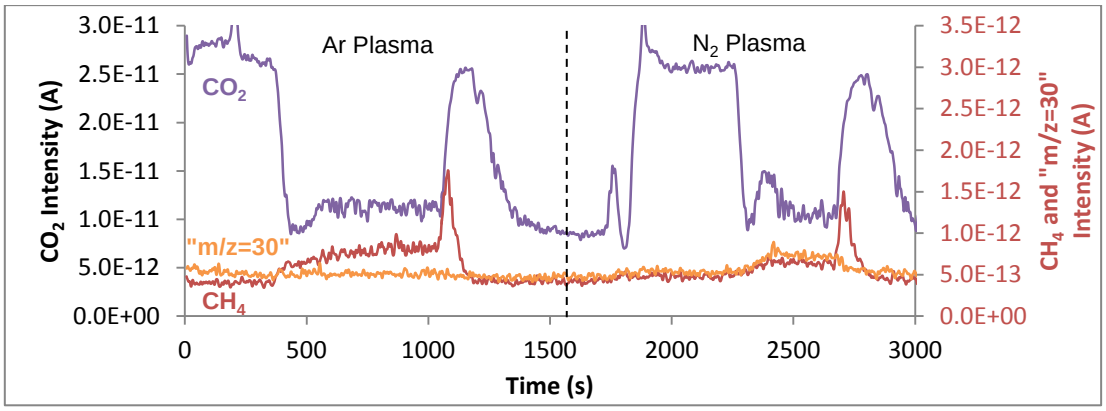

Figure 15 - Test reaction: Ar plasma *vs* N2 plasma.

As N_2 is a diatomic gas, its ionization caused by the glow-discharge is higher than the one obtained with Ar, due to the greater ionization ratio of the gas, the properties of the plasma, such as: composition, temperature, electron density or density are changed. This may affect the results of the reaction [55]. According with Figure 16, plasma which is generated with diatomic gases such as H_2 or N_2 has a tendency to reach higher temperatures, which can be related with higher ionization of the gas and consequent increase of free electrons amount.

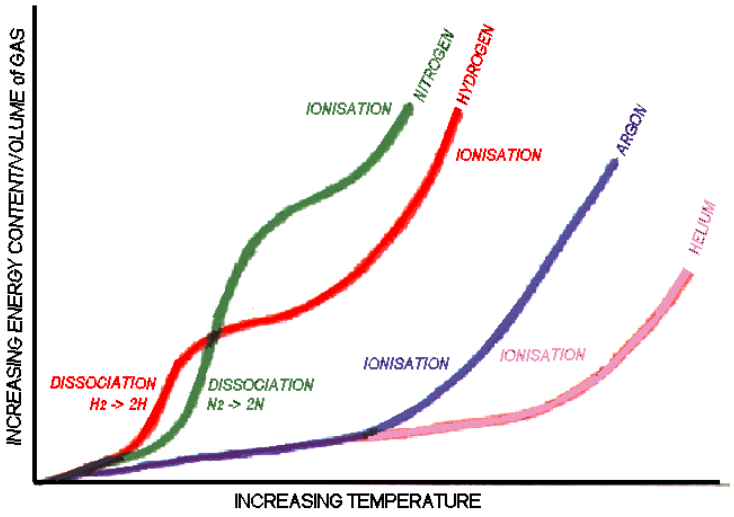

Figure 16 - Increasing energy content of the gas *vs* Temperature for different kind of plasma gas media[56].

As it was referred in chapter 2.5, in non-thermal plasma discharges, the temperature of the electrons is much greater than that of the heavy particles. As a consequence of the higher ionization of nitrogen, in comparison to that of argon, a higher part of plasmas energy is consumed in the dissociation of N_2, resulting in less energy being applied in the CO_2 dissociation. According with [57] argon also has a lower breakdown voltage than nitrogen (see Appendix A5).

It was also noticed that, while using N_2 as an inert, during plasma activity a compound with a mass to charge ratio (*m/z*) of 30 would be produced. This signal may be associated to nitrogen monoxide (NO) which has a molecular weight of 30.01 g/mol or to any other molecule that results from the reaction between the plasma-ionized nitrogen and the remaining species in the reactor. Therefore, a reactional mixture containing Ar should be preferential to one containing N_2 as this last seems to participate in the plasma-assisted reaction.

Another advantage of using an argon plasma is the fact that the mass t charge ratio of nitrogen detected by the mass spectrometer is usually m/z = 28, which is the same value as one of the reactions sub-product, carbon monoxide (CO). Then, the use of Ar as inert allows a better performance of the reaction as well as avoids misinterpretations of the measurements done.

Three kinds of experiments were performed under this system:

1. The conventional heating experiment, in which the reaction was conducted under heating at temperatures from 200 to 450ºC with an increment of 50ºC between each temperature.
2. The plasma reaction, in which cold plasma is formed by the electrodes through catalyst bed, without any heating besides the heating inherent to the plasma activity.
3. The combination of both heating and plasma, studied at temperatures between 200 and 350ºC, once again using the 50ºC increment.

After starting the inlet stream the plasma was turned on for a few moments until the MS signal show stability and then extinguished. After this measurement the reactor was heated and measurements at the desired temperatures were performed in the same way. The heating rate used for each heating step was 10ºC/min. Once each temperature was reached and the MS signal is stable, measurements of the reaction without plasma and with plasma were performed. For the temperatures of 400ºC and 450ºC the plasma measurements were not performed due to instability of the plasma observed during one of the initial experiments. At these temperatures it was observed that at the bottom of the reactor the plasma would exhibit a very dense reddish color. When the plasma discharge is applied to a gas, the electrons of the gas molecules are excited. As these electrons return to their original state they emit light. The color of that light is defined by its wavelength which is related to the amount of energy released by the electron. Then, each gas emits a different color when it is submitted to the electrical discharge. During experiments it was noticed that hydrogen plasma emitted a red color, which based on Figure 17, is due to the electron transition of N=3 to N=2. The other compounds of the reactional mixture presented color of purple, in the case of Argon, and white in the case of CO and CO_2.

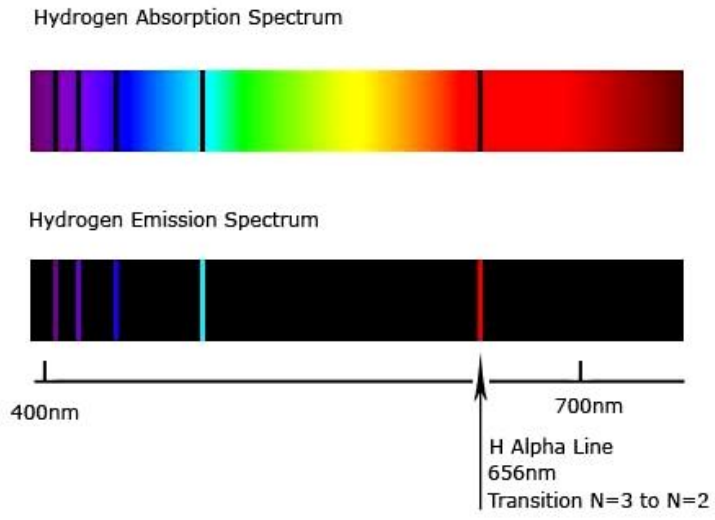

Figure 17 - Hydrogen absorption and emission spectra [56].

Based on this information, the detection of the reddish color at the base of the reactor was attributed to the presence of hydrogen and the strong intensity of that light, according with Beer-Lambert's law, was related with the high amount of this gas in the base of the reactor. This accumulation may be explained by the increase of the pressure drop that occurs due to the augmentation of the gas temperature in the reactor. High temperatures increase the volumetric flow of the gas that goes through the catalytic bed and, therefore, its superficial velocity, leading to a higher pressure drop. Also, as hydrogen is a very low density gas it accumulates on the upper zone of the bottom of the reactor, bellow the quartz frit, while the other gaseous compounds keep descending, being sucked by the vacuum pump due to their higher densities. This contributes to the creation of a hydrogen rich zone that represents a danger of possible explosion.

As hydrogen is a flammable gas, in order to avoid its accumulation under high temperatures (400 and 450ºC) it was decided that the plasma experiment was not going to be performed above 350ºC.

The samples used for this experiment and its characteristics are shown in Table 7.

Table 7 - Characteristics of the catalyst samples used in the packed-bed reaction [52].

Zeolite	Crystallinity (%)	Ni content (wt.%)	Si/Al molar ratio
USY(30)	>99	14	30
USY(40)	>99	14	40
USY(40)(IWI)	-	14	40
ZSM-11	>99	5	17
ZSM-11	>99	2.5	17

Typically, the mass to charge ratios followed in the MS for each of the species throughout this work are the ones in Table 8.

Table 8 - Species followed with the MS and corresponding m/z signals.

Specie	*m/z*
H_2	2
C	6
CH_4	13; 15
H_2O	18
CO	28
N_2	14; 28
O_2	32
Ar	40
CO_2	44

3.3.2. In-Plasma *vs* Post-Plasma Catalysis

Despite of the plasma-catalyst interaction being thought to have a strong influence in catalysis there is still much lack of knowledge about its causes. For this reason, based on the results of the plasma reaction with the packed-bed reactor, it was decided that the study of the influence of the

contact of plasma with catalyst bed could be interesting. In order to do that, a modification in the packed-bed reactor was made, adding to it a second electrode entry above the catalytic bed in order to be able to operate under an In-plasma or Post-plasma catalysis configuration, as schematized in Figure 18.

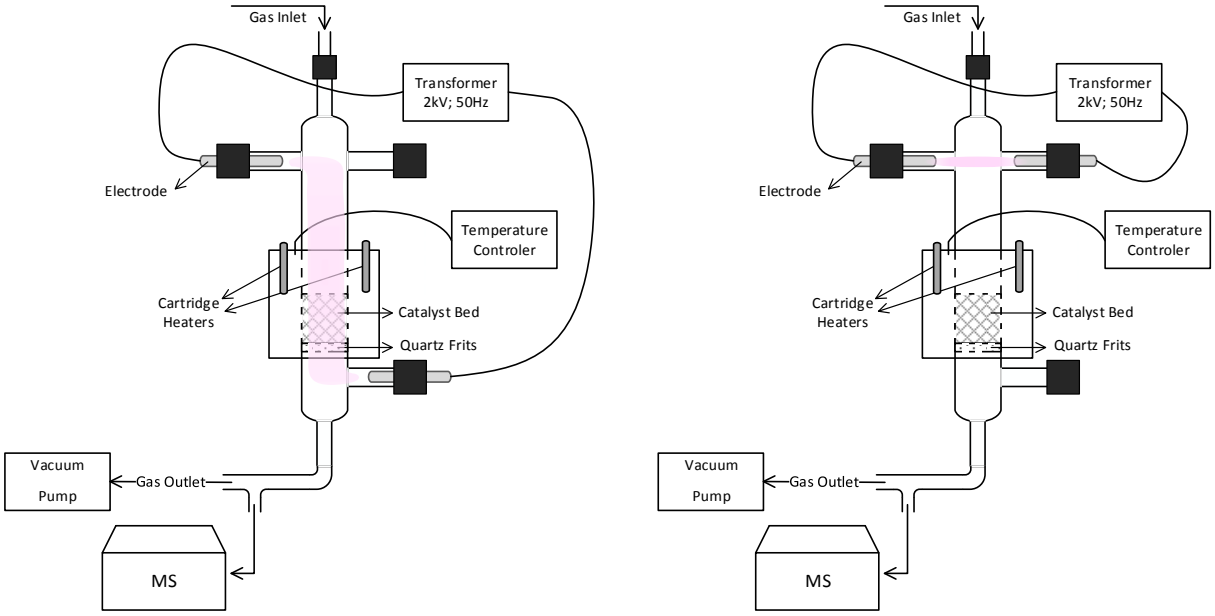

a) In-Plasma Catalysis Configuration **b) Post-Plasma Catalysis Configuration**

Figure 18 - Different plasma-catalysis configurations. a) IPC; b)PPC.

The IPC and PPC catalytic experiments performed using the Ni/USY(40) sample as catalyst.

Measurements with plasma activity were made, with and without catalyst, for inlet flows of 10, 15, 20, 30, 50, 80 and 100 mL/min, in order to evaluate the effect of the residence time of the reactants through the catalyst bed, maintaining the $H_2/CO_2/Ar=4/1/5$ molar ratio. The temperature of the reactor was ≈125ºC, measured with a Raytek Infrared Temperature Measurement Sensor.

3.4. *Operando* Infrared (IR) measurements

Based on the results obtained in the packed-bed reactor, and in order to have a better understanding of the species that are formed and consumed by plasma influence, an Infrared spectroscopy study was performed. A Bruker Vertex 80v FTIR (Fourier transform infrared) spectrometer was used for this effect. Using the software OPUS 7.5, IR spectra were acquired between 4000 cm^{-1} and 1000 cm^{-1}, to the catalyst samples in Table 9.

Table 9 - Catalyst samples used in the IR measurements and characteristics.

Sample	Ni content (wt.%)	Si/Al molar ratio
Ni/USY(40)(IWI)	14	40
Ni/ZSM-11	5	17
Ni/ZSM-11	2.5	17
Ni/SiO_2	14	-
Ni/Al_2O_3	14	-

In order to perform the IR study the reactional system was changed to a static infrared cell (schematized in Figure 19 a)). In this cell, a self-supported wafer of the studied catalyst is held by a sample-holder that allows the user to place the sample at the heater level, for pre-treatment purposes, or at the IR-beam position for the FTIR measurements. The reactor placed at the infrared position is also equipped with two electrodes, see Figure 19 b), for plasma generation across the wafer.

Each catalyst sample was reduced *in-situ* before reaction according with the procedure explained in section 3.2.4.

After the reduction step, IR measurements were performed before, during and immediately after plasma activity. Additionally, measurements were performed 5 and 10 minutes after plasma extinction in order to see the evolution of the spectra after the plasma-assisted reaction. A measurement with no reactants was also performed for each catalyst in order to identify the reactants IR bands.

The measurements were performed in *Operando* mode with a inlet stream of 20 mL/min with a composition of $H_2/CO_2/Ar$ = 4/1/5 like the one used in the packed-bed reaction. The IR cell was also put under high vacuum with a pressure of approximately 2.040 Torr being reached when the reactional mixture was sent into the system.

All the IR measurements were also followed by mass spectrometry in order to control the composition of the outlet mixture of the reactor, allow CO_2 conversion, CH_4 and CO selectivity and yield values calculations as well as for safety purposes.

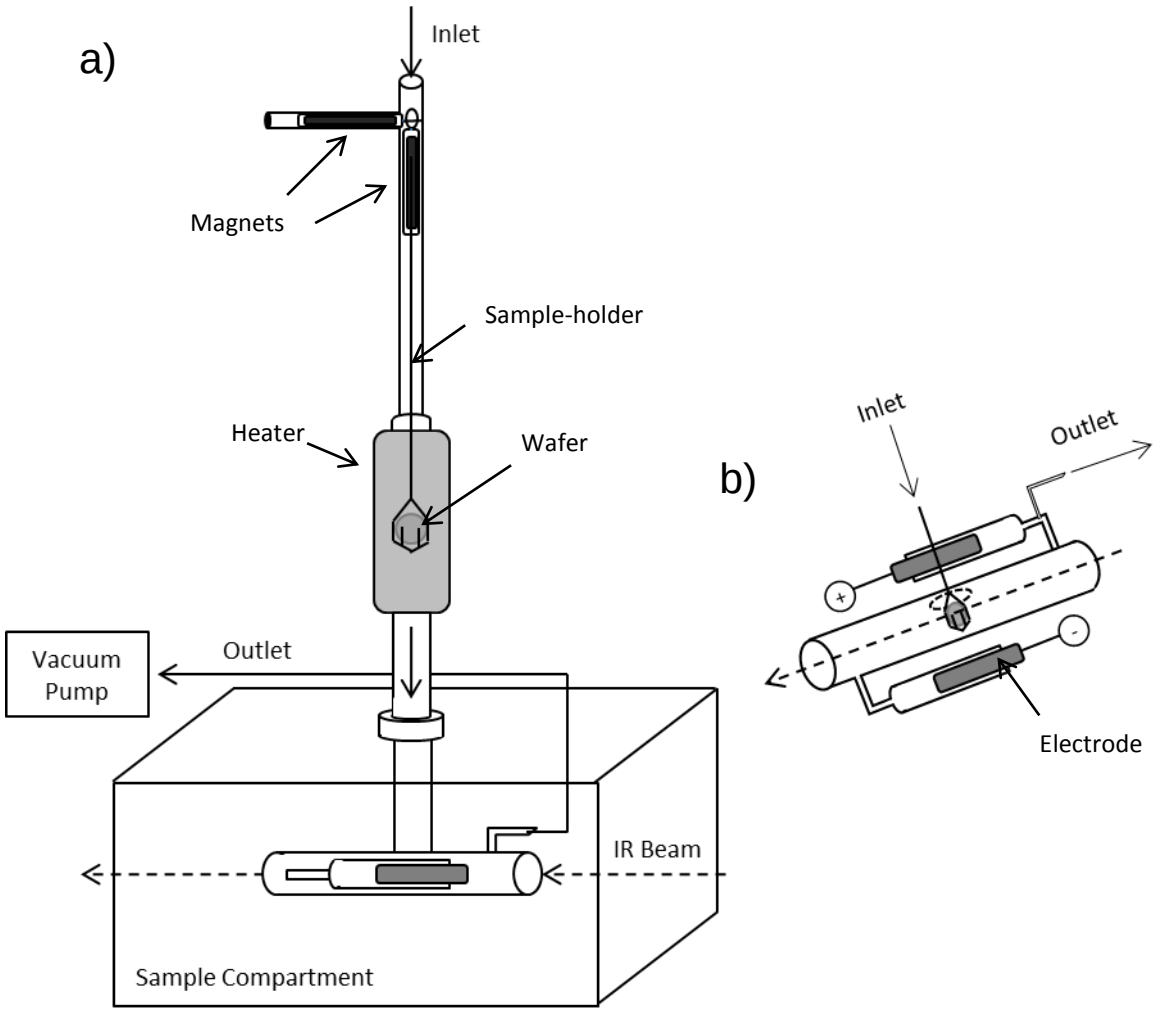

Figure 19 - a) IR cell scheme; b) Plasma reactor detail placed at the IR beam level.

4. Results

4.1. Characterization of the catalysts

4.1.1. Verification of crystalline structure of the zeolites

The XRD patterns obtained for the Ni based USY and ZSM-11 samples do not indicate any crystalline structure modification throughout the reactions and all the treatments applied to the catalysts, as the crystallinity obtained was higher than 99% for all of them (see Table 10).

4.1.2. Determination of catalysts surface area, micro- and mesopores volume

The results obtained for the surface areas as well as microporous and mesoporous volumes of the analyzed catalyst samples are presented in Table 10.

Table 10 - Surface area and pore volume of the FAU and MEL catalyst samples.

Zeolite	Crystallinity (%)	Si/Al molar Ratio	Ni content (wt.%)	Reduced Ni fraction (%)	Internal surface area (m^2/g)	External surface area (m^2/g)	Micropores volume (cm^3/g)	Mesopores volume (cm^3/g)
USY(30)	>99%	30	14.0	13.4	513	106	0.197	0.201
USY(40)	>99%	40	14.0	17.4	632	107	0.252	0.201
USY(40)(IWI)	-	40	14.0	24.3	-	-	-	-
ZSM-11	>99%	17	5.0	6.6	252	57	0.085	0.154
ZSM-11	>99%	17	2.5	16.6	291	69	0.107	0.195

It can be observed that as the Si/Al ratio diminishes the internal surface area tends to decrease as well as the micropores volume. In [52], F. Azzolina-Jury explains this with the increase of Al in the zeolite framework that, due to the isomorphic substitution of Al for Si leads to an increase of the negative charges in the zeolite, increasing the number of exchangeable sites enhancing the hostage of cations such as Ni^{2+} inside of the structure.

The difference of reduced Ni fraction obtained for the FAU samples, despite of having the same Ni content, can be explained once again recurring to the difference in the Si/Al ratio [52]. As USY(30) has a higher Al quantity, the amount of Nickel that is deposited in the structure under Ni^{2+} form is higher. As reported in [17], Ni^{2+} ions are difficult to reduce, as temperatures higher than the ≈500ºC used during the H_2TPR-MS are needed. Therefore, the quantity of nickel in the form of Ni^{o} is lower than the one obtained for the USY(40) sample.

Regarding the ZSM-11 samples, the higher Nickel content of one of them and, therefore, Ni^{2+} ion increase, diminishes its micropores volume, and due to that internal surface area. For this zeolite in particular it also seems to have some influence in the mesopores volume. In addition a higher Ni^{2+} quantity decreases the reduced Ni fraction obtained for said sample.

The external surface area is related with the size of the particles of each catalyst, then, it can be concluded that ZSM-11 samples have smaller size particles than the Ultra-stable Y Zeolite samples [52].

4.1.3. Scanning electron microscopy (SEM) of the catalysts

The SEM images of the ZSM-11 and USY samples at scales of 2 µm, 1 µm and 500 nm are shown in Figure 20.

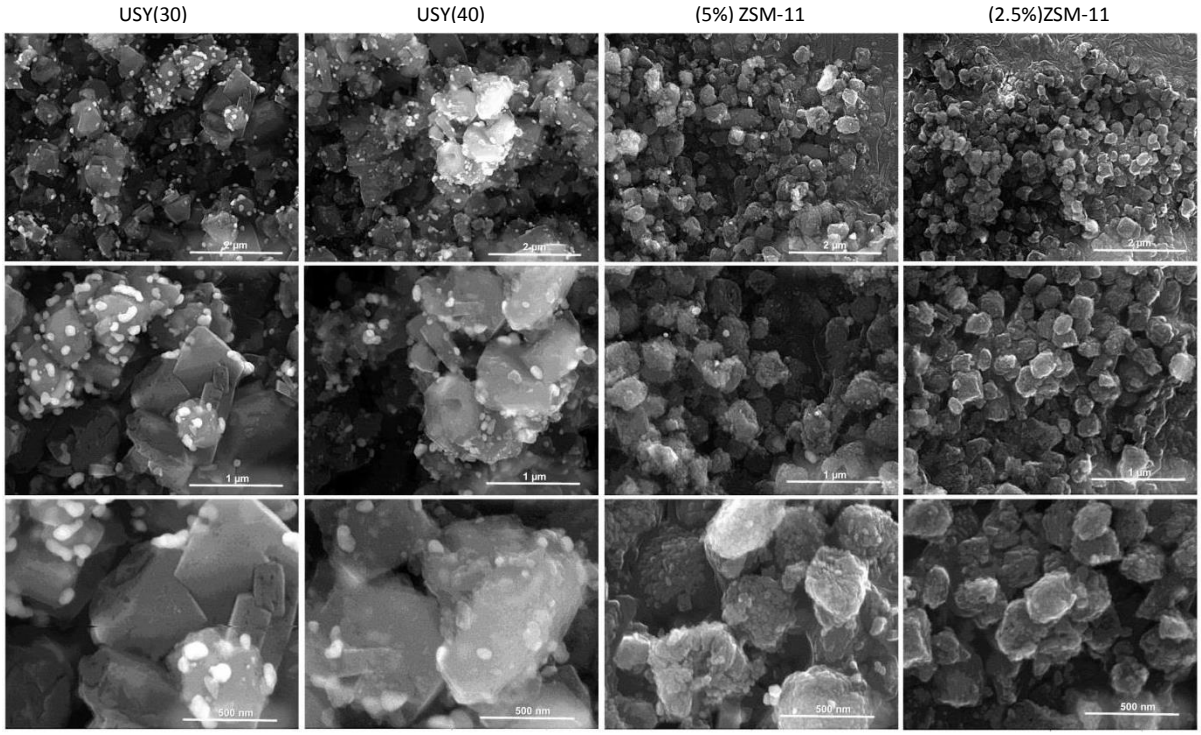

Figure 20 - SEM images of FAU and MEL catalyst samples [52].

This figure shows that the USY samples have a particle size of approximately 500 nm while ZSM-11 ones have nearly 250 nm of size. These results are compatible with the deduction about the relative particle size of the samples based on the values of the external surface area.

The white spots that can be observed in the figure correspond to Nickel oxide agglomerates. They have about 50 nm of diameter in all the analyzed samples and their density is proportional to the Nickel content of each catalyst. For this reason we can see that the USY samples clearly have a lot more agglomerates than the ZSM-11 samples. In the sample with 2.5 wt.% of Ni they can hardly be seen due to its low quantity.

4.1.4. Temperature-programmed reduction (H_2TPR-MS)

Based on the *in-situ* reduction hydrogen consumption profiles obtained for each catalyst sample, it is possible to estimate the amount of Nickel on its surface and pores that was reduced. According to the equation (3.1), that describes the reduction of Nickel to the state of Ni^o, and with the mass spectrometer measurement for Hydrogen (*m/z*=2) throughout the process, Figure 21, the Hydrogen consumption was calculated.

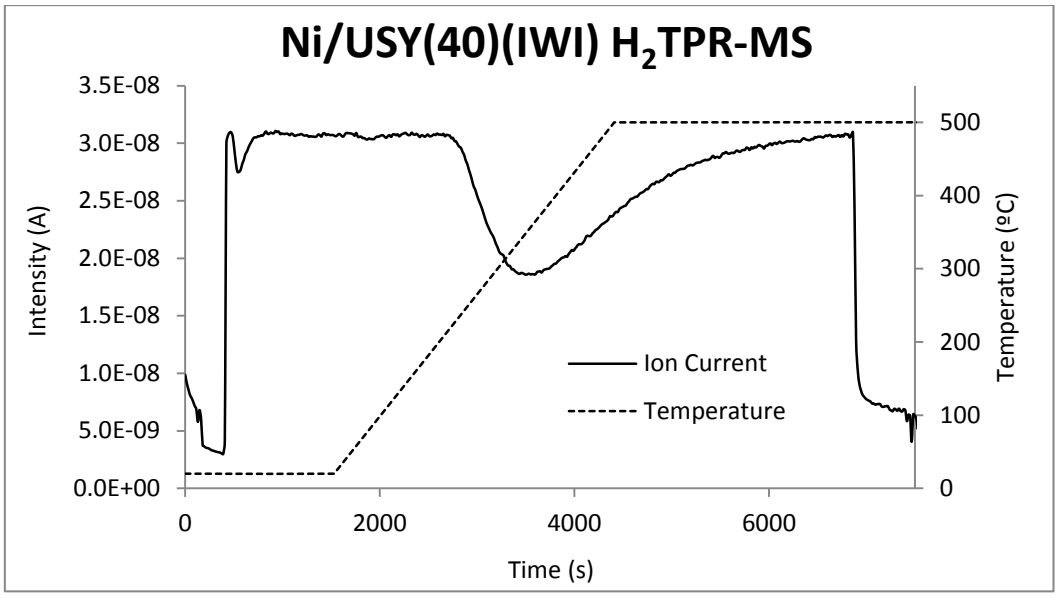

Figure 21 - H_2TPR-MS data obtained for the USY(40) (IWI) sample.

In Figure 22 the hydrogen consumption evolution of the Ni/USY(40)(IWI) catalyst with the temperature can be observed.

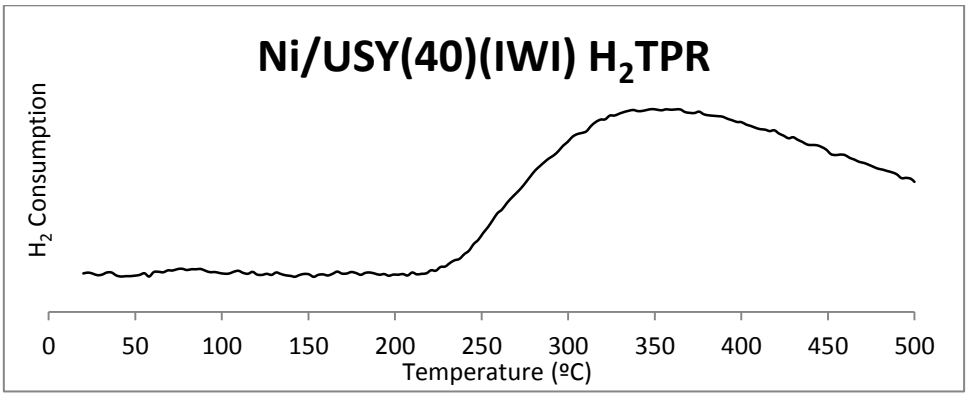

Figure 22 - Hydrogen consumption profile with the temperature.

In order to calculate the H_2 consumption, the area beneath the ion current was subtracted the area below the initial gas concentration in the time interval which the reduction takes place. This process is exemplified in Figure 23. The reduction interval is defined since the beginning of hydrogen signals decrease until it returns to stability at its original value. The area that results from this subtraction, *A* (A.s), is then used to determine the amount of H_2 that reacted with the NiO in the catalyst to produce Niº.

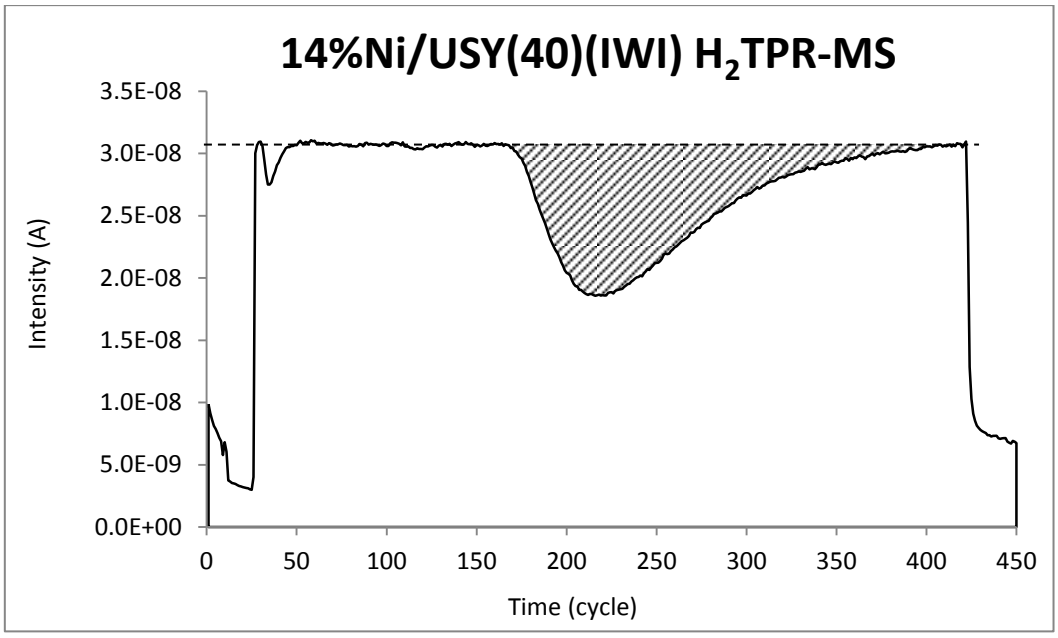

Figure 23 - H_2TPR-MS signal of Ni/USY(40)(IWI) catalyst with the H_2 consumption area.

Knowing that the total flow of H_2 that is used in each reduction is 1.5 mL/min and assuming a perfect gas behavior inside the reactional system, an initial flow ($F_{initial}$) of 6.14x10^{-5} mol/min (1.02x10^{-6} mol/s) of H_2 is obtained applying equation 4.1. With *p* and *T* the atmospheric pressure (atm) and temperature (K), respectively, *V* is the volume of the gas in L, which, in this case, was considered to 1 minute time base and *R* the gas constant.

$$pV = nRT \quad (4.1)$$

If the initial intensity ($I_{Initial}$) corresponds to this flow, the amount of H_2 consumed in the reduction can be calculated by the proportion in equation 4.2.

$$n_{H_2 Consumed}(mol) = \frac{A(A.s) \times F_{initial}\left(mol/s\right)}{I_{initial}(A)} \quad (4.2)$$

Once the amount of consumed H_2 is quantified and knowing the total amount of nickel in mol (Ni_{Total}) in each catalyst sample, which can be easily calculated from the respective weight percentages, the fraction of reduced Ni, Ni^o_{frac} (%), can be calculated by equation 4.3, where $Ni_{Reduced}$ is the mole number of nickel that is reduced during the process. It was assumed that all the consumed H_2 is used in the conversion of NiO into Ni according with equation 3.1.

$$Ni^0{}_{frac}\ (\%) = \frac{Ni_{Reduced}}{Ni_{Total}} \quad (4.3)$$

Attending to the equation of the NiO reduction (equation 3.1) and its stoichiometry, the ratio of consumed H_2 to reduced nickel amount in the catalyst is 1:1. Therefore, $n_{H_2 Consumed}(mol) = n_{Ni^0}(mol)$ (4.4).

As the Ni^{2+} species in the exchangeable sites are not likely to be reduced at temperatures up to 500ºC [17] it can be considered that only the NiO species at the surface and pores of the catalyst take part in the hydrogen consumption.

The results of reduced nickel quantity obtained for each catalyst sample are displayed in the Table 11.

Table 11 - Nickel content, Ni^o_{frac} and percentage of reduced nickel of each sample.

Catalyst Sample	Ni (wt.%)	Ni^o_{frac}	$\mathbf{Ni^0}/_{\mathbf{Catalyst\ mass}}$ $(\mathbf{wt.\%})$
Ni/USY(30)	14.0	13.4	1.9
Ni/USY(40)	14.0	17.4	2.4
Ni/USY(40) IWI	14.0	24.3	3.4
Ni/ZSM-11	2.5	16.8	0.4
Ni/ZSM-11	5.0	6.6	0.3
Ni/Al2O3	14.0	1.4	0.2
Ni/SiO2	14.0	21.1	3.0

4.2. Packed-bed system: Conventional heating *vs* plasma-assisted CO_2 hydrogenation

All the calculations referring to the packed-bed experiments were done based on the signal measured by the mass spectrometer and recorded using the *Quadstar* software based on the *m/z* ratios presented in Table 12.

In order to evaluate and compare the performance of the catalyst samples, calculations of CO_2 consumption (CO_2Conv), selectivity (S_i) and yield (Y_i) towards the products and the carbon balance ($C_{balance}$) to the reactor were calculated according with the equations presented in Table 12.

Table 12 - Equations used in the calculations of the packed-bed reaction.

	Equation	Equation number
CO_2 Conversion (%)	$CO_2Conv = \frac{CO_{2_{in}} - CO_{2_{out}}}{CO_{2_{in}}} \times 100\%$	(4.5)
Selectivity of a product *i* (%)	$S_i = \frac{i_{produced}}{CO_{2_{in}} - CO_{2_{out}}} \times 100\%$	(4.6)
Yield of a product *i* (%)	$Y_i = \frac{i_{produced}}{CO_{2_{in}}} \times 100\% = CO_2Conv(\%) \times S_i(\%)$	(4.7)
Carbon balance	$C_{balance} = \frac{n_{C\ out}}{n_{C\ in}} \times 100\%$	(4.8)

Where CO_2Conv expresses the carbon dioxide conversion, CO_{2in} and CO_{2out} refer to the inlet and outlet molar or volumetric flow values of CO_2, respectively, once the ideal gas approximation can be done without significant deviation from reality for the reactional systems used in this work. S_i and Y_i stand for the selectivity and yield concerning product *i*, and $i_{produced}$ is the molar or volumetric flow of product *i* that is produced through the reaction. $n_{c\ in}$ and $n_{c\ out}$ are the molar amounts of carbon in the inlet and outlet stream of the reactor and $C_{balance}$ expresses the carbon balance completion percentage.

In order to calculate the CO_2 conversion from the raw MS readings it was considered that the intensity detected for each m/z signal is proportional to the concentration of the corresponding compound. Average values of the initial intensity value $I_{initial}$ (when C_{CO2}=10%) and of the value

obtained for each operating condition, *I*, were corrected by subtracting the signal intensity obtained when the CO_2 concentration in the system is 0, $I_{baseline}$. Corrected values were then obtained, $I'_{initial}$ and *I*' respectively (see Figure 24).

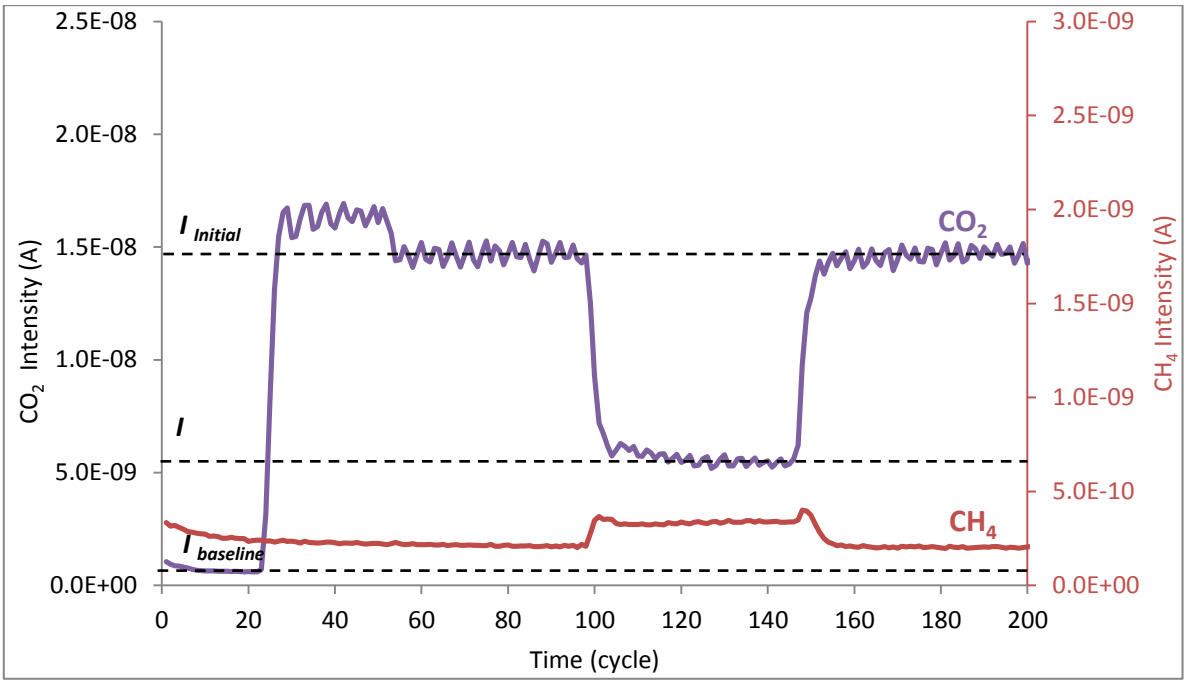

Figure 24 - Example of the intensity values considered in the CO_2 conversion calculations.

Knowing the operating conditions, based on those values a calibration line of CO_2 quantity in function of its intensity values was obtained (4.9) which allows calculating the amount of CO_2 at the outlet.

$$CO_2(mol) = (5.770 \times 10^3) \times I(A) - 3.606 \times 10^{-6} \quad (4.9)$$

With the values of CO_2 quantity obtained, by applying equation 4.5, one is able to find the CO_2 Conversion value.

In order to calculate the methane formation during each experiment it was necessary to make a calibration curve (Appendix A7). Equation 4.10, expresses the concentration of CH_4, C_{CH4} (ppm), in function of the intensity, *I*(A), obtained for the m/z=15 signal.

$$C_{CH4} = (6.898 \times 10^{12}) \times I(A) - 2.607 \times 10^3 \quad (4.10)$$

However, as the baseline of each m/z signal changes slightly from experiment to experiment. In order to achieve more accurate values of CH_4 formation, these variations had to be minimized by performing a correction. To the C_{CH4} value that matches each I_{CH4} was subtracted the concentration value obtained for the baseline intensity, $C_{baseline}$, according with equation 4.11. From this subtraction the corrected methane concentration, C'_{CH4} (ppm), is obtained.

$$C'_{CH4} = C_{CH4} - C_{baseline} \quad (4.11)$$

A calibration curve was also obtained for CO, but during calculations it was verified that the CO concentrations obtained through its utilization did not match the observed values and did not close the carbon molar balance. This may be due to the *m/z* = 28 ion current signal additionally being responsive to molecular Nitrogen which shares the molecular weight of 28 g/mol with CO. Then, as it was not observed the formation of any other reaction products besides H_2O, CO and CH_4, it was considered that $S_{CO} = 1 - S_{CH_4}$ (4.12). Attending to the stoichiometric coefficient of the CO_2 hydrogenation reaction into CO the amount of carbon monoxide can be calculated by equation 4.13.

$$n_{CO} = n_{CO_2\,Consumed} \times S_{CO}(\%) \quad (4.13)$$

Where n_{CO} and $n_{CO2Consumed}$ are the number of moles of CO that were formed and CO_2 that were consumed in the reaction and S_{CO} the CO selectivity value in percentage.

The catalytic results under different conditions are summed in the Figures 25, 26 and 27.

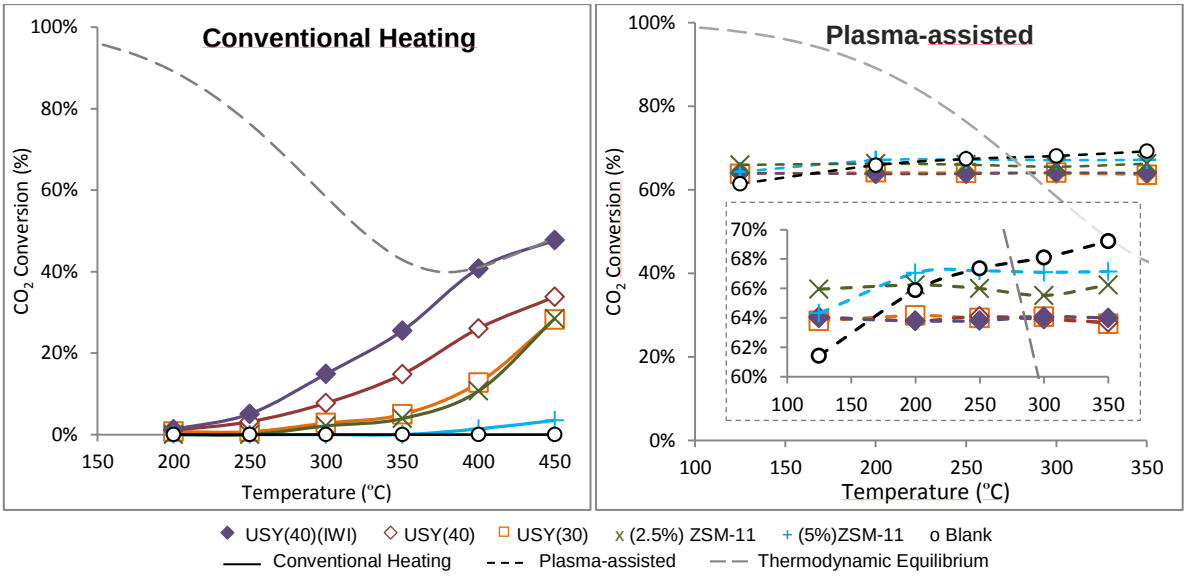

Figure 25 - CO_2 conversion results under conventional heating and plasma-assisted reaction.

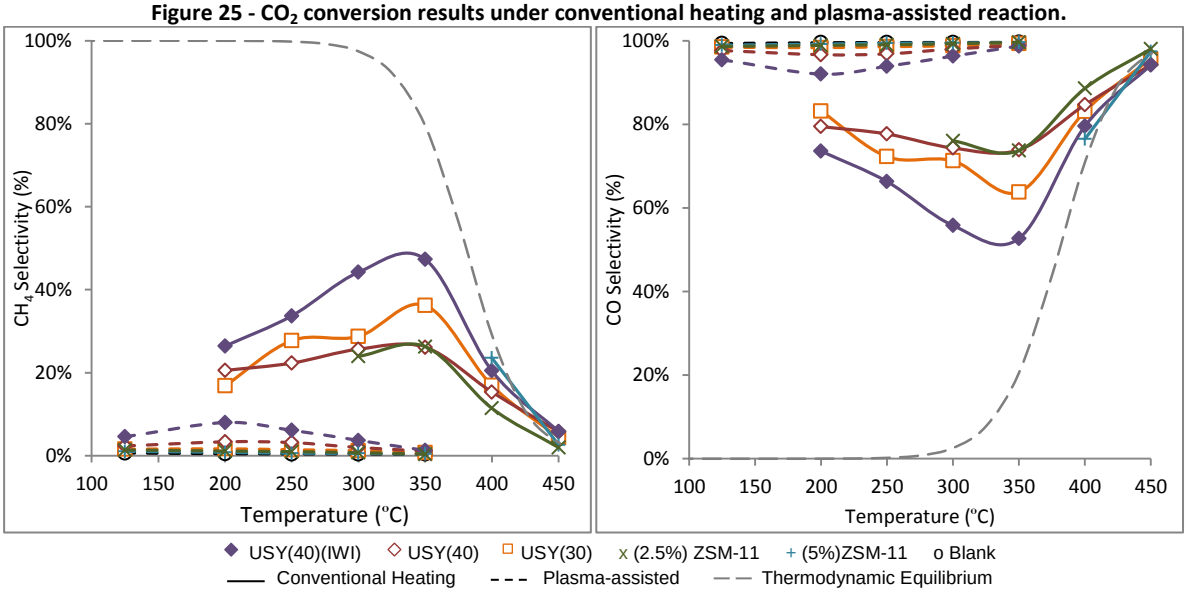

Figure 26 – CH_4 and CO selectivity results for the conventional heating and plasma-assisted reaction.

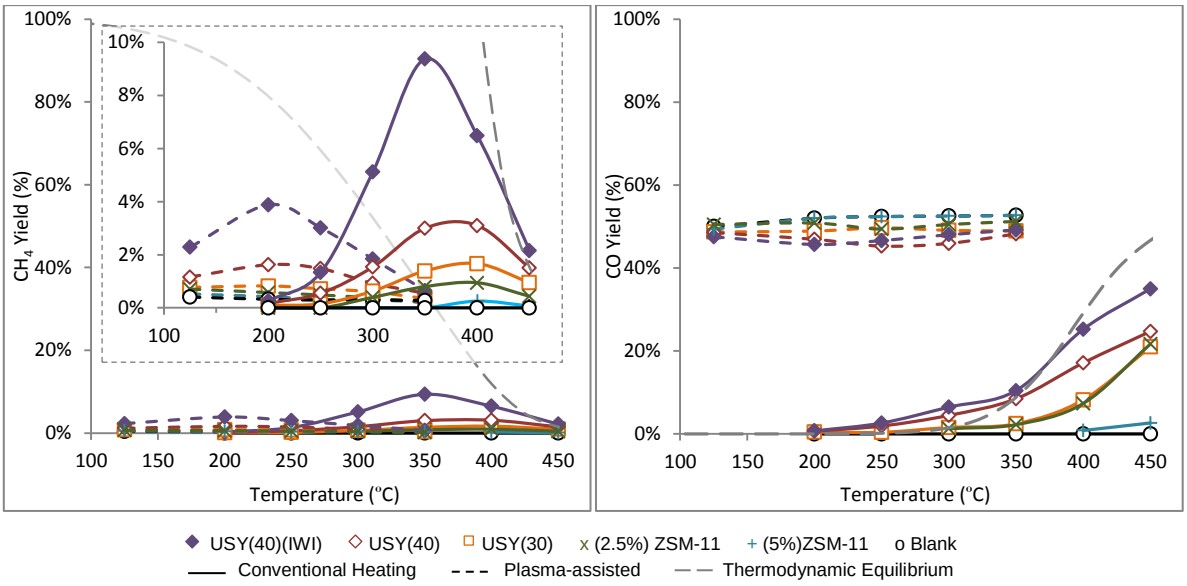

Figure 27 - CH_4 and CO yields results for the conventional heating and plasma-assisted reaction.

The tables with the values correspondent to these figures are in Appendix A8.

According with the results obtained for the classical heating reaction in this temperature range and pressure, the CO_2 conversion, which increases with the heating (Figure 25), seems to be improved by the increasing amount of reduced Nickel in each catalyst (see Table 11). The role of nickel in the catalyst is to adsorb and dissociate the Hydrogen molecules, facilitating the reduction of CO_2 into CO, as well as into CH_4 [52]. With the exception of the Ni/USY(40)(IWI) sample, the CO_2 conversion values for the classical heating reaction didn't go above 35%, which, in comparison with the thermodynamically calculated for this reaction, at the working pressure (Figure 3), can still be improved. However, the FAU zeolite impregnated by the incipient wetness method (IWI) revealed to achieve CO_2 conversion values very close to the thermodynamic limit. The main difference between these two catalysts is the higher Ni^{o}_{frac} achieved by the more effective impregnation method. Its higher amount of reduced nickel seems to take a significant effect, at least, in the reduction of CO_2 into CO. Due to its very low amount of reduced nickel, the 5%Ni/ZSM-11 sample showed poor activity being comparable to the blank experiment for the conventional heating reaction.

When non-thermal plasma was applied to the reactional system, the CO_2 conversion values reveal a significant improvement. Under plasma activity CO_2 is ionized and dissociated into CO* and O*. The conversion happens not only in the catalyst surface but also, and mostly, in the gas phase before it reaches the packed-bed. This statement is supported by the CO_2 conversion values obtained in the blank experiment, comparable to the ones obtained with the catalyst samples. It can also be observed that zeolites with the same frameworks exhibit similar CO_2 conversion values under plasma activity. In fact, for temperatures above 250ºC, the carbon dioxide conversion is higher when no catalyst is used. This increase is related with the enhancement of plasma energy with the increase of temperature [59]. When the catalyst samples are used it is noticeable that, at higher temperatures CO_2 conversion is lower than in the blank experiment. This is possibly due to some plasma energy that is consumed by plasma-catalyst interaction [52], therefore not being applied to the dissociation of the molecules. The explanation for the higher CO_2 dissociation obtained at lower temperatures for all the

samples in relation to the blank experiment may rely on the formation of hot-spots inside of the catalytic bed due to the microdischarges that are caused by the interaction of plasma with the sample pellets, Figure 28. As explained in chapter 2.6, the localized heating that results from this phenomenon may stimulate catalytic activity [52].

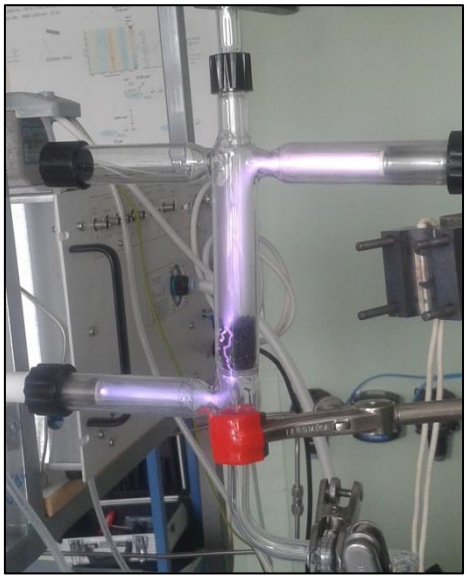

Figure 28 – Plasma-assisted reaction in the packed-bed reactor with formation of micro-discharges across the catalyst.

The temperature increase improves the plasma energy which is directly related with the dissociation of molecules of carbon dioxide [60]. It can also be verified that ZSM-11 samples reveal a slightly higher conversion than the Ultrastable zeolite Y. As an electric field is applied on the catalyst adsorption can be induced in the catalyst by enhancement of the electric field [40]. Besides that, the adsorption-desorption equilibrium of the zeolite is strongly affected by the occurrence of microdischarges in the catalytic bed [29]. The electric field in each catalyst is related to the complex permittivity value of the sample material [61, 62]. As FAU zeolites have a higher complex permittivity value than MEL zeolites [63], they are more easily affected by the electric field existent in the reactor. Therefore, a bigger part of plasma's energy is consumed by plasma-catalyst interaction and, as consequence, less energy is applied in the conversion of the reactants [52].

Analysing the results in terms of selectivity, two main factors can be related with the production of methane: a) the amount of Ni^o, where the dissociative adsorption of H_2 occurs, which, due to the abundance of Hydrogen favors the hydrogenation of the CO_2 and CO adsorbed in the catalyst; b) the adsorption capacity of each catalyst which is associated with the zeolite framework. In the conventional heating case, overall, higher selectivity towards CH_4 can be associated to the FAU zeolites, being the USY(40)(IWI) sample noticeably more methane selective. The better performance of this catalyst can be related with its higher Ni^o_{frac} value. The maximum CH_4 selectivity obtained at 350ºC is explained by the compromise between adsorption-desorption equilibrium and the CO dissociation on the zeolite which are affected by the temperature. The dissociation of CO has been reported to be the rate-determining step for the CO_2 methanation reaction [28, 52]. Above 350ºC the

CH_4 selectivity decrease observed during the experiments seems to match the equilibrium selectivity calculated thermodynamically. This can be explained by the fact that the high temperatures favor the RWGS reaction, which is a concurrent reaction of the CO_2 methanation, due to its endothermicity. As CO_2 conversion values for the 5%Ni/ZSM-11 sample were not observed before 400ºC, a proper analysis of this catalysts selectivity or yield towards any product could not be performed. These experiments also revealed that, apart from the Ni/USY(40)(IWI) sample, the USY(30) catalyst revealed to be more CH_4 selective than the regular USY(40) which has a closer reduced Ni amount than its IWI version. This may mean that the lower Si/Al ratio of USY(30) also plays a role in the selectivity of the catalyst towards certain compounds. This hypothesis is also supported by the fact that the ZSM-11 sample with the lowest nickel amount, which has an even lower Si/Al ratio (17) reaches methane selectivity values very close to the ones obtained with USY(40) (Si/Al=40). Based on these results, higher conventional heating selectivity towards methane can be associated to higher reduced nickel amount or, also, the structure of the support zeolite.

When the reaction is performed under plasma activity, the effect of plasma-induced adsorption enhancement must be taken into account. As the faujasite zeolites complex permittivity values are more expressive than MEL zeolites, the effect of the induced adsorption of the reactants on them is higher. This, associated to the amount of reduced Nickel in each sample provides a higher CH_4 selectivity for Ni/USY(40) (IWI), followed by Ni/USY(40), Ni/USY(30), 2.5%Ni/ZSM-11 and 5%Ni/ZSM-11 showing the worst results. A maximum of CH_4 selectivity was observed at 200ºC for every catalyst due to higher amounts of methane being produced (as the CO_2 conversion tends to be constant for plasma reactions). This is possibly due to the compromise between the plasma induced adsorption of species into the zeolite and the temperature promoted desorption. If above 200ºC the most important factor is the second one, then the hydrogenation of adsorbed molecules of CO into CH_4 will decrease as higher temperatures are provided. It increases with temperature possibly due to the enhancement of plasmas energy which causes more induced adsorption on the zeolite.

As the only products identified with the mass spectrometer through the methanation reactions were methane and carbon monoxide, the selectivity towards CO was calculated according with:

$$S_{CO} = 1 - S_{CH_4} \quad (4.14).$$

Based on the values obtained for CO_2 conversion and CH_4 and CO selectivity, the yield of the reaction in terms of each one of the products was calculated. The yields were normalized with respect to 1g of catalyst for all the catalytic tests.

By analysing the CO_2 conversion and selectivity values, the best catalyst in terms of CH_4 yield is 14%Ni/USY(40) (IWI), followed by 14%Ni/USY(40), 14%Ni/USY(30), then 2.5%Ni/ZSM-11, and at last 5%Ni/ZSM-11. This order of CH_4 yield is verified for both conventional heating and plasma experiments.

Plasma operation led to a shift of the thermodynamic equilibrium to lower temperatures. An optimal temperature of 400ºC was obtained in conventional heating reaction while only 200ºC were obtained as the optimal temperature of the plasma experiment.

It is interesting to notice that, under plasma conditions, despite achieving better conversion of carbon dioxide, the CH_4 yield at the optimal temperature is lower than half of the one obtained for

conventional heating optimal temperature due to the poor CH_4 selectivity observed for the plasma reaction.

4.2.1. Methane release phenomenon

While performing the plasma-assisted experiments a new phenomenon was noticed. After operating, upon switching off the transformer and extinguishing the plasma, a sudden increase of CH_4 would occur while every reactant, as well as other products such as water and CO, would have its signal return to the original value for each temperature, Figure 29. This increase, to values significantly higher than the ones obtained during reaction, would last only for a few seconds, and then the signal of methane would gradually return to its baseline.

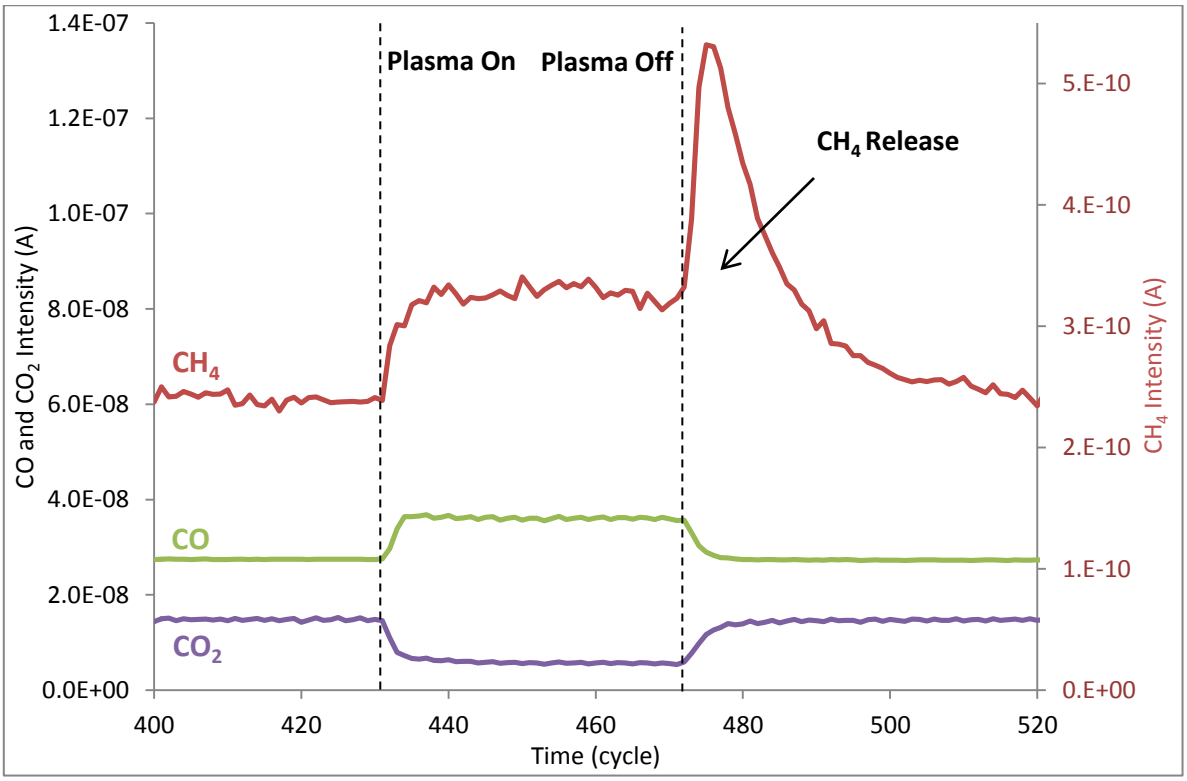

Figure 29 - Plasma experiment MS signals of CH_4, CO and CO_2. Putting in evidence the CH_4 increase phenomenon after plasma.

It was verified that, ignoring this occurrence, the carbon balance to the reaction would not be complete. For the majority of the plasma experiments the ratio between the number of carbon atoms that was detected in the outlet of the reactor and the carbon amount on the inlet stream revealed values of approximately 99% without considering the methane increase and 100% after considering it. The calculations of the carbon balance and respective results are shown in Appendix A9.

Regardless of the reason for this behavior, as this increase was not negligible and it was verified for practically every plasma experiment involving a catalyst, this amount of methane was taken into account for selectivity and yield calculations. By integrating the CH_4 signal area corresponding to

this increase, the amount of methane released was calculated and employed in selectivity and yield calculations. It is then necessary to subtract the area beneath the *I(A)*, the filled zone in Figure 30, that corresponds to each temperature steady state production, otherwise the value obtained will be affected by the conventional heating methane formation.

The corrected area value that results from the integration, expressed in A.cycle, where a cycle is a time measure used by the mass spectrometer that corresponds to approximately 11.5 seconds, is divided by the number of cycles of the same interval in order to obtain a value of intensity equivalent to the amount of methane detected in the release that is product of the plasma reaction. This intensity is then converted into concentration values with the calibration equation (equation 4.10) which is added to the steady state production quantity.

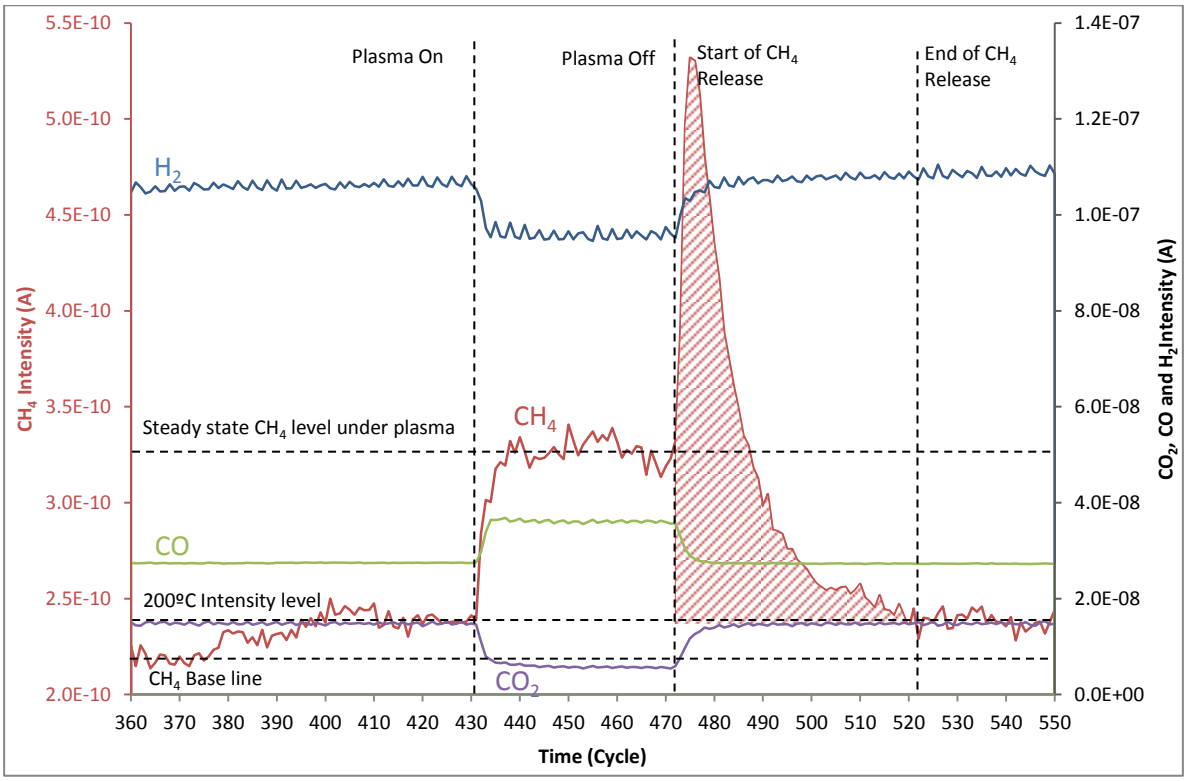

Figure 30 - Example of CH_4 signal intensity considerations for the methane release quantification.

As shown in Figure 31, by considering this occurrence, plasma experiments results get their selectivity improved, in terms of CH_4, and by consequence the respective yield.

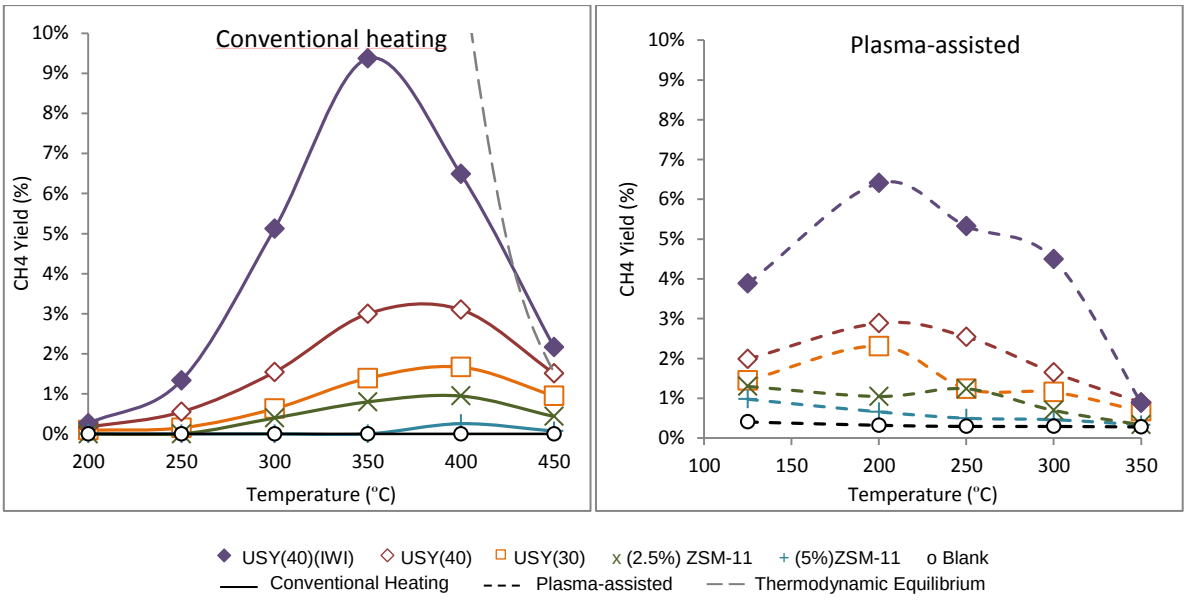

Figure 31 - CH_4 yield results for conventional heating and conventional heating + plasma after considering the CH_4 release.

Analysing the results calculated by considering the methane release an increase of CH_4 yield per gram of catalyst is noticed in respect to the previously calculated values under plasma activity. A new comparison between conventional heating and the plasma-assisted reaction methane yields is also possible. The new methane yield values, for the plasma experiments optimal temperature of 200ºC, seem to match or even surpass the optimal temperature yield values of the conventional heating reaction, with the exception of the most active catalyst. As a consequence of its high Ni^{o}_{frac}, under conventional heating, the USY(40)(IWI) catalyst achieved both CO_2 conversion and CH_4 selectivity values much greater than the ones obtained with the remaining samples. As seen in equation 4.7, the yield of a reaction is dependent of these two factors. According with the results presented in Figures 28 and 29, plasma has a positive effect on the first but a negative one in the last. The influence of the NTP discharge in the reaction CH_4 Yield results of a compromise between CO_2 conversion increase and CH_4 selectivity decrease. In a general scenario, it was noticed that plasma triggered the increase of CO_2 Conversion into values between 61 and 69%. Usually it is a very significant increase that has more influence in the CH_4 yield than the decrease of the selectivity decrease towards this product that is verified in the NTP-assisted reaction. In the case of the USY(40) IWI sample, as a consequence of the higher activity and methane selectivity values obtained under conventional heating, the high selectivity value dropped significantly and the increase of the already high CO_2 conversion did not increase so much as the one obtained with the other samples. As the first factor did not assume higher importance than the second, a lower optimal yield for the plasma reaction was obtained than the one for conventional heating.

In general, the plasma reaction yield values at their optimal temperature of 200 ºC largely exceed the CH_4 yield obtained at the same temperature of the reaction with only heating. Then, plasma operation appears to be a great alternative to the conventional heating CO_2 methanation reaction.

Due to the lack of bibliographical information about plasma catalysis, especially on the methanation topic, it is difficult to predict the effects of NTP application to the catalytic conversion of carbon dioxide into methane. So, in order to have better understanding of this phenomenon and to try to take advantage of plasma full potential, further study under different operating conditions such as: temperature range, system pressure, catalyst, plasma operation time or plasma properties. This could be useful in order to optimize the operating conditions and take possibly advantage of this phenomenon.

As an attempt to explain the observed phenomenon of increasing CH_4 after extinguishing the plasma in the reactor some hypothesis were tested.

One of the possible explanations that were tested was the double ionization of the species analyzed by the mass spectrometer. Usually, mass spectrometry is based on the readings of the mass to charge ratio (*m/z*) of the analyzed stream which is previously ionized by an electron beam. The double ionization theory suggests that, while operating under plasma, the stream is ionized by the action of plasma and, at the time of its analysis, after leaving the plasma comprehended area of the reactor, would reach the MS partially ionized and suffer a second ionization inside the device, affecting the value of *m/z* and, therefore, detecting a significant part of the methane under other values than the usual *m/z*=15. Upon extinguishing the plasma the first ionization would cease and the residual methane from the plasma reaction detected by the mass spectrometer would return to its usual value, causing the increasing signal and then decreasing due to the stopping of the reaction.

Another possibility, based on the knowledge that plasma can affect the properties of the catalyst and induce adsorption of compounds, is the release of adsorbed methane radicals under plasma activity. The species formed by the ionization of methane, methane radicals, such as CH_3*, CH_2*, CH* and C*, are thought to be adsorbed in the catalyst due to their polarity. This adsorption would cause a diminution of the methane MS signal due to two main reasons: the retaining of methane, which is adsorbed by the catalyst, and so, not read by the mass spectrometer while the plasma is operating; and the blockage of part of the catalysts active sites caused by this adsorption, reducing catalytic performance. It was suggested by F. Azzolina-Jury that when the plasma ceases, the adsorbed radicals may aggregate with the hydrogen attached with the Nickel in the catalyst, forming CH_4, which is desorbed. During this process of desorption the amount of methane on the outlet of the reactor will increase and then decrease as the catalyst runs out of methane/methane radicals, causing the sudden increase followed by decrease of the methane signal.

In order to evaluate the veracity of the double ionization explanation a test was made in which a short plasma reaction was performed while following mass to charge ratios that were not usually followed such as *m/z* = [4, 5, 6, 7, 8, 12, 14] as well as the usual *m/z* = 15 that is typically used for methane detection.

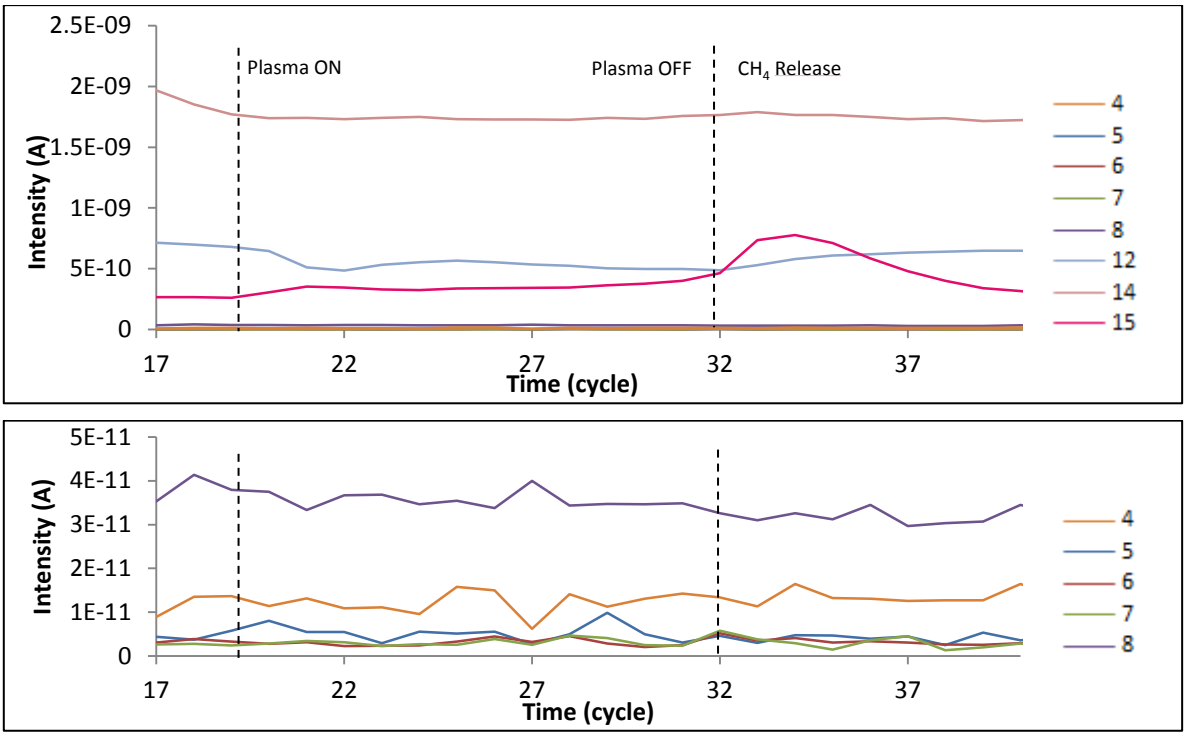

Figure 32 - Double ionization experiment MS results.

In Figure 32 is displayed the Intensity *vs* Time plot for this test. It is possible to observe that, aside from *m/z* = 14, which responds to the presence of nitrogen, and *m/z* = 12, that usually responds to the carbon from CO_2, no significant changes were observed from mass to charge ratios other than the usual 15. This suggests the double ionization phenomenon did not occur and does not take a role in the unexplained methane increase.

In order to evaluate the possibility of the adsorption of methane radicals a small test was conducted. CH_4 from a 1%CH_4/Ar bottle was fed to the packed-bed reactor filled with Ni/USY(30) catalyst. Plasma was applied in order to observe the behavior of methane under these conditions. If the radicals adsorption hypothesis is correct, then upon turning on the plasma, its signal should decrease, and increase again with a release after ceasing the plasma.

Figure 33 shows the evolution of the methane signal during this test.

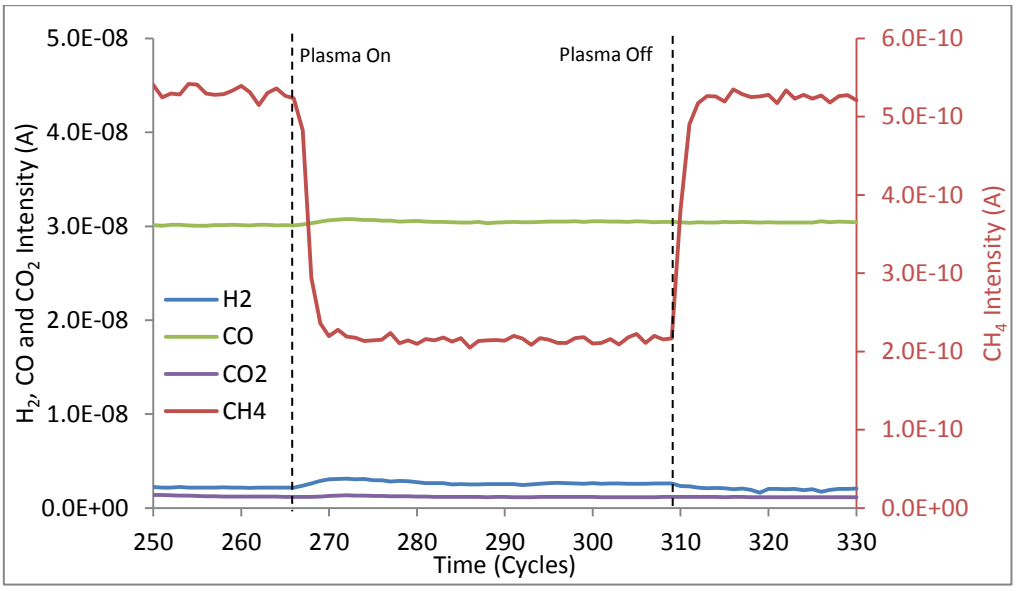

Figure 33 - Methane adsorption test.

As it is possible to observe, the behavior of the methane signal is according to the described above. It supports the theory that methane radicals are formed by plasma and adsorbed by the catalyst, being released afterwards. They were also noticed very low amounts of CO and H_2 being detected during plasma activity. The H_2 may be created by some Hydrogen atoms that dissociate from CH_4 molecules while the small CO increase can be due to desorption of traces of carbon oxides that were retained in the catalyst.

In order to have further information and confirmation of this occurrence, IR measurements were done to 14%Ni/USY(40) catalyst under plasma and after plasma.

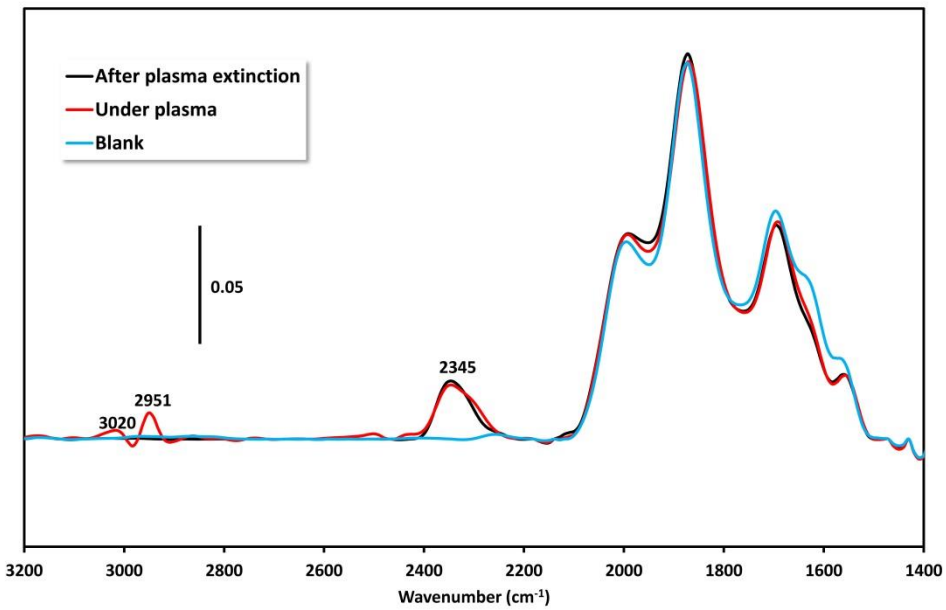

Figure 34 - IR spectra of the USY(40) sample during and after plasma reaction [52].

From the analysis of the spectra from Figure 34, two bands at 3020 and 2951 cm^{-1} that correspond to the v_3 antisymmetric C-H stretching mode of free and adsorbed methane, respectively, can be observed when plasma is under activity, suggesting that in fact there is methane (or methane radicals) adsorption caused by the plasma activity. After extinguishing the plasma, these bands are no longer observed. The band at 2345 cm^{-1} corresponds to the asymmetric stretching vibration of CO_2 [52].

4.3. In-plasma *vs* Post-plasma catalysis

From the experiments described in 3.3.2 was obtained the plot from Figure 35.

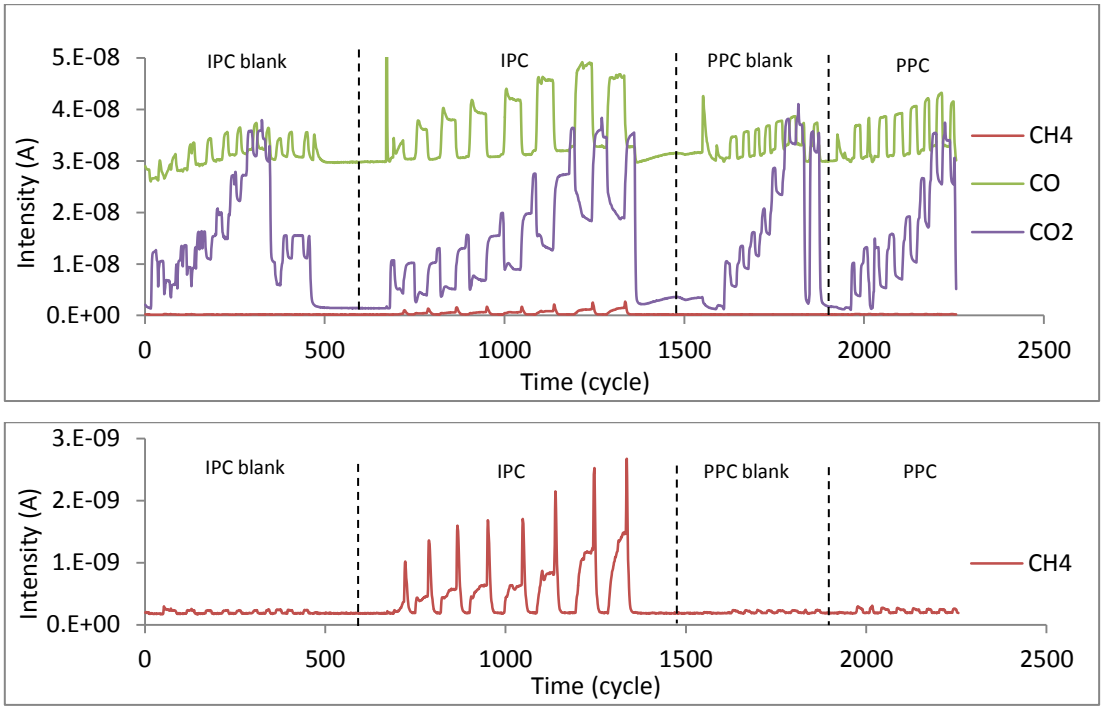

Figure 35 - MS results of the IPC and PPC experiments.

Based on these values, calculating the CO_2 conversion by the same method applied before in chapter 4.2, it is possible to obtain the CO_2 conversion values displayed in Figure 36.

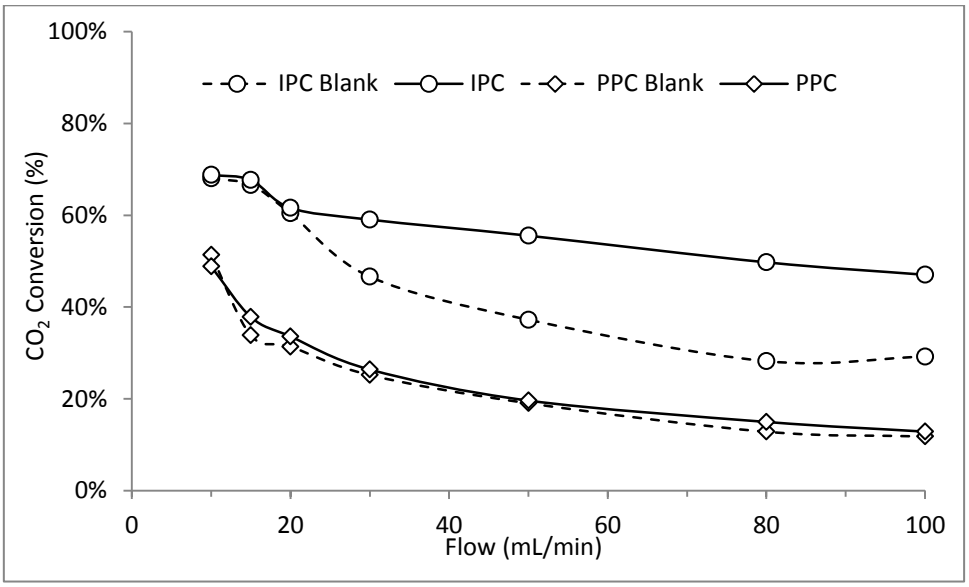

Figure 36 - CO_2 conversion results for the IPC and PPC experiments.

From the comparison of the CO_2 conversion values between IPC and PPC configurations, can be easily observed that IPC, either with our without catalyst reveals greater conversions than the PPC configuration. This performance is justified by the residence time of the inlet gas into the ionized zone inside of the reactor. The IPC configuration has a much bigger volume of the reactor under plasma (≈25.1 cm^3) than in the PPC configuration (3.1≈ cm^3) (Figure 37), which allows the stream to be affected by plasma during a longer time, resulting in more CO_2 plasma inducted dissociation. It has been estimated that the in-plasma residence time for the ICP configuration varies from 73 to 232 ms according with the inlet flow used while the PPC configuration has values ranging from 9 to 29 ms.

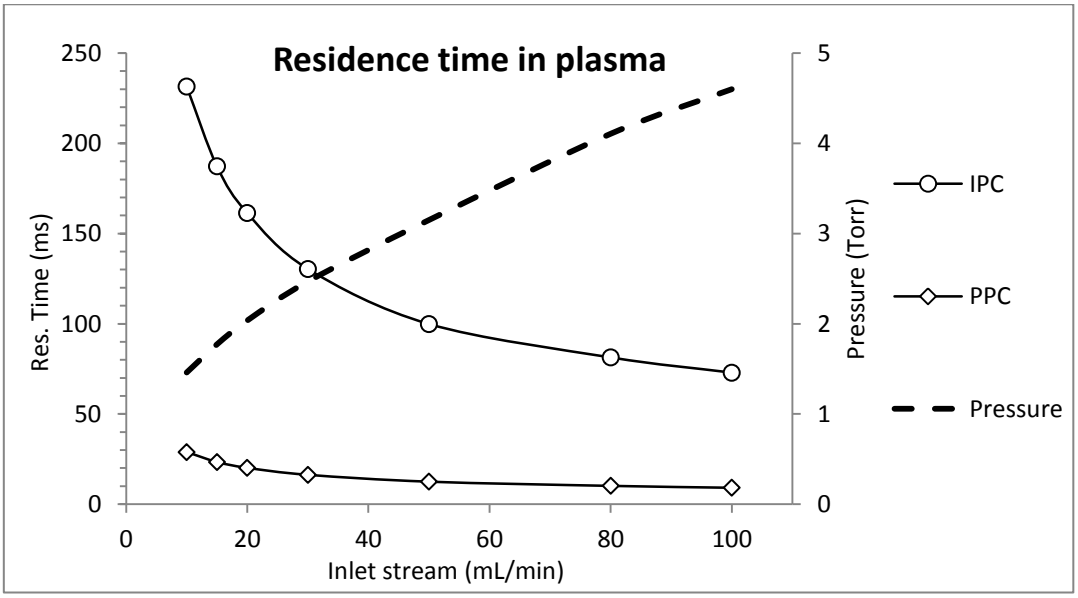

Figure 37 - Residence time in plasma and pressure obtained for each configuration between 10 and 100 mL/min.

Detailed calculations on the residence time in plasma for each experiment in function of the inlet flow are presented in Appendix A11. In IPC system, the presence of catalyst seems to improve significantly the conversion. As explained in chapter 2.6, when plasma is in contact with the catalyst, the properties of both can change. There is formation of hot-spots inside the catalytic bed which can improve CO_2 ionization. The catalytic conversion of CO_2 is also enhanced due to induced adsorption. As seen in Figure 25, the temperature increase tends to favor it. Another factor that can be involved in the better performance of the IPC configuration, in specific in the presence of catalytic bed, is the fact that with this configuration, plasma affects not only the reactants but also the products of the reaction, including water, which is easily dissociated into OH^- and H^+. According with the principle of Le Chatelier, the consumption of the products of the reaction favors consumption of CO_2.

The influence of the residence time of the stream under plasma can also explain the decrease of the overall CO_2 conversion with the increase of the flow.

It was noticed a change of slope of the CO_2 conversion plot for the IPC catalytic system. This variation, which occurs between 20 and 30 mL/min of inlet steam, as proposed in [52], may be explained by the compromise between two factors: the diminution of the residence time of the gas in the plasma discharge zone and the enhancement of the reactions rate by increasing the special

velocity of the ionized stream, and sending a greater amount of reactive species with short lifetimes to the catalyst bed. Between 10 and 20 mL/min the first factor assumes a bigger importance in this equilibrium, causing a more significant conversion decrease as the flow increases. From 30 mL/min onwards the second phenomenon assuming a bigger influence justifies the change in slope to a weaker decrease of consume with higher stream values.

Looking into the results in terms of product selectivity (Figure 38), a similar modification of behavior can be verified between these flow values. As the selectivity of products also seems to be affected by the change in compromise between these two factors, it can be assumed that as more active species are adsorbed into the catalyst, a change in the reaction mechanism may occur in a way that improves CH_4 selectivity [52].

With the PPC configuration, due to the reduced exposure time of the inlet stream to plasma, as well as the absence of plasma-catalyst contact, the CO_2 conversion takes place solely in the gas phase. Besides that, in this configuration there is no adsorption capacity enhancement, resulting on a very low CH_4 productivity.

As the catalyst is the main responsible for the selectivity towards methane, each configuration's blank experiment reveal, as expected, lower CH_4 selectivity than the respective catalytic reaction.

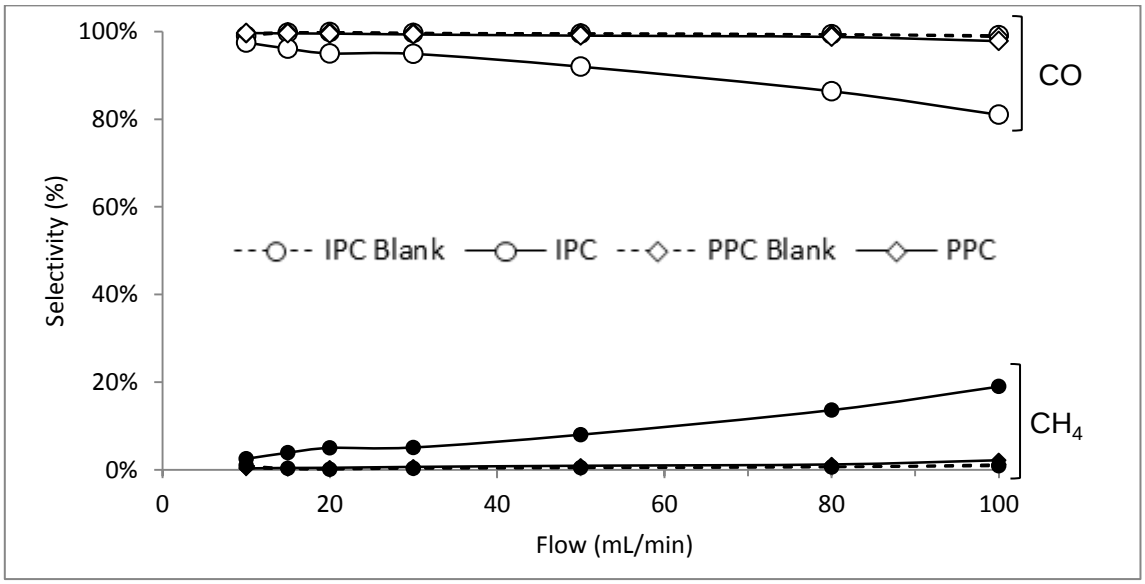

Figure 38 - IPC and PPC Selectivity results towards CH_4 and CO.

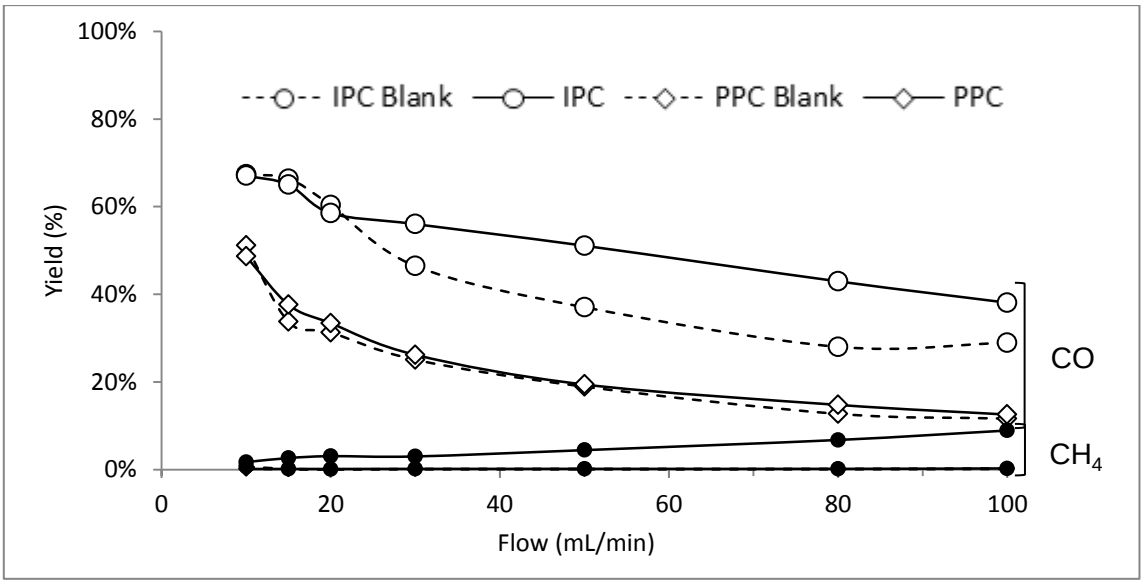

Figure 39 - IPC and PPC yield results towards CH_4 and CO.

In a general scenario, the performance with respect to methane selectivity of the reaction follows the order: IPC_{cat} > IPC_{blank} > PPC_{cat} > PPC_{blank}. The increasing of the inlet flow to the reactor has a positive impact in these results which is more noticeable in the IPC catalytic configuration.

Then, looking into the CH_4 and CO yield of these reactions, Figure 39, calculated by the CO_2 conversion and CH_4 selectivity values, the use of a catalytic bed in the IPC configuration reveals clearly the best yield, which can be clearly seen in Figure 35, reaching approximately 3% at the higher volumetric flow. This configuration is followed by post-plasma catalysis, which achieves nearly 0.5% for the higher inlet flow, and is closely followed for the blank experiments for both configurations.

Based on these results it can be concluded that, despite of the possible benefits of the post plasma catalysis configuration, in this study, in-plasma catalysis revealed to be much more productive, mostly due to the higher residence time of the gas in plasma and due to the plasma-catalyst contact.

In Appendix 10 are presented tables with the results obtained in the IPC *vs* PPC study.

4.4. *Operando* Infrared (IR) measurements

The results obtained by the infrared measurements for each sample are shown in Figures 42 to 46. These measurements were performed before, during and after plasma activity. Afterwards, measurements 5 and 10 minutes after the NTP extinction were done and a final measurement under a flow of pure argon was performed.

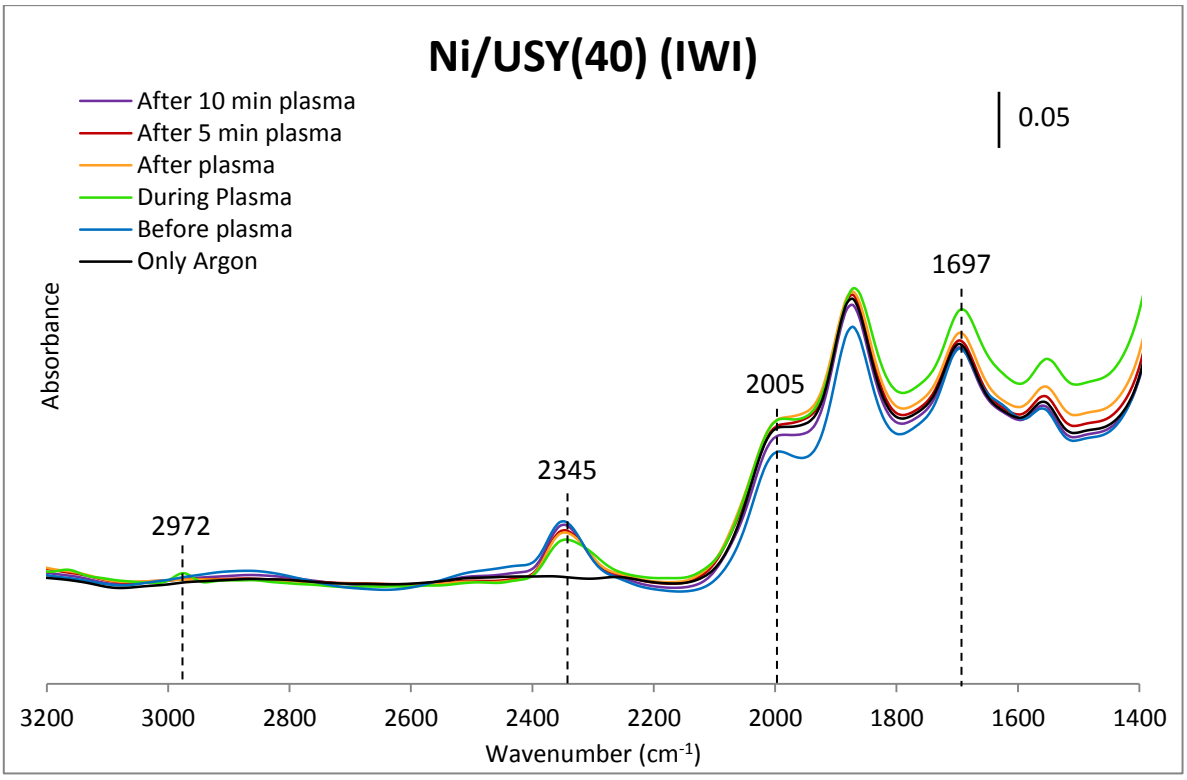

Figure 40 - IR spectra before, during and after plasma activity for the Ni/USY(40) catalyst sample.

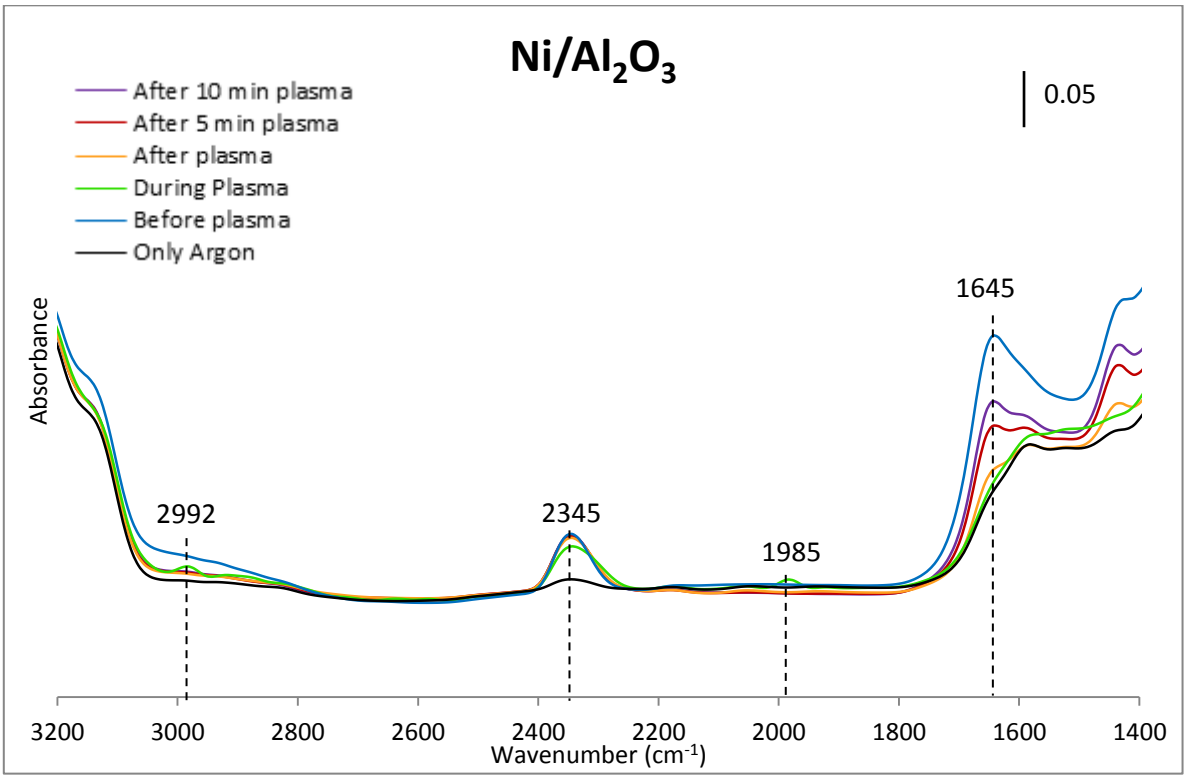

Figure 41- IR spectra before, during and after plasma activity for the Ni/Al2O3 catalyst sample.

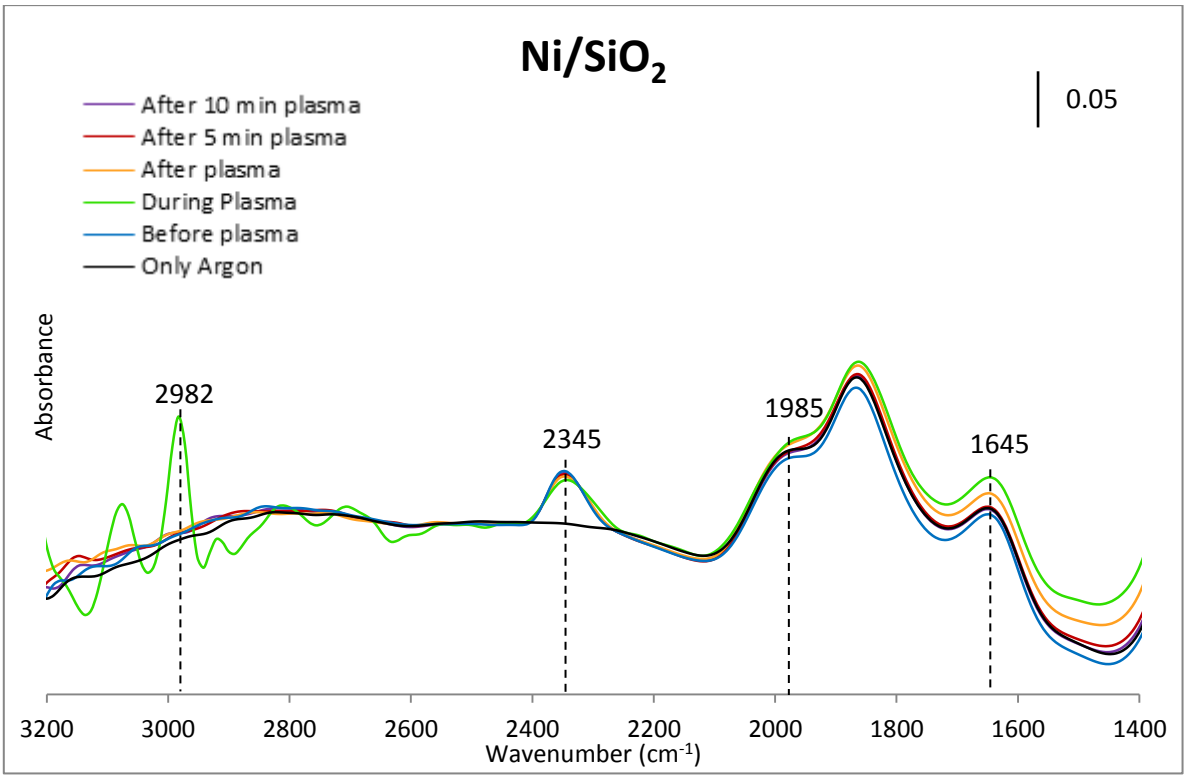

Figure 42 - IR spectra before, during and after plasma activity for the Ni/SiO2 catalyst sample.

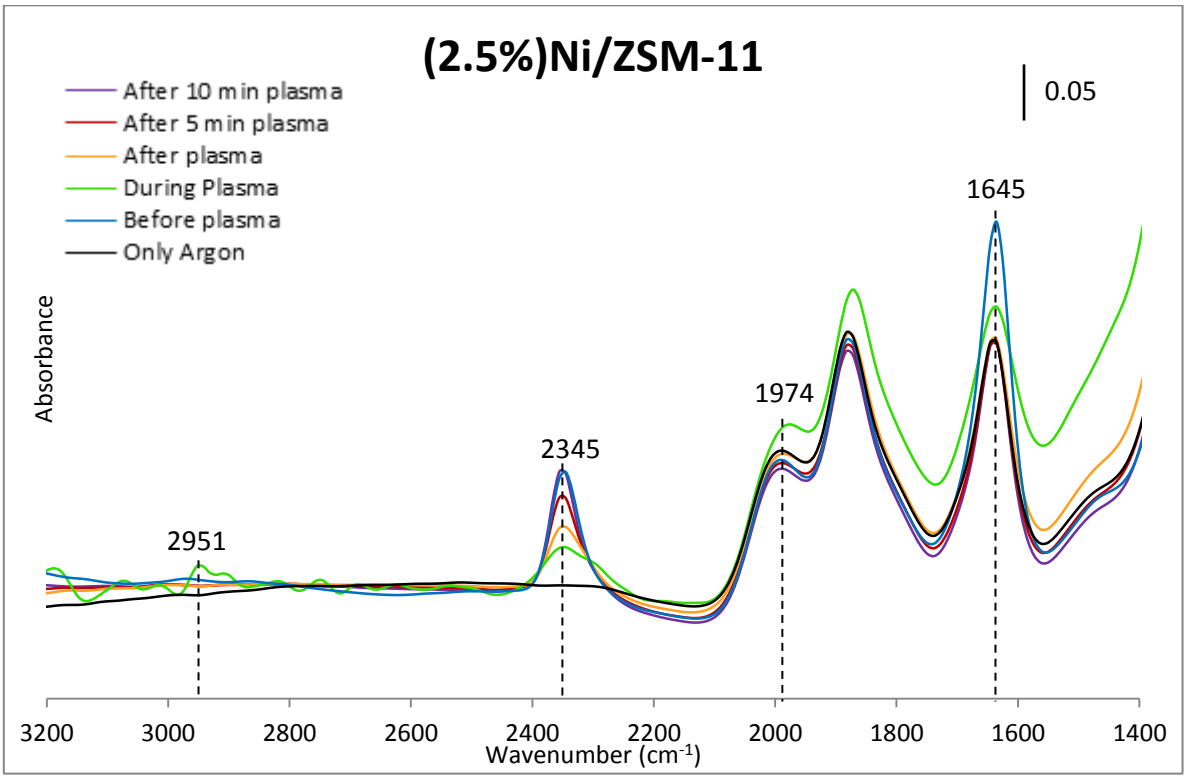

Figure 43 - IR spectra before, during and after plasma activity for the (2.5%)Ni/ZSM-11 catalyst sample.

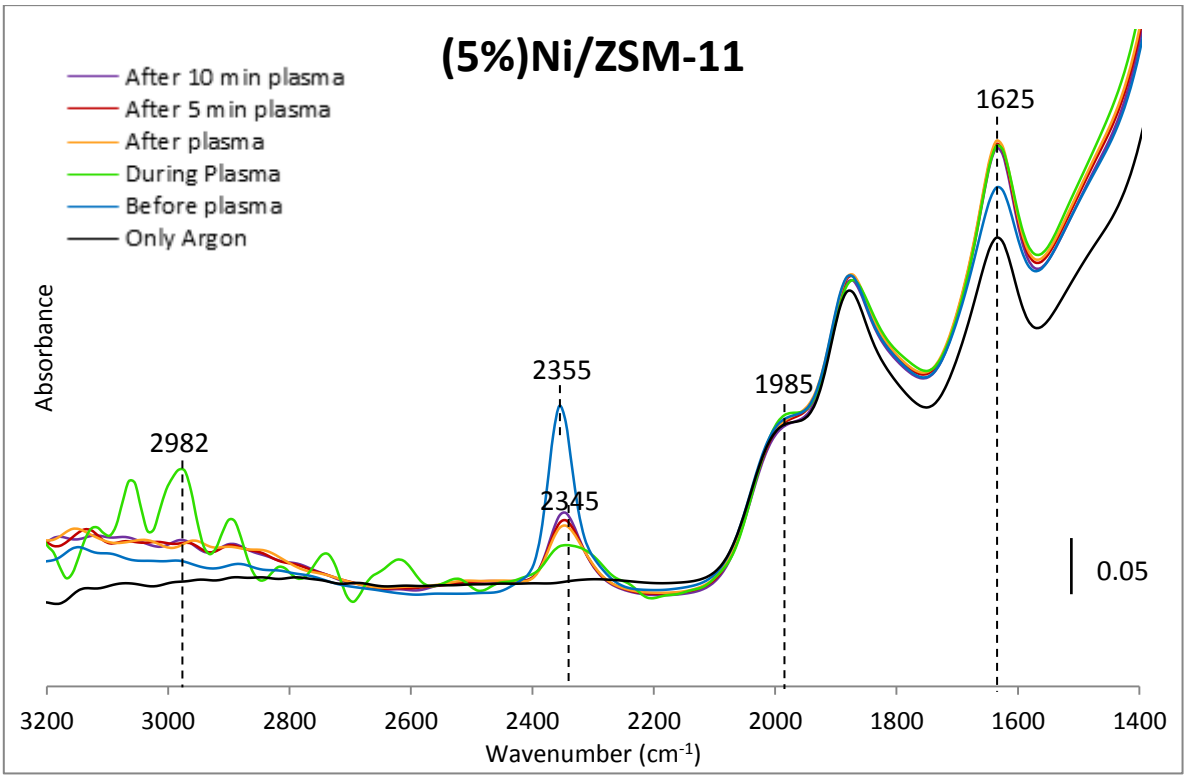

Figure 44 - IR spectra before, during and after plasma activity for the (5%)Ni/ZSM-11 catalyst sample.

It can be noticed that, for every catalyst sample, when the reactants are sent into the reactor, in the measurements performed before plasma activity, a band at 2345 cm^{-1} appears, which is reported to correspond to the asymmetric stretching vibration of CO_2 [11,64]. Both Ar and H_2, the other components of the inlet stream, are not detected by IR as they do not have dipole moment changes. Argon is a noble gas (single atom) and hydrogen, as a diatomic homonuclear molecule, the only vibration mode is the symmetric stretch <-H-H->. Therefore, these species are IR inactive.

Looking into the measurement results performed under plasma, it is evident that plasma triggers the reaction. It was noticed that for every catalyst sample, once the discharge is applied bands at approximately 2980 cm^{-1}, 1980 cm^{-1} and 1645 cm^{-1} appear. These bands are attributed to the υ3 antisymmetric C-H stretching mode of CH_4 [55-57], to the adsorption of CO [19] and to the H-O-H bending mode of H_2O [11,19,68], respectively, all products of the hydrogenation of CO_2. This reveals plasmas influence in the dissociation of carbon dioxide as well as in the further hydrogenation of CO into CH_4.

After plasma extinction the product bands that were noticed to appear during the discharge decrease due to the stopping of the reaction. CO and H_2O bands were noticed to gradually decrease over time. These species have tendency to adsorb in the catalysts due to their polarity. As they are produced, part of these species is stored, and after plasma activity due to these compounds affinity with the catalysts support, they slowly desorb as a consequence of the high vacuum in the system. However, this is not observed in the CH_4 case. It can be noticed in these figures, that the band around 2980 cm^{-1} immediately disappears after the plasma reaction. Methane, as a non-polar molecule, usually is not adsorbed in the catalyst. But, as it was referred before in chapter 4.2.1, plasma induced

adsorption of CH_4 takes place during the reaction. This is evidenced by the methane adsorption band that was observed for every catalyst sample during plasma activity. The absence of CH_4 traces after plasma suggests that, when plasma extinguishes, it quickly desorbs from the catalyst, matching with the methane release hypothesis proposed in [52].

Between 2000 and 1500 cm^{-1} it is possible to observe bands that appear due to the Si atoms interaction present in the support of zeolite (MEL and FAU) and SiO_2 catalysts. In the alumina catalysts case, bands of the Al atoms interaction can be seen between 1700 and 1400 cm^{-1}. These bands can be seen in Figure 45, in which the effect of Si and Al atoms can be seen for different Si/Al ratios [69].

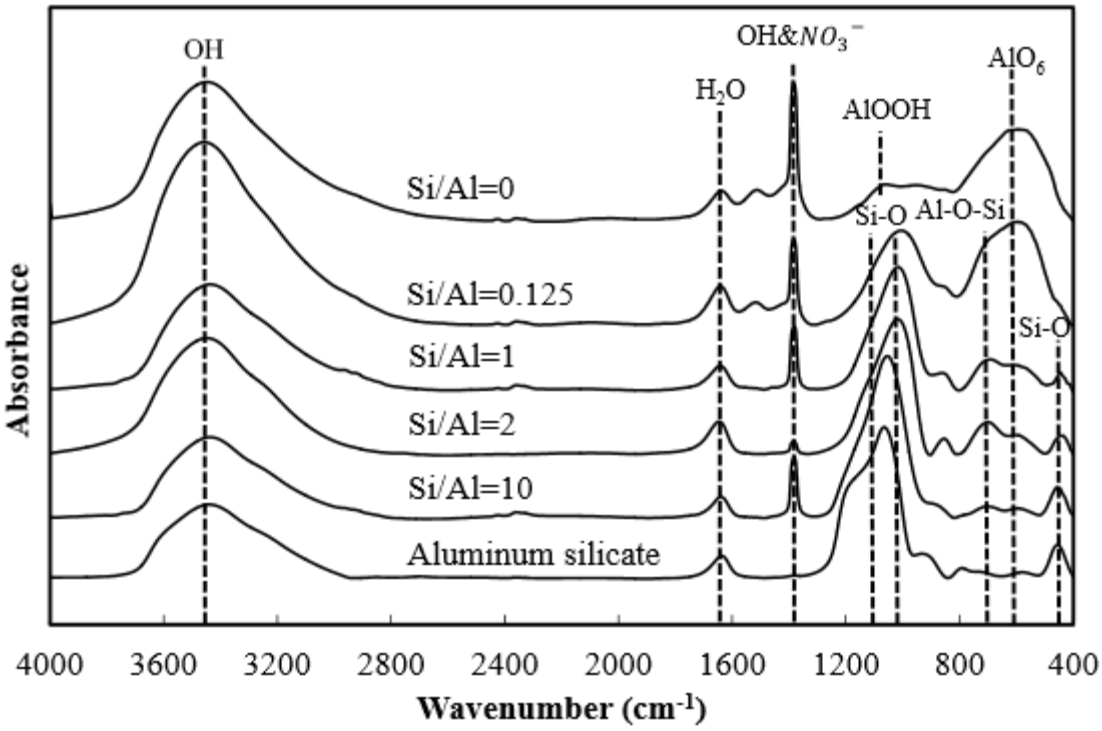

Figure 45 - IR spectra of Si-Al samples with different Si/Al ratios [69].

Despite of the, overall, similar behavior of every catalyst sample, in concern to the plasma influence on the reaction, some differences between the spectra can be analyzed and interpreted. The Ni/Al_2O_3 sample spectra, in comparison to the other samples, revealed lower absorbance values, under plasma, of the peaks at 2992, 1985 and 1645 cm^{-1}, that express CH_4, CO and H_2O (respectively), in comparison to the base values obtained with pure argon. These low intensities suggest, on one hand, low adsorption capacity of these compounds in this sample and, on the other hand, low catalytic activity as low product formation is revealed. The low adsorption capacity of this catalyst can be explained if it is assumed that the plasma interaction with this catalyst does not (or does in very small proportions) enhance the adsorption of species in it. It was already referred that the complex permittivity values of MEL zeolites, with Si/Al=17 are lower than the ones obtained for FAU zeolites [52], with Si/Al ratios of 30 and 40. Then, it can be assumed that the complex permittivity value of each catalyst may be related to its silica and alumina content. Increasing with the content

increase of silica and decreasing as the alumina content decreases. As this catalyst support is solely alumina, a lower plasma induced-adsorption can be anticipated based on these suppositions. This low adsorption associated with its poor Ni^{o}_{frac} value, calculated through the H_2TPR-MS for this sample, can explain the low product formation observed in the IR experiment.

Both ZSM-11 samples presented peaks of higher intensity than the other sampes. This can be explained by the lower Ni load of these catalysts (2.5 and 5 wt.%), compared with that of the remaining samples (14 wt.%), which diminishes the opacity of the samples leading to more intense readings.

Taking a look at Figure 46, the IR spectra under plasma of each sample can be compared in order to have a better look at the behavior of the different catalyst samples during the reaction.

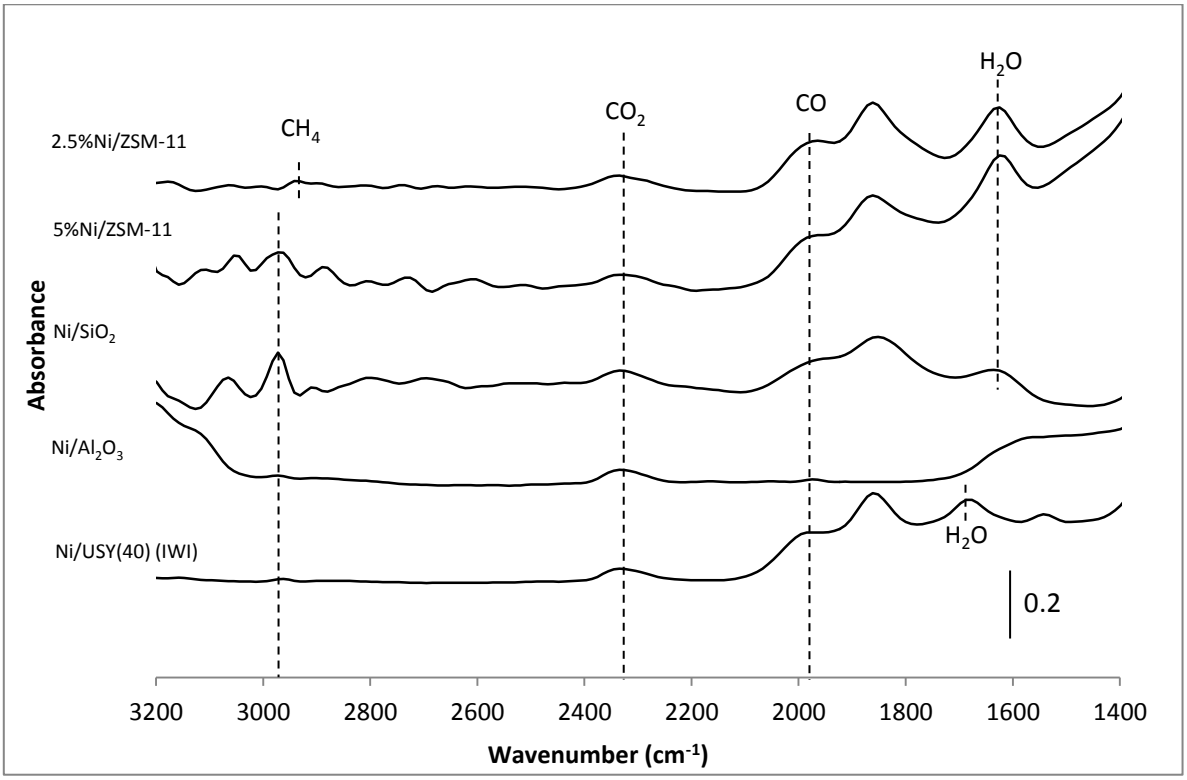

Figure 46 – IR spectra during plasma activity for every catalyst sample analyzed.

In this figure the poor activity of the Ni/Al_2O_3 sample is evidenced by the low intensity of the bands that represent the reactions products. The methane corresponding band (≈2982cm^{-1}) exhibits a very low absorbance as well as the bands that were attributed to CO (≈1980 cm^{-1}) and H_2O (≈ 1640 cm^{-1}) in the catalyst.

Based on the mass spectrometer reading of these experiments, CO_2 conversion as well as CO and CH_4 selectivity and yield values were determined. The results obtained are summed in Table 13. All the yield values were normalized for a catalyst mass of 18 mg, which is the approximate mass of the wafers used in each experiment.

Table 13 - CO_2 conversion, CO and CH_4 selectivity and yield resuts.

	Ni/USY(40)(IWI)	Ni/Al_2O_3	Ni/SiO_2	(5%)Ni/ZSM-11	(2.5%)Ni/ZSM-11
CO_2 Conversion (%)	56.2	55.9	56.1	54.4	55.7
CH_4 Selectivity (%)	3.4	1.5	1.7	1.2	1.8
CH_4 Yield (%)	1.9	0.9	1.0	0.7	1.0
CO Selectivity (%)	96.6	98.5	98.3	98.8	98.2
CO Yield (%)	54.3	55.0	55.2	53.7	54.7

Very similar CO_2 conversion values were obtained for every catalyst sample. As it was verified before, in chapter 4.3, when the reaction is performed under plasma activity, CO_2 dissociation takes place in the gaseous phase. The catalyst does not assume a great importance in this step of the reaction. However, it assumes a bigger importance in the selectivity towards methane. The best performance in terms of CH_4 selectivity was clearly obtained for the USY(40) sample that due its high nickel content and Ni^o_{frac} improves the catalysts capacity to hydrogenate the CO molecules that are originated by the dissociation of CO_2. This catalyst is followed by 2.5%Ni/ZSM-11 which slightly surpasses the silica supported catalyst. Just like the FAU sample, the Ni/SiO_2 catalyst was prepared with 14 wt. % of Nickel and with the incipient wetness impregnation method which allowed achieving high reduced Ni contents. However, the ZSM-11 catalyst with less Ni^o_{frac} and a nickel content of only 2.5% was able to achieve better methane selectivity values. The explanation for these results relies on the difference between the structures of the zeolite and that of SiO_2. The alumina present in ZSM-11 zeolites increases the basicity of the catalyst and interacts more strongly with the carbon oxides, favoring the hydrogenation into methane. The lower values obtained for the alumina and 5%Ni/ZSM-11 samples are justified by their low reduced nickel amount. Between these two catalysts, the higher CH_4 selectivity obtained with Ni/Al_2O_3 can be related with its higher alumina content and nickel load.

5. Conclusions and future perspectives

In this work the study of the CO_2 methanation reaction was focused on some main aspects such as the effects of: the framework type of the catalyst, its nickel content, reduced Ni fraction and impregnation method used, the operating conditions at which the reaction is carried, the application of plasma to the reaction and the way it is used.

The catalysts characterization was performed with the USY and the MEL catalysts. Its results revealed that zeolite properties like micro- and mesoporous volume as well as the surface area, are influenced by the zeolite framework, by the Si/Al ratio and Ni load of each catalyst. Pore volume and surface area were found to decrease as more Ni^{2+} is hosted in the exchangeable sites of the zeolite. Higher alumina content of the zeolite increases its negative charge and promotes the deposition of Ni under the form of cations. Higher amounts of nickel also were found to increase the Ni^{2+} quantity in the catalyst. These results reveal that despite of the positive influence of the higher Ni load in the amount of Ni^o obtained after reduction, it has a negative influence in the properties of the zeolite. In order to define the optimal Ni quantity in each zeolite, the compromise between these two aspects must be studied.

SEM images of the nickel-loaded FAU and MEL zeolites revealed crystal sizes of 500 and 250 nm respectively. The lower values obtained for the ZMS-11 samples explains their lower external surface areas. The nickel oxide agglomerates, with ≈50 nm in these images were also found to be proportional to the Ni load of each catalyst.

The H_2TPR-MS experiments conducted revealed that the metallic nickel content in each catalyst after reduction mainly depends on two factors: the alumina content of the zeolite and the impregnation method used in the deposition of the metal in the zeolite. Unlike NiO, Ni^{2+} species require higher temperatures to be reduced. Due to the positive alumina content effect on Ni^{2+} hostage, its increase leads to lower metal reduction levels. The higher reduced Ni amount obtained for the USY(40)(IWI) sample in comparison to the USY(40) sample suggests that the incipient wetness impregnation allows achieving a more effective nickel spreading in the zeolite structure.

The catalytic tests carried in the packed-bed reactor in which the conventional heating reaction was compared to a plasma-assisted one showed that, during conventional heating operation, the catalytic conversion of CO_2 tends to increase with the temperature. At temperatures below 400ºC the conversion of carbon dioxide ranged between 0 and 25% as a consequence of the high activation energy that is necessary to dissociate the stable CO_2 molecule. From this temperature on the conversion values seem to increase noticeably. 48% of CO_2 conversion was achieved at 450ºC for the USY(40)(IWI) catalyst, being very close to the thermodynamic value estimated for this temperature and pressure. By comparison between the several catalysts used a global trend of higher conversions being linked to higher Ni^o content was verified. In conventional heating the CO_2 molecules are adsorbed in the catalyst and are reduced to CO and CH_4 by reacting with the hydrogen that is adsorbed in the Ni^o particles. Higher Ni^o content means greater facility in converting carbon dioxide. These results evidence the importance of the nickel load and Ni^o_{frac}, especially this last one, of a catalyst in the catalytic activity.

Looking at the results in terms of selectivity, under conventional heating operation a maximum of methane selectivity was observed at 350ºC. It was found to decrease after this temperature due to the thermodynamically favored RWGS reaction which is a concurrent reaction of the CO_2 methanation. A maximum value of 47% was obtained for the USY(40)(IWI) catalyst, which was the more active one. It can also be related with the high-temperature induced desorption of the species in the zeolite compromising the catalytic activity towards CH_4 formation. As adsorption capacity is also known to affect the selectivity of the reaction, the close values obtained for the 14%Ni/USY(30) and 2.5%Ni/ZSM-11 samples (26% for 350ºC) also suggest that MEL zeolites have a higher adsorption capacity than FAU and/or more CO_2 methanation active sites in detriment of those that favor the RWGS reaction. This conclusion is based on the similar results obtained for these two samples despite of the much lower total Ni load of ZSM-11 as well as Ni^o content.

When the reaction was performed with plasma-assistance different behaviors were observed for both CO_2 conversion and selectivity towards products. Unlike what was observed for the conventional case scenario, under plasma, the temperature effect in CO_2 conversion was not found to be so relevant. The dissociation of carbon dioxide under plasma was found to occur due to its ionization by the plasma discharge. Conversions between 60 and 70% were obtained for temperatures between 125 (NTP temperature) and 350ºC. Then, plasma is able to dissociate CO_2 in a more effective and efficient way than conventional heating. The thermodynamic equilibrium conversion was trespassed due to the formation of highly reactive species consequent of plasma ionization of the reactional mixture. In terms of catalyst comparison, the conversion values obtained with the analyzed catalysts were found to differ based on the zeolite used. FAU zeolites achieved conversion values of ≈64% while MEL zeolites achieved ≈67%. This slight difference is related to the interactions between plasma and catalyst. These interactions consume part of the energy of plasma, thus, decreasing the amount of energy applied to CO_2 dissociation. The strength of these interactions is influenced by the complex permittivity of each zeolite which was found to be greater for FAU zeolites. However, these interactions were found to enhance the adsorption capacity of the catalysts during plasma activity. This effect was verified by the little higher CH_4 selectivity that was obtained under plasma for the USY catalysts.

Overall, the application of plasma to the hydrogenation of CO_2 increases significantly the conversion of CO_2 while decreasing the selectivity towards methane. Analysing the yield of both kinds of reaction towards the obtained products it was possible to observe that at an optimal temperature of 200ºC plasma was able to reach CH_4 yield values of 6% (using the USY(40)(IWI) catalyst) while values near 0% are obtained in conventional heating conditions for the same temperature. The plasma-assisted reaction methane yield values at this temperature are found to match or even surpass those obtained under thermal operation at its optimal temperature of 400ºC, with the exception of the most active catalyst. Hereby, the methanation of CO_2 is found to be performed in a more energy efficient way since it can be performed at 200ºC less than the conventional heating reaction without achieving worse results. NTP is also found to be beneficial for the catalysts health by preventing its poisoning or sintering.

Despite of the obtained CH_4 selectivity and its consequent yield being below 10% for conventional heating and plasma experiments, the conversion of CO_2 into CO, which together with CH_4 were the only observed products, is also very interesting in an industrial point of view. CO and H_2 can be applied to synthesis gas chemistry to the production of liquid hydrocarbon fuels or other chemical products. A resulting stream containing high quantities of CO together with CH_4 as well as some unconverted H_2 and CO_2 can be submitted to separation processes in order to recuperate the products or can even be applied to some chemical processes as syngas without further separation.

In terms of catalyst comparison, USY(40)(IWI) achieved the best results, followed by USY(40) which presented the same Ni load but less Ni^o_{frac}. USY(30) was found to have a slightly worse performance due to its lower Si/Al ratio (higher Al content) which promotes the hostage of Ni^{2+} and lowers the Ni^o content after reduction. This catalyst was followed by 2.5%Ni/ZSM-11 and finally 5%Ni/ZSM-11 which revealed the lowest Ni^o content and the worst activity. This catalytic-performance order was observed for both conventional heating and plasma-assisted reactions in respect to methane production.

Methane storage and release phenomena were observed during and after, respectively, plasma-activity when the discharge is created across the catalyst bed. It was noticed that without considering the released CH_4 upon plasma extinction the carbon balance to the reactor would reach 99% instead of 100%. IR measurements performed before, during and after plasma-activity proofed these phenomena to be a consequence of the plasma-catalyst interaction which induces the adsorption of methane on the zeolite during the discharge under the form of methyl groups. Upon the extinction of plasma, the adsorbed methane radicals are thought to react with the dissociated hydrogen on the surface of the metallic nickel of the catalyst and desorb as CH_4. These were previously unreported occurrences that were found to highly affect the methane yield of the reaction. It was estimated that the amount of CH_4 that is trapped in the catalyst during plasma activity would be ≈44% of the total produced amount. It was found to have greater importance to catalysts that are strongly affected by plasma such as the FAU zeolite catalysts. These phenomena are very interesting since they suggest that if the trapping and release of CH_4 are better understood the reaction conditions can be optimized in order to take full advantage of it, making it possible to achieve even higher methane yield values.

The IPC *vs* PPC experiments carried out with the USY(40) catalyst revealed the importance of the plasma-catalyst interactions as well as the flow effect in the reaction. In terms of CO_2 conversion, two main aspects were identified as relevant on the results obtained: the residence time of the reactional mixture in plasma and the plasma-catalyst interactions. The flow increase led to a decrease of CO_2 conversion as a consequence of the diminution of the contact time between the gas and the discharge. This conclusion was supported by the comparison between conversion values while using the IPC and PPC configurations. Values of residence time ranging between 73 and 232 ms for the IPC configuration and 9-29 ms for the PPC. Lower contact times between plasma and reactional mixture lead to lower CO_2 dissociation. The fact that considerable conversion values were achieved with the blank experiments (69% and 49% at 10 mL/min for IPC and PPC blank experiments, respectively) supports the idea that under plasma activity the CO_2 dissociation occurs mainly in the gas phase. The

comparison of both configurations with the respective blank experiments revealed a considerable catalyst effect while performing the reaction in an in-plasma catalysis system. The presence of catalyst pellets allowed higher CO_2 conversion values to be achieved. Probably this is due to micro-discharges that occur across the catalytic bed which create localized heating (hot-spots) and enhance the dissociation of CO_2.

A modification in the reaction mechanism was observed with the volumetric flow increase in the IPC configuration. For flows above 30 mL/min it is thought that the reaction rate is increased by sending a higher amount of plasma-created reactive species with short lifetimes. These species, due to their high excitation state may provide an alternative pathway to the reaction which is supported by the change of CO_2 and selectivity observed above this flow.

A selectivity analysis to this set of experiments supports the idea that catalyst plays a very active role in the production of methane from the dissociated species which are created by CO_2 ionization under plasma. A considerable amount of produced CH_4 was only verified for the IPC configuration with catalyst. CH_4 selectivity is found to increase with the flow

The blank experiments exhibited CO selectivity values of almost 100% due to the absence of catalyst and the PPC catalytic experiment revealed similar values since the active species created by plasma were not able to reach the catalyst before the end of their lifetime.

In terms of yield, for both products the observed trend was IPC>>IPC_{blank}>PPC>PPC_{blank}. The volumetric flow was observed to favor methane production, increasing its yield from 0 to 9 (IPC), while decreasing that of CO from 67 to 38% (IPC), at 10 and 100 mL/min, respectively.

The catalytic activity study within the IR cell revealed that, in respect to methane production, Ni/USY(40)(IWI)>2.5%Ni/ZSM-11>Ni/SiO_2>Ni/AL_2O_3>5%Ni/ZSM-11. As before, the USY(40)(IWI) catalyst was the most active due to its high Ni load and Ni^o_{frac}. The 2.5%Ni/ZSM-11 sample, despite having a much lower Ni content and also lower Ni^o_{frac} than the Ni/SiO_2 sample, revealed a slightly higher yield towards methane which can be explained by the Si/Al ratio as alumina increases the catalyst basicity, interacting strongly with carbon oxides. The low Ni^o content of the Ni/Al_2O_3 5%Ni/ZSM-11 led to their lower performance. The first catalyst revealed a slightly better performance than the last due to its little higher Ni^o amount and the higher alumina content of the support.

Based on the results and conclusions achieved through this work there are some aspects which future study may be of interest. One of them being the study/development of an optimal catalyst for its application in plasma-assisted hydrogenation of CO_2 based on the characteristics that were found to have greater influence in the catalytic activity such as: Ni load and reduction level, framework type and Si/Al ratio. The study of the CO_2 hydrogenation mechanism under plasma and the lifetime of the active species created in the discharge as well as a study about the plasma-catalyst interactions that may occur could also be of some interest in order to fully understand phenomena such as the methane storage and release. This knowledge may be useful in the development of catalysts and to set the properties of the plasma discharge in a more efficient way. Further optimization of the reactional can also be done by studying with more detail the effect of parameters such as: pressure, temperature, residence time, reactional mixture composition, catalyst mass as well as plasma type and volume.

References

[1] http://www.bp.com/en/global/corporate/energy-economics/statistical-review-of-world-energy/2014-in-review.html. [Accessed: Oct-2015]

[2] REN21, “Renewables 2012 Global Status Report 2012,” p. 172, 2012

[3] http://www.conserve-energy-future.com/advantages-and-disadvantages-of-renewable-energy.php. [Accessed: Oct-2015]

[4] EPA, http://www.epa.gov/climatechange/ghgemissions/gases/co2.html. [Accessed: Oct-2015].

[5] J. B. Sabatier, P. Senderens, Acad. Sci. 1902

[6] S. Hwang, J. Lee, U. G. Hong, J. G. Seo, J. Ind. Eng. Chem., vol. 17, no. 1, pp. 154–157, 2011

[7] S. Rahmani, M. Rezaei, and F. Meshkani, J. Ind. Eng. Chem., vol. 20, no. 4, pp. 1346–1352, 2014

[8] N. E. A. A. PSI, “Trends in global CO2 emissions, 2014 Report,” 2014

[9] IPCC, “Fourth Assessment Report,” 2007

[10] M. A. A. Aziz, A. A. Jalil, S. Triwahyono, and M. W. A. Saad, Chem. Eng. J., vol. 260, pp. 757–764, 2015

[11] A. Westermann, B. Azambre, M. C. Bacariza, I. Graça, M. F. Ribeiro, J. M. Lopes, and C. Henriques, Appl. Catal. B Environ., vol. 174–175, pp. 120–125, 2015

[12] J. Gao, Y. Wang, Y. Ping, D. Hu, G. Xu, F. Gu, and F. Su, RSC Adv., vol. 2, no. 6, p. 2358, 2012

[13] M. Jacquemin, A. Beuls, and P. Ruiz, Catal. Today, vol. 157, no. 1–4, pp. 462–466, 2010

[14] A. Wokaun, Phys. Chem. Chem. Phys., pp. 5071–5080, 1999

[15] L. Cerveny, Catalytic Hydrogenation, vol. 27. 1986

[16] J.-N. Park and E. W. McFarland, J. Catal., vol. 266, no. 1, pp. 92–97, 2009

[17] I. Graça, L. V. González, M. C. Bacariza, a. Fernandes, C. Henriques, J. M. Lopes, and M. F. Ribeiro, Appl. Catal. B Environ., vol. 147, pp. 101–110, 2014

[18] P. A. U. Aldana, F. Ocampo, K. Kobl, B. Louis, F. Thibault-Starzyk, M. Daturi, P. Bazin, S. Thomas, and a. C. Roger, Catal. Today, vol. 215, pp. 201–207, 2013

[19] S. Tada, O. J. Ochieng, R. Kikuchi, T. Haneda, and H. Kameyama, Int. J. Hydrogen Energy, vol. 39, no. 19, pp. 10090–10100, 2014

[20] M. Guo and G. Lu, Catal. Commun., vol. 54, pp. 55–60, 2014

[21] A. Westermann, B. Azambre, M. C. Bacariza, I. Graça, M. F. Ribeiro, J. M. Lopes, and C. Henriques, Appl. Catal. B Environ., vol. 174–175, pp. 120–125, 2015

[22] H. Liu, X. Zou, X. Wang, X. Lu, and W. Ding, J. Nat. Gas Chem., vol. 21, no. 6, pp. 703–707, 2012

[23] F.-W. Chang, M.-T. Tsay, and S.-P. Liang, Appl. Catal. A Gen., vol. 209, no. 1–2, pp. 217–227, 2001

[24] C. Jia, J. Gao, J. Li, F. Gu, G. Xu, Z. Zhong, and F. Su, Catal. Sci. Technol., vol. 3, no. 2, pp. 490–499, 2013

[25] “Recognizing the Best in Innovation: Breakthrough Catalyst,” R&D Mag., no. September, p. 20, 2005

[26] F. A. Jury, “Préparation et Caractérisation de Zéolithes Dopées par des Métaux de Transition” 2013

[27] IZA Structure Commission, http://www.iza-structure.org/; [Accessed: Oct-2015]

[28] E. Jwa, S. B. Lee, H. W. Lee, and Y. S. Mok, Fuel Process. Technol., vol. 108, pp. 89–93, 2013

[29] M. Magureanu and P. Lukes, Plasma Chemistry and Catalysis in Gases and Liquids. 2013

[30] O. Martín-Belloso and R. Soliva-Fortuny, Nonthermal Processing Technologies for Food. 2010
[31] E. C. Neyts and A. Bogaerts, J. Phys. D. Appl. Phys., vol. 47, no. 22, p. 224010, 2014.
[32] W. Somers, a. Bogaerts, a. C. T. van Duin, and E. C. Neyts, Appl. Catal. B Environ., vol. 154–155, pp. 1–8, 2014
[33] U. Roland, F. Holzer, and F. D. Kopinke, Appl. Catal. B Environ., vol. 58, no. 3–4, pp. 217–226, 2005.
[34] Y. F. Guo, D. Q. Ye, K. F. Chen, and J. C. He, Catal. Today, vol. 126, no. 3–4 SPEC. ISS., pp. 328–337, 2007
[35] H. L. Chen, H. M. Lee, and S. H. Chen, Ind. Eng. Chem. Res., vol. 47, no. 7, pp. 2122–2130, 2008
[36] Y.-P. Zhang, P.-S. Ma, X. Zhu, C.-J. Liu, and Y. Shen, Catal. Commun., vol. 5, no. 1, pp. 35–39, 2004
[37] M. Young Sun, K. Ho-Chul, K. Dong Jun, S. Dong Nam, and B. Joon Hyun, J. Korean Phys. Soc., vol. 57, no. 3, p. 451, 2010
[38] H. K. Song, J.-W. Choi, S. H. Yue, H. Lee, and B.-K. Na, Catal. Today, vol. 89, no. 1–2, pp. 27–33, 2004
[39] J. C. Whitehead, Pure Appl. Chem., vol. 82, no. 6, pp. 1329–1336, 2010.
[40] H. H. Kim, A. Ogata, and S. Futamura, IEEE Trans. Plasma Sci., vol. 34, no. 3 PART 3, pp. 984–995, 2006
[41] L. Grond, P. Schulze, and J. Holstein, DNV Kema, vol. GCS 13.R.2, pp. 1–70, 2013
[42] O. Strohbach, “Wolrd premiere: Audi opens power-to-gas facility.” 2013
[43] B. Stefansson, “emissions to methanol Brief history of CRI,” 2015
[44] http://www.sunfire.de/; [Accessed: Oct-2015]
[45] S. H. Jensen, C. Graves, M. Mogensen, C. Wendel, R. Braun, G. Hughes, Z. Gao, and S. a. Barnett, Energy Environ. Sci., 2015
[46] M. Sterner, M. Jentsch, and U. Holzhammer, “Energiewirtschaftliche und ökologische Bewertung eines Windgas-Angebotes,” p. 46, 2011
[47] http://www.materialsviews.com/race-for-a-co2-to-fuel-technology/; [Accessed: Oct-2015]
[48] Sunfire, “sunfire GmbH / Hintergrund Allgemein,” 2015
[49] http://cleantechnica.com/2014/11/24/power-liquids-demonstration-plant-opens-dresden/; [Accessed: Oct-2015]
[50] S. Becker and L. Sebastian, “Power-To-Liquids,” Fact Sheet, p. 1237, 2015
[51] J. Haber, J. H. Block, and B. Delmon, Pure Appl. Chem., vol. 67, no. 8–9, pp. 1257–1306, 1995
[52] F. Azzolina Jury and F. Thibault-starzyk, “Plasma effects on CO 2 hydrogenation over Ni-based zeolites under high vacuum", Unpublished work
[53] X. Zhang, W. Sun, and W. Chu, J. Fuel Chem. Technol., vol. 41, no. 1, pp. 96–101, 2013.
[54] X. Yan, Y. Liu, B. Zhao, Z. Wang, Y. Wang, and C. Liu, Int. J. Hydrogen Energy, vol. 38, no. 5, pp. 2283–2291, 2013
[55] D. Rankovic, M. Kuzmanovic, M. S. Pavlovic, M. Stoiljkovic, and J. Savovic, “Properties of Argon–Nitrogen Atmospheric Pressure DC Arc Plasma,” Plasma Chem. Plasma Process., 2015
[56] http://cronodon.com/Atomic/AtomTech3.html; [Accessed: Oct-2015]
[57] https://en.wikipedia.org/wiki/Paschen’s_law#/; [Accessed: Oct-2015]
[58] L. Yingxin, C. Jixiang, and Z. Jiyan, Chinese J. Chem. Eng., vol. 15, no. 1, pp. 63–67, 2007
[59] M. Leštinský and K. Hensel, IEEE Trans. plasma Sci., vol. 39, no. 2186–2187, 2011
[60] M. Heintze and B. Pietruszka, Catal. Today, vol. 89, no. 1–2, pp. 21–25, 2004
[61] B. Lu, K. Kawamoto, J. of Envir. Chemical Engineering, Vol.1, Issue 3, September 2013, p.300-309

[62] F. Azzolina Jury, I. Polaert, L. Estel, and L. B. Pierella, Appl. Catal. A Gen., vol. 453, pp. 92–101, 2013
[63] F. Azzolina Jury, I. Polaert, L. B. Pierella, and L. Estel, Int. J. Chem. React. Eng., vol. 13, no. 2, pp. 169–175, 2015
[64] L. Ohlin, P. Bazin, F. Thibault-Starzyk, J. Hedlund, and M. Grahn, J. Phys. Chem. C, vol. 117, no. 33, pp. 16972–16982, 2013
[65] L. Y. Chen, L. W. Lin, Z. S. Xu, T. Zhang, Q. Xin, P. L. Ying, G. Q. Li, and C. Li, J. Catal., vol. 161, no. 1, pp. 107–114, 1996
[66] D. Scarano, S. Bertarione, G. Spoto, a. Zecchina, and C. Otero Areán, Thin Solid Films, vol. 400, no. 1–2, pp. 50–55, 2001
[67] M. Kimura, T. Miyao, S. Komori, A. Chen, K. Higashiyama, H. Yamashita, and M. Watanabe, Appl. Catal. A Gen., vol. 379, no. 1–2, pp. 182–187, 2010
[68] M. A. A. Aziz, A. A. Jalil, S. Triwahyono, R. R. Mukti, Y. H. Taufiq-Yap, and M. R. Sazegar, Appl. Catal. B Environ., vol. 147, pp. 359–368, 2014
[69] C. Tokoro, S. Suzuki, D. Haraguchi, and S. Izawa, Materials (Basel), vol. 7, no. 2, pp. 1084–1096, 2014
[70] https://en.wikipedia.org/wiki/Catalysis; [Accessed: Oct-2015]
[71] Micromeritics Instrument Corporation, “Gas Adsorption Theory,” p. 1, 1AD
[72] http://particle.dk/methods-analytical-laboratory/surface-area-bet/surface-area-bet-theory/; [Accessed: Oct-2015]
[73] M. Birkholz, “Thin Film Analysis,” no. WILEY-VCH Verlag GmbH & Co. KGaA, Weinheim, 2006
[74] http://web.pdx.edu/~pmoeck/phy381/Topic5a-XRD.pdf; [Accessed: Oct-2015]
[75] G. A. Lomi, E. E. Ki, G. C. Bo, R. P. Marinkovi, N. Sad, and B. C. Lazara, System, vol. 280, pp. 67–77, 2004
[76] T. Jones, “EXPLOSIVE NATURE PARTIAL-PRESSURE VACUUM Case Study :,” no. February, pp. 43–46, 2009
[77] D.H. Kim, S. W. Han, J. Ind. Engineering Chemistry, 2015, p.67-71
[78] F. Bustamante, R. Enick, Fuel Chemistry Division Preprints, 2002, 47(2), p.663-664
[79] K. Oshima, T. Shinagawa, Cat. Today, Vol. 232, Sept. 2014, p.27-32
[80] W. Wang, Y. Zhang, Cat. Today, Vol, 259, Jan. 2016, p.402-408
[81] www.personal.utulsa.edu; [Accessed: Dec-2015]
[82] F. Azzolina-Jury, “Préparation et caractérisation de zéolithes dopées par des métaux de transition”, Institut National des Sciences Appliquées de Rouen

This page was intentionally left blank

Appendixes

A1 - Catalysis Principles

Catalysis is the modification of a chemical reaction rate caused by the reactant species interaction with a substance which remains chemically unchanged at the end of the reaction (catalyst). The presence of a catalyst provides an alternative reactional mechanism with lower activation energy than the one without catalyst. This is schematized in Figure A1. 1 with X and Y represent reactants and Z the product of the reaction.

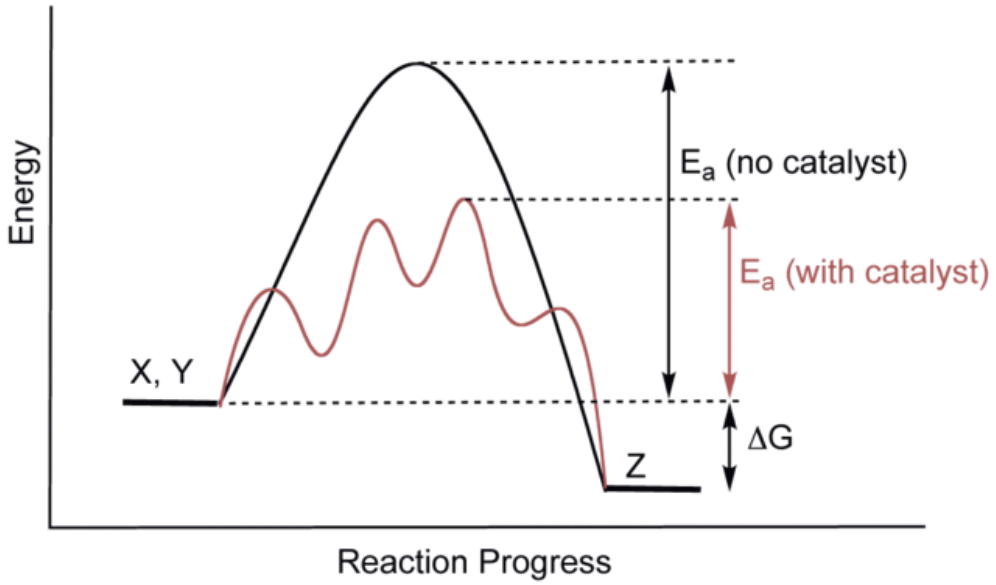

Figure A1. 1 - Influence of catalysis in the potential energy of a reaction [70].

As a catalyst, by definition, is not consumed by the reaction, usually, low amounts of it are necessary to obtain significant changes in the reaction rate. However, the catalyst can be affected by possible secondary reactions, leading to loss of activity by its deactivation, inhibition or destruction for example by sintering, poisoning, fouling or coking.

Typically, a catalyst reacts with one or more reactants, forming intermediates that will react to form the final product.

A simple example of the standard catalytic reaction is the following:

Adsorption of reactant A in X: $A + X \rightarrow AX \quad (A1.1)$

Adsorption of reactant B in X: $B + AX \rightarrow ABX \quad (A1.2)$

Reaction between the two adsorbed reactants to form P: $ABX \rightarrow PX \quad (A1.3)$

Desorption of the product: $PX \rightarrow P + X \quad (A1.4)$

Overall, catalysis can be classified in three major types according to the phase in which catalyst and reactants are:

- Homogeneous catalysis: In which the catalyst is in the same phase as the reactants.

- Heterogeneous catalysis: In which the catalyst and reactants are in different phases.
- Enzymatic (or biochemical) catalysis: In which the catalysts are enzymes.

In homogeneous catalysis, usually, the catalysts and the reactants are both in liquid phase, being also common that they are dissolved in a solvent, forming a one phase solution. This kind of catalysis is very often used in organocatalysis and biological processes involving enzymes and biocatalysts. Processes which implement this kind of catalysts tend to have as advantage a very good contact between catalyst and reactants, but also the disadvantage of requiring a separation step of the catalyst afterwards in order to recycle it and recover the reactants. The separation step tends to be difficult as well as expensive once these kinds of catalysts can be damaged due to the high temperatures required for the distillation step. Some examples of homogeneous catalysis are acid or basic catalysis or organometallic catalysis. It is often applied in the synthesis of organic compounds, biofuel production and fine chemicals industry.

Enzymatic catalysis may also be considered a sort of homogeneous catalysis, with the particularity of the catalysts being amino acid chains known as enzymes. This kind of catalyst is highly efficient and has a highly specific nature, achieving very high selectivity values. The drawbacks of its utilization are the extreme sensitivity to the temperature and pH of the medium. It is mainly used in industries such as paper production, food processing and molecular biology,

Heterogeneous catalysis, typically happens with the catalyst is in the solid state and the substrates in liquid or gaseous state. Unlike homogeneous catalysis one of the advantages of this kind of processes relies in the easy separation of catalyst and products, on the other hand, the amount of catalyst that is effectively used is lower due to the reaction taking place only on its surface and pores (in the case of porous materials being used). This kind of catalysis has application in environmental protection (e.g. VOC treatment), mechano-catalysis and bulk chemical as well as fine chemical industry.

In this kind of catalysis, the surface area is one of the more influent parameters in the catalysts activity, since it relies on the presence of active sites. In order to maximize the surface area of the catalyst and, therefore, active site abundance, heterogeneous catalysis is usually supported. This means that the catalyst is normally dispersed on the surface of a host material (support), diminishing the particle size and increasing its superficial area.

Although the support can be just a surface where the catalyst is dispersed, it can be extremely advantageous that both catalyst and support interact between each other and with reactants or products of the reaction in order to improve conversion of reactants, selectivity towards specific products and, overall, reaction yield.

In order to make the surface area as big as possible, microporous materials are highly preferred as supports. Some of the most common materials used for this effect include alumina (Al_2O_3), silica (SiO_2), titania (TiO_2), activated carbon and zeolites.

Catalytic activity can be affected by the presence of certain substances in the catalyst. This kind of substances on catalysts can be classified in three different types:

- Promoters: If it increases catalytic activity.
- Inhibitors: If they decrease the catalytic activity and their connection to the catalyst is reversible.
- Poison: If they decrease the catalytic activity and their connection to the catalyst is irreversible.

Besides both inhibitors and poisons having negative influence in the catalytic behavior, the first ones are often intentionally used as means of improving selectivity towards a desired product.

A2- Characterization Methods

Brunauer-Emmett-Teller (BET) surface area and Barret-Joyner-Halenda (BJH) pore size and volume analysis

The adsorption, just like superficial tension, is a consequence of superficial energy. In a solid, most of the atoms are connected to other atoms by all sides. On the other hand, the superficial atoms are incompletely bound and therefore less stable than the first ones. Due to Van der Waals forces of interaction, the superficial atoms are more reactive, attracting gas, vapor and liquids in order to reach higher stability by lowering the imbalance of atomic forces [71].

The BET analysis of a material sample allows obtaining information about its superficial area. This can is done by the adsorption of a gas (usually N_2) and calculation of the amount of adsorbate gas molecules that corresponds to the formation of a monolayer on the surface of the adsorbent.

This method is performed according with the following steps:

- Outgassing of the sample. This step is performed by submitting the sample to heat and vacuum, forcing the desorption of possible contaminants that exist within its pores. These contaminants are usually gases like CO_2 or H_2O that are adsorbed due to atmospheric exposure.
- Cooling of the sample under vacuum. Usually until cryogenic temperature (77K).
- Dosing of the adsorptive to the sample. This process is performed in controlled measurements and after each dose the adsorbed quantity is calculated.

The quantity adsorbed at each pressure defines an adsorption isotherm that can be used to determine the amount of gas needed to form a monolayer over the external surface.

The BET equation (A2.2) allows the calculation of the volume of gas necessary to the formation of a monolayer of gas [72]:

$$\frac{1}{V_a\left(\frac{P_0}{P^*}-1\right)} = \frac{C-1}{V_m C} \times \frac{P^*}{P_0} + \frac{1}{V_m C} \quad (A2.1)$$

C – Adimensional constant related with the enthalpy of adsorption of the adsorbate in the sample.

P – Parcial pressure of the adsorbate vapor at the working temperature (Pa)

*P** – Saturation pressure of the adsorbate. (Pa)

V_a – Adsorbed gas volume at STP conditions. (mL)

V_m – Adsorbed gas volume necessary to the monolayer formation at STP conditions. (mL)

By plotting $\frac{1}{V_a\left(\frac{P_0}{P}-1\right)}$ *vs* $\frac{P}{P_0}$ it is possible to determine V_m. With this value, the specific surface area of the sample can be calculated by equation (A2.2)., where 22400 is the volume of 1 mol of adsorbate in STP conditions in mL.

$$S = \frac{V_m . N_a}{m \times 22400} \quad (A2.2)$$

S – Specific surface area (m^2/g)

N_a – Avogadro's number

m – Sample mass (g)

Applying these principles it is also possible to determine the porosity, pore size and pore distribution of the sample. In the BJH method these characteristics can be determined performing an adsorption-desorption test. In this process the conditions to the adsorption of a monolayer of molecules are created. Then, more gas is sent into the sample so that the gas starts to condensate inside its pores. This allows the evaluation of the fine pores of the material. As the gas pressure increases the pores will gradually be filled from the smaller to the bigger ones. When the saturation of the material occurs and the pores of the sample get filled with liquid. After saturation the adsorptive gas is removed incrementally and from the obtained isotherm it is possible to obtain information about size, volume and area of the pores. This process is exemplified in Figure A2.1.

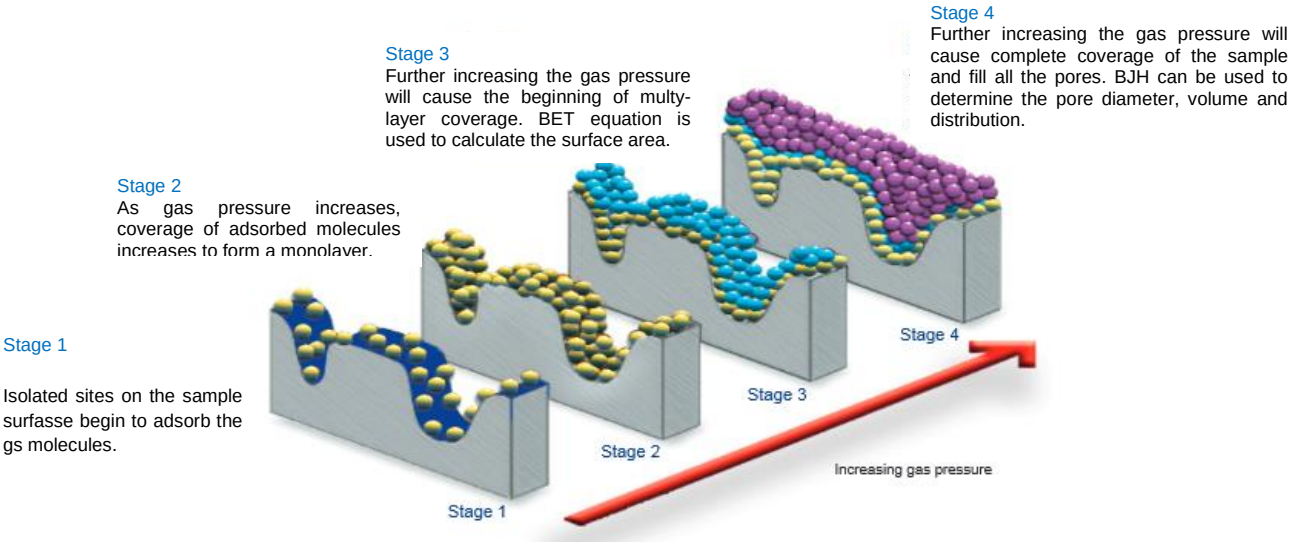

Figure A2. 1 - BJH analysis explained by steps (adapted from [71]).

X-Ray diffraction (XRD) crystalline structure analysis

The X-ray diffraction analysis provides information about the structure of the material. It can be used to:

- Measure average spacing between layers or rows of atoms;
- Determine the orientation of a single crystal or grain;
- Determine the crystal structure of unknown materials;
- Measure the size, shape and internal stress of small crystalline region.

It assumes a particular importance in heterogeneous catalysis since it allows the verification of the crystalline structure of the catalyst support.

During pre-treatment steps or catalytic activity tests, catalyst samples may lose some of their crystalline structure due to high temperatures, leading to porosity and surface area loss and consequent activity drop.

In XRD the X-rays are produced by bombarding a metal target (Cu or Mo) with an electron beam emitted from a hot filament. They are emitted to the catalyst sample with a certain angle θ and are partially diffracted with 2θ as schematized in Figure A2.2. The diffracted radiation only occurs in directions that verify Bragg's Law (equation A2.3) [73]. *n* is any integer number, *d* the spacing between diffracting planes and λ the wavelength of the beam (cm^{-1}).

$$n\lambda = 2dsin\theta \quad (A2.3)$$

Then, a diffractometer detects the incoming radiation, amplifyies and records it.

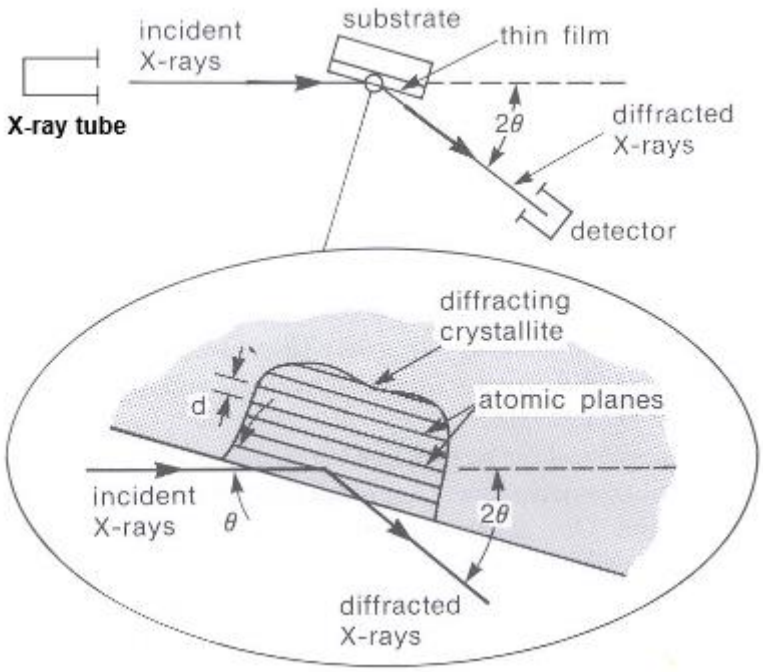

Figure A2. 2 - XRD analysis schematization [74].

The obtained XRD pattern can be compared with the standard patterns for crystalline structures of the corresponding material that can be obtained in [27]. The comparison between the

intensity of the standard peaks for the crystalline structure and the ones obtained with the XRD results in the determination of the crystalline structure percentage of the analysed sample (Figure A2.3).

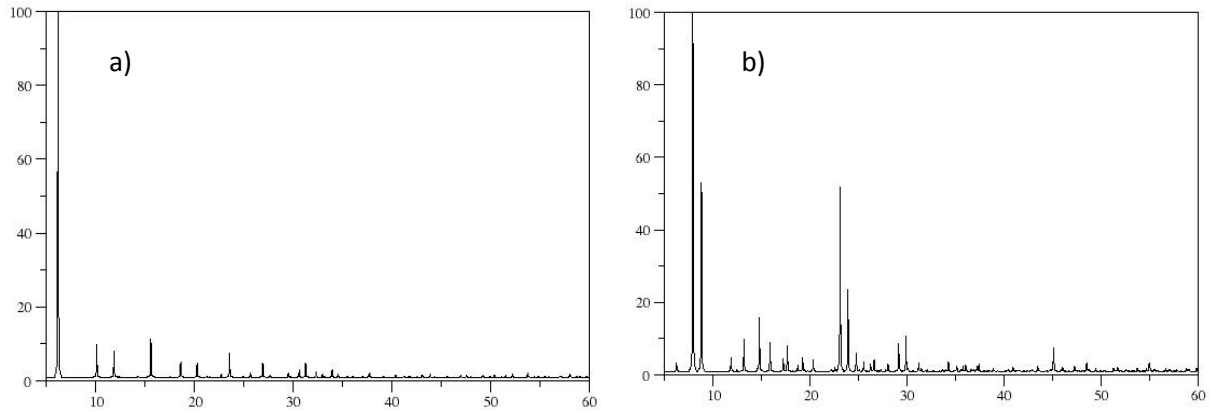

Figure A2. 3 - XRD patterns of: a) crystalline FAU zeolite; b) crystalline MEL zeolite.

Scanning electron microscopy (SEM) analysis

SEM analysis provides information about the morphology/topography, composition and particle size of a material sample at the nanometric scale. It allows 3D visualization of the analysed sample.

The scanning electron microscope uses a focused probe of electrons that is scanned across the sample while the electrons emitted from the surface are analysed to form an image of the material.

In heterogeneous catalysis, usually the catalysts consist of metal particles in oxidic materials. In this case SEM can be used to study not only the shape of the support but also the shape, size and distribution of the metal particles which play a crucial role in catalytic activity [75].

A3 - Safety Calculations

Hydrogen is much known for its high flammability. Special measures have to be taken while operating with this gas, especially when there is the possibility of contact with oxygen that may cause an explosion if certain conditions are met.

During the hydrogenation of CO_2, as well as in the H_2TPR-MS, the reactor is heated up until 500ºC. As it was referred in chapter 3.2.1, a perfect isolation of the reactor could not be achieved, therefore, due to the high vacuum achieved inside the reactor some atmospheric air was leaking inside the reactor. This leak could be noticed by the pressure increase inside the reactor whenever the connection to the vacuum pump was interrupted. In order to understand if this leak could represent a potential danger to the material and to the people in the surroundings of the reactional system, some research was made about the explosivity of H_2/O_2 and H_2/Air mixtures.

According with [76] the explosivity range of a mixture of hydrogen and air under partial-pressure vacuum was studied under different furnace designs. The results of this study are summed in Figure A3. 1.

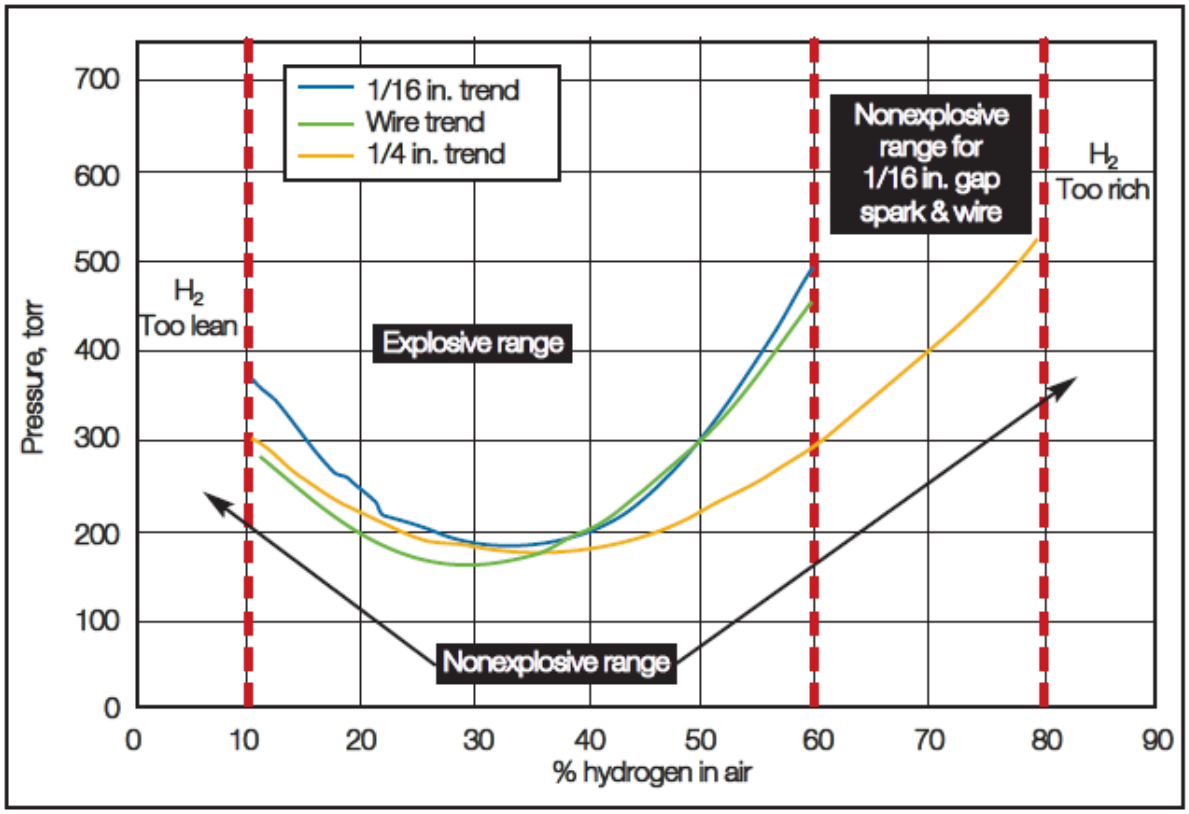

Figure A3. 1 - Explosivity range of an H2/Air mixture [76].

As the hydrogen risk is more relevant in the reduction of the catalyst than in the CO_2 hydrogenation reaction, because higher temperatures are achieved (500ºC) and the hydrogen does not react as it does in contact with the carbon dioxide, the safety calculations were performed for the reduction scenario which is the most likely to represent some kind of danger. Also, in order not to use

pure hydrogen during the reduction, it was mixed with nitrogen to lower its concentration, diminishing the risk of explosion.

At *p*=2.4 Torr, which is approximately the working pressure during the reduction procedures, and temperature T=470ºC, knowing that the reactor has 10 cm of height and 2 cm of inner diameter ($V_{reactor}$=3.14x10^{-5} m^3), the amount of species inside the reactor is 1.56x10^{-6} mol, calculated with equation A3.1, assuming a perfect gas behavior.

$$pV = nRT \quad (A3.1)$$

For a molar concentration of 5% H_2 in the H_2/N_2 feed mixture a value of 7.82x10^{-8} mol of hydrogen is obtained inside of the reactor.

The leak of air into the reactor was measured by registering the increase of pressure over time after blocking the connection between the reactor and the vacuum pump. The leak caused a pressure increase speed of 0.01 Torr/min that, at room temperature and pressure, result in 1.69x10^{-8} mol of air (applying equation A3.1).

Then the amount of hydrogen in the mixture with air is given by the equation A3.2 and its 82.2%.

$$H_2/_{Air}\,(\%) = \frac{n_{H_2}}{n_{H_2} + n_{Air}} \quad (A3.2)$$

According with figure A1.1, besides working at 2.400 Torr, a pressure much lower to the approximately 150 Torr that are necessary in order to reach the explosivity region of the mixture, the hydrogen concentration in air for this mixture composition is within the “too rich” H_2 zone, which means that there is no O_2 enough to represent danger of explosion.

Based on these results, it was considered that the reaction could be performed under safety.

A4 - Estimative of the pressure drop in the packed-bed reactor

The pressure drop felt by the gaseous mixture across the catalyst bed was calculated applying the Ergun general equation for packed-beds (equation A4.1).

$$-\frac{\Delta P}{H} = 150\frac{\mu.u(1-\varepsilon)^2}{d^2\varepsilon^2} + 1.75\frac{\rho_f u^2(1-\varepsilon)}{d.\varepsilon^3} \quad (A4.1)$$

With:

ΔP – Pressure drop;

H – Bed length;

μ – Fluid viscosity;

u – Superficial fluid velocity;

d – Equivalent diameter of the catalyst particles;

ε – Porosity of the packed-bed;

ρ_f – Fluid density.

The equivalent diameter of the particles is the diameter of a spherical particle with a surface area equivalent to that of the actual particles and it was calculated based on an approximate 3mm diameter of the pellets and 1mm of height. It was obtained d=3.383x10^{-3}cm.

The superficial fluid velocity was calculated according with equation A4.1. With Q_r the volumetric flow of the gas at the reactors conditions and A_s the area of the section of the reactor. In which A_s was calculated based on the 2 cm of inner diameter of the reactor.

$$u = {Q_r}/{A_s} \quad (A4.2)$$

Q_r, was determined by equation A4.3, attending to the temperature and pressure inside the reactor, T_r and P_r, respectively, as well as the flow, temperature and pressure at standard conditions, Q_0, T_0, and P_0.

$$Q_r = Q_0\frac{P_0.T_r}{P_r.T_0} \quad (A4.3)$$

Tables A4.1 and A4.2 present the parameters used in the calculation of the pressure drop in function of the reactional system, the temperature and volumetric flow used in the CO_2 methanation experiments using ≈1.2g (H=0.5cm) of catalyst as well as in the IPC *vs* PPC experiment in which ≈4g of catalyst were used (H=3.0cm). It was assumed a value of catalyst-bed porosity of 0.8. The viscosity and density values of the gas were estimated using Aspen Plus V8.4 for a stream with the same composition and flow as the inlet stream used.

Table A4. 1 - Values and results of pressure-drop calculation in the experiments from chapter 3.3.1.

T	P	Q_0	Q_r	μ	ρ_f	u	ΔP	ΔP
(ºC)	(Torr)	(mL/min)	(mL/min)	(Pa.s)	(kg/m^3)	(m/s)	(Torr)	(%)
25	2.040	20	8132.9	2.39×10^{-5}	2.76×10^{-3}	0.43	0.05	2.28%
125			10860.7	2.39×10^{-5}	2.07×10^{-3}	0.58	0.06	3.04%
200			12906.6	2.39×10^{-5}	1.74×10^{-3}	0.68	0.07	3.61%
250			14270.5	2.39×10^{-5}	1.58×10^{-3}	0.76	0.08	3.99%
300			15634.4	2.39×10^{-5}	1.44×10^{-3}	0.83	0.09	4.37%
350			16998.3	2.39×10^{-5}	1.32×10^{-3}	0.90	0.10	4.76%
400			18362.2	2.39×10^{-5}	1.22×10^{-3}	0.97	0.10	5.14%
450			19726.1	2.39×10^{-5}	1.14×10^{-3}	1.05	0.11	5.52%

Table A4. 2 - Values and results of pressure-drop calculation in the experiments from chapter 3.3.2.

T	P	Q_0	Q_r	μ	ρ_f	u	ΔP	ΔP
(ºC)	(Torr)	(mL/min)	(mL/min)	(Pa.s)	(kg/m^3)	(m/s)	(Torr)	(%)
125	1.460	10	6514.9	2.39×10^{-5}	2.17×10^{-3}	0.35	0.04	2.55%
	1.772	15	8051.7	2.39×10^{-5}	1.92×10^{-3}	0.43	0.05	2.59%
	2.036	20	9343.6	2.39×10^{-5}	2.20×10^{-3}	0.50	0.05	2.62%
	2.468	30	11562.1	2.39×10^{-5}	2.20×10^{-3}	0.61	0.07	2.67%
	3.150	50	15098.1	2.39×10^{-5}	2.67×10^{-3}	0.80	0.09	2.74%
	4.106	80	18532.5	2.39×10^{-5}	3.41×10^{-3}	0.98	0.11	2.58%
	4.600	100	20677.8	2.39×10^{-5}	4.50×10^{-3}	1.10	0.12	2.57%

A5 -Plasma discharge breakdown voltage

In order to create plasma in a gaseous medium between two electrodes it is necessary to apply a voltage such that provides enough energy to ionize the gas atoms and allows the removed electrons an amount of energy that makes them able to ionize atoms which they collide with. This voltage is called the Breakdown Voltage and it depends on the gas composition, conditions and electrode distance.

When a voltage is applied to a gas the particles the species present in the gas are ionized and the freed electrons are accelerated. The more distance they travel without colliding with other particles, the more energy they gain. This distance is called the mean free path and it is inversely proportional to the pressure of the gas. If these electrons achieve energy equal or higher than the ionization energy of the other species in the gas, when a collision occurs it will cause the ionization of another atom or molecule, starting a chain reaction (avalanche breakdown) and creating plasma, hence the dependence of the breakdown voltage with the pressure and gas composition.

The breakdown voltage, V_B, for each gas can be determined by Paschen's Law (equation A5.1) in function of the pressure multiplied by the distance between the electrodes, *p.d*, with *a* and *b*, experimental parameters that depend on the gas composition.

$$V_B = \frac{a \times p.d}{\ln(p.d) + b} \quad (A5.1)$$

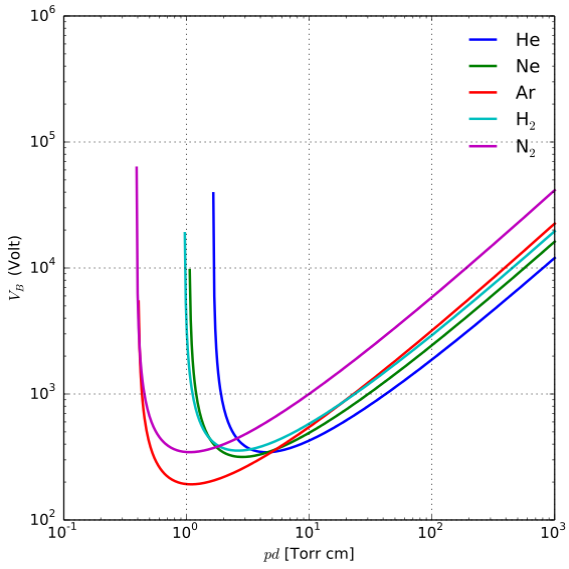

Figure A5. 1 - Breakdown voltage in function of gas type and p.d. [57].

A6 - Mass spectrometer calibrations

In order to calculate the concentration of CH_4 and CO at the outlet of the reactor in a more accurate way calibration experiments were performed for these two compounds.

CH_4 Calibration

The methane calibration was performed by measuring the *m/z* = 15 ion current intensity of CH_4 for several concentrations. The reactor was fed with a mixture of pure Argon and CH_4 that was in a bottle of 1%CH_4/Ar. As the mass spectrometer responds to the concentration of each compound, 15 mL/min of total volumetric flow was fed to the reactor for 1%CH_4/Ar quantities ranging from 0 to 10 mL/min (which was the limit of the flow meter controller that was used for the methane/Argon stream). The CH_4 concentration obtained for each set of values of this calibration experiment as well as the ion current intensities for *m/z* = 15 are shown in Table A6. 1.

Table A6. 1 - CH4 signal intensity in function of its concentration.

Total Flow (mL/min)	1%CH_4/Ar Flow (mL/min)	CH_4 Flow (mL/min)	Pure Ar Flow (mL/min)	CH_4 Concentration (ppm)	m/z=15 Intensity (A)
15	0.0	0.000	15	0	$3.82x10^{-10}$
15	1.5	0.015	13.5	1000	$5.36x10^{-10}$
15	2.0	0.020	13	1333	$5.79x10^{-10}$
15	3.0	0.030	12	2000	$6.52x10^{-10}$
15	5.0	0.050	10	3333	$8.47x10^{-10}$
15	7.0	0.070	8	4667	$1.05x10^{-9}$
15	9.0	0.090	6	6000	$1.25x10^{-9}$
15	10.0	0.100	5	6667	$1.35x10^{-9}$

By plotting the obtained intensity in function of each methane concentration value in ppm and making a linear regression of these values it is obtained the calibration curve in Figure A6. 1

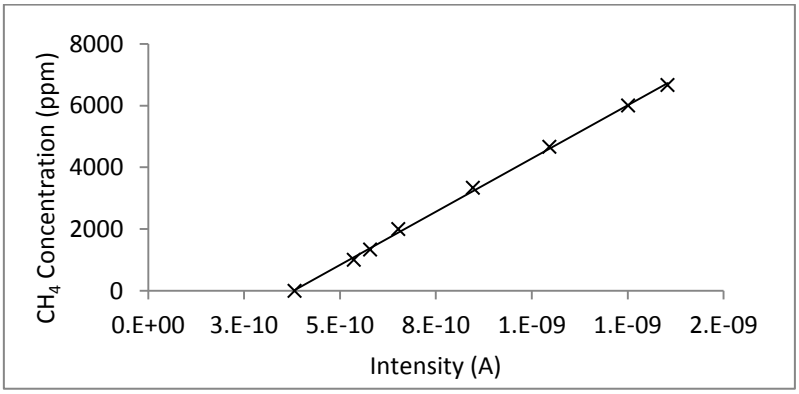

Figure A6. 1 - CH_4 calibration curve.

The equation obtained with the linear regression which expresses the methane concentration (C_{CH4}) in ppm for each intensity (A) is $I(A) = (6.898107 \times 10^{12}) \times C_{CH4} - 2.607427 \times 10^{3}$ $(A6.1)$, with $R^2 = 0.999$.

CO Calibration

The calibration of CO was performed in an analogue way to the one performed for CH_4. The concentration of carbon monoxide in Argon was changed from 0 to 12.5 % (volume) in a 20 mL/min flow mixture. The obtained *m/z* = 28 intensity values for each carbon monoxide concentration are shown in Table A6. 1.

Table A6. 2 - CO signal intensity in function of its concentration.

Total Flow (mL/min)	Ar Flow (mL/min)	CO Flow (mL/min)	CO Concentration (%)	m/z=28 Intensity (A)
20	20.0	0	0	2.94×10^{-8}
20	19.5	0.5	2.5	3.80×10^{-8}
20	19.0	1	5	4.34×10^{-9}
20	18.5	1.5	7.5	4.54×10^{-8}
20	18.0	2	10	5.04×10^{-8}
20	17.5	2.5	12.5	5.53×10^{-8}

With these values the Intensity (A) *vs* Concentration (%) plot obtained and corresponding linear regression curve are the ones shown in **Erro! A origem da referência não foi encontrada.**.

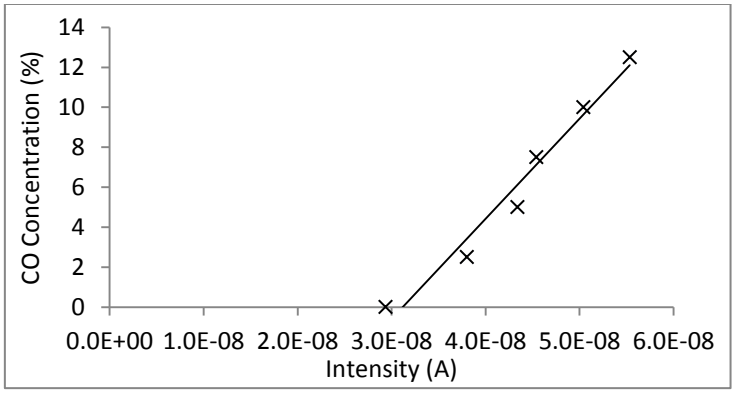

Figure A6. 2 - CO calibration curve.

The linear regression equation which expresses the carbon monoxide concentration, C_{CO}, in % (vol) in function of the ion current intensity *I(A)* is $I(A) = (5.014977 \times 10^{8}) \times C_{CO} - 1.564351 \times 10$ (A6.2) with $R^2 = 0.969$.

A7 - Packed-Bed CO_2 hydrogenation results

Table A7. 1 - Packed-bed reaction results for the blank experiment.

Blank	Conventional Heating						Plasma + Heating				
Temperature (ºC)	200	250	300	350	400	450	125	200	250	300	350
CO_2 Conversion (%)	0.0	0.0	0.0	0.0	0.0	0.0	61.4	65.9	67.4	68.1	69.2
CH_4 Selectivity (%)	-	-	-	-	-	-	0.7	0.5	0.4	0.4	0.4
CH_4 Yield (%)	-	-	-	-	-	-	0.4	0.3	0.3	0.3	0.3
CO Selectivity (%)	-	-	-	-	-	-	99.3	99.5	99.6	99.6	99.6
CO Yield (%)	-	-	-	-	-	-	61.0	65.6	67.1	67.8	68.9

Table A7. 2 - Packed-bed reaction results for the Ni/USY(30) catalyst.

Ni/USY(30)	Conventional Heating						Plasma + Heating					Plasma + Heating (with release)				
Temperature (ºC)	200	250	300	350	400	450	125	200	250	300	350	125	200	250	300	350
CO_2 Conversion (%)	0.7	0.7	2.8	4.9	12.7	28.3	63.8	64.2	65.0	64.1	63.6	63.8	64.2	65.0	64.1	63.5
CH_4 Selectivity (%)	16.8	27.7	28.7	36.2	16.9	4.3	1.6	1.7	1.4	1.2	0.7	2.9	4.6	2.5	2.3	1.4
CH_4 Yield (%)	0.1	0.2	0.6	1.4	1.7	0.9	0.8	0.8	0.7	0.6	0.3	1.5	2.3	1.2	1.2	0.7
CO Selectivity (%)	83.2	72.3	71.3	63.8	83.1	95.7	98.4	98.3	98.6	98.8	99.3	97.1	95.4	97.5	97.7	98.6
CO Yield (%)	0.5	0.4	1.6	2.4	8.2	21.0	48.7	48.9	49.7	49.1	49.0	48.0	47.4	49.2	48.5	48.6

Table A7. 3 - Packed-bed reaction results for the Ni/USY(40) catalyst.

Ni/USY(40)	Conventional Heating						Plasma + Heating					Plasma + Heating (with release)				
Temperature (ºC)	200	250	300	350	400	450	125	200	250	300	350	125	200	250	300	350
CO_2 Conversion (%)	1.1	3.2	7.7	14.8	26.1	33.8	64.1	62.6	60.3	60.4	62.9	64.1	62.6	60.3	60.4	62.9
CH_4 Selectivity (%)	20.5	22.3	25.7	26.1	15.3	5.8	2.3	3.3	3.2	2.0	1.1	4.0	6.0	5.4	3.5	1.8
CH_4 Yield (%)	0.2	0.5	1.5	3.0	3.1	1.5	1.2	1.6	1.5	0.9	0.5	2.0	2.9	2.5	1.6	0.9
CO Selectivity (%)	79.5	77.7	74.3	73.9	84.7	94.2	97.7	96.7	96.8	98.0	98.9	96.0	94.0	94.6	96.5	98.2
CO Yield (%)	0.7	1.9	4.5	8.5	17.1	24.7	48.5	46.9	45.3	45.9	48.2	47.7	45.7	44.2	45.2	47.9

Table A7. 4 - Packed-bed reaction results for the 5%Ni/ZSM-11 catalyst.

5%Ni/ZSM-11	Conventional Heating						Plasma + Heating					Plasma + Heating (with release)				
Temperature (ºC)	200	250	300	350	400	450	125	200	250	300	350	125	200	250	300	350
CO_2 Conversion (%)	0.0	0.0	0.0	0.0	1.4	3.5	64.3	67.6	68.0	68.1	68.2	64.3	67.6	68.0	68.1	68.2
CH_4 Selectivity (%)	-	-	-	-	23.5	2.6	1.0	0.8	0.6	0.6	0.4	2.0	1.3	0.9	0.9	0.6
CH_4 Yield (%)	-	-	-	-	0.3	0.1	0.5	0.4	0.3	0.3	0.2	1.0	0.7	0.5	0.5	0.3
CO Selectivity (%)	-	-	-	-	76.5	97.4	99.0	99.2	99.4	99.4	99.6	98.0	98.7	99.1	99.1	99.4
CO Yield (%)	-	-	-	-	0.8	2.6	49.4	52.0	52.4	52.5	52.7	48.9	51.8	52.2	52.3	52.6

Table A7. 5 - Packed-bed reaction results for the 2.5%Ni/ZSM-11 catalyst.

2.5%Ni/ZSM-11	Conventional Heating						Plasma + Heating					Plasma + Heating (with release)				
Temperature (ºC)	200	250	300	350	400	450	125	200	250	300	350	125	200	250	300	350
CO_2 Conversion (%)	0.0	0.0	2.1	3.9	10.7	28.5	66.0	66.2	64.2	65.5	66.2	66.0	66.2	65.0	65.5	66.2
CH_4 Selectivity (%)	-	-	23.9	26.3	11.4	2.0	1.4	1.1	1.0	0.7	0.4	2.5	2.0	2.5	1.4	0.7
CH_4 Yield (%)	-	-	0.4	0.8	0.9	0.4	0.7	0.6	0.5	0.4	0.2	1.3	1.0	1.2	0.7	0.3
CO Selectivity (%)	-	-	76.1	73.7	88.6	98.0	98.6	98.9	99.0	99.3	99.6	97.5	98.0	97.5	98.6	99.3
CO Yield (%)	-	-	1.3	2.2	7.3	21.7	50.5	50.8	49.4	50.5	51.2	49.9	50.4	49.2	50.2	51.1

Table A7. 6 - Packed-bed reaction results for the Ni/USY(40)(IWI) catalyst.

Ni/USY(40) (IWI)	Conventional Heating						Plasma + Heating					Plasma + Heating (with release)				
Temperature (ºC)	200	250	300	350	400	450	125	200	250	300	350	125	200	250	300	350
CO2 Conversion (%)	1.3	5.1	14.9	25.3	40.7	47.7	64.5	62.3	63.2	64.1	66.2	64.5	62.3	63.2	64.1	66.2
Selectivity CH_4 (%)	26.4	33.7	44.2	47.3	20.5	5.8	4.6	8.0	6.1	3.7	1.3	7.7	13.2	10.8	9.0	1.7
CH_4 Yield (%)	0.3	1.3	5.1	9.4	6.5	2.2	2.3	3.9	3.0	1.8	0.7	3.9	6.4	5.3	4.5	0.9
Selectivity CO (%)	73.6	66.3	55.8	52.7	79.5	94.2	95.4	92.0	93.9	96.3	98.7	92.3	86.8	89.2	91.0	98.3
CO Yield (%)	0.7	2.6	6.5	10.4	25.2	35.0	47.9	44.6	46.2	48.0	50.8	46.3	42.1	43.9	45.4	50.6

A8 - Carbon balance results

During the plasma experiments performed with the IPC configuration the carbon molar balance was calculated by applying the equation 4.8 from chapter 4.2.

Table A8. 1 - Carbon balance to the IPC plasma experiments performed in chapter 4.2.

CB (%)	Plasma + Heating (without CH_4 release)					Plasma + Heating (with CH_4 release)				
Temperature (ºC)	125	200	250	300	350	125	200	250	300	350
Ni/USY(30)	99.1	98.1	99.3	99.3	99.6	100	100	100	100	100
Ni/USY(40)	98.9	98.4	98.6	99.1	99.6	100	100	100	100	100
Ni/USY(40) (IWI)	98.0	96.8	97.0	96.6	99.7	100	100	100	100	100
5%Ni/ZSM-11	99.4	99.7	99.8	99.8	99.9	100	100	100	100	100
2.5%Ni/ZSM-11	99.2	99.4	99.8	99.6	99.8	100	100	100	100	100

A9 - IPC *vs* PPC reactions results

Table A9. 1 - IPC blank results from the IPCvsPPC experiment.

IPC Blank							
Flow (mL/min)	**10**	**15**	**20**	**30**	**50**	**80**	**100**
CO_2 Conversion (%)	68	67	60	47	37	28	29
CH_4 Selectivity (%)	1	0	0	0	0	1	1
CH_4 Yield (%)	1	0	0	0	0	0	0
CO Selectivity (%)	99	100	100	100	100	99	99
CO Yield (%)	67	66	60	46	37	28	29

Table A9. 2 - IPC results from the IPCvsPPC experiment.

IPC							
Flow (mL/min)	**10**	**15**	**20**	**30**	**50**	**80**	**100**
CO_2 Conversion (%)	69	68	62	58	56	50	47
CH_4 Selectivity (%)	3	4	5	5	8	14	19
CH_4 Yield (%)	2	3	3	3	4	7	9
CO Selectivity (%)	97	96	95	95	92	86	81
CO Yield (%)	67	65	59	56	51	43	38

Table A9. 3 - PPC blank results from the IPCvsPPC experiment.

PPC Blank							
Flow (mL/min)	**10**	**15**	**20**	**30**	**50**	**80**	**100**
CO_2 Conversion (%)	51	34	31	25	19	13	12
CH_4 Selectivity (%)	0	0	0	0	0	1	1
CH_4 Yield (%)	0	0	0	0	0	0	0
CO Selectivity (%)	100	100	100	100	100	99	90
CO Yield (%)	51	34	31	25	19	13	12

Table A9. 4 - PPC results from the IPCvsPPC experiment.

PPC							
Flow (mL/min)	**10**	**15**	**20**	**30**	**50**	**80**	**100**
CO_2 Conversion (%)	49	38	34	26	20	15	13
CH_4 Selectivity (%)	0	0	0	1	1	1	2
CH_4 Yield (%)	0	0	0	0	0	0	0
CO Selectivity (%)	100	100	100	99	99	99	98
CO Yield (%)	49	38	33	26	19	15	13

A10 - Determination of residence time in plasma in IPC and PPC configurations

The calculation of the gas residence time inside the plasma-affected zone, $t_{res\ plasma}$, in both IPC and PPC configurations was done according with equation A10.1. V_{plasma} expresses the volume of the plasma zone in mL and Q_r the gas flow in mL/min inside the reactor.

$$t_{res_{plasma}} = \frac{V_{plasma}}{Q_r} \quad (A10.1)$$

As the reactor is under effect of high vacuum and plasma causes temperature increase of the gas to values near 125ºC, Q_r (mL/min) was calculated for each set flow and configuration by assuming the ideal gas case and using equation (A10.2). In this expression, Q_0 is the volumetric flow at room temperature, T_0 (K), and pressure, P_0 (Torr), while T_r and P_r are the temperature in Kelvin degrees and pressure in Torr inside the reactor, respectively. The pressure inside the reactor for each flow was registered during the IPC and PPC studies in order to proceed to these calculations.

$$Q_r = Q_0 \frac{P_0 . T_r}{P_r . T_0} \quad (A10.2)$$

The volume of plasma was calculated knowing that the plasma height was approximately 8 cm in the ICP configuration and 1 cm in the PPC configuration and the reactor has an inner diameter of 2 cm. Assuming a cylindrical geometry of the plasma inside the reactor, volumes of 25.1 and 3.1 mL were obtained for each configuration, respectively.

The residence time results obtained for each configuration and gas volumetric flow between 10 and 100 mL/min are summed in Table A10. 1.

Table A10. 1 - Residence time of the reactional mixture in plasma for the IPC and PPC configurations.

			IPC	PPC
Q_0 (mL/min)	P_r (Torr)	Q_r (mL/min)	$t_{res\ plasma}$ (ms)	$t_{res\ plasma}$ (ms)
10	1.460	6515	231.5	28.9
15	1.772	8052	187.3	23.4
20	2.036	9344	161.4	20.2
30	2.468	11562	130.4	16.3
50	3.150	15098	99.9	12.5
80	4.106	18532	81.4	10.2
100	4.600	20678	72.9	9.1